

DTIC FILE COPY

2

GL-TR-89-0288

AD-A227 588

Analysis of Significant Weather on Meso-Alpha  
Scales Using Conventional and Remotely-Sensed  
Data - Further Studies

Gregory S. Forbes  
Timothy Dye  
Ming-Tzer Lee  
Dennis W. Thomson  
John J. Cahir  
Scott R. Williams  
Arthur A. Person

Pennsylvania State University  
Department of Meteorology  
University Park, PA 16802

August 1990

Final Report  
February 1986-February 1988

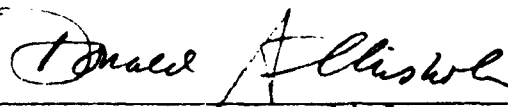
DTIC  
ELECTE  
OCT 17 1990  
E D

APPROVED FOR PUBLIC RELEASE; DISTRIBUTION UNLIMITED

GEOPHYSICS LABORATORY  
AIR FORCE SYSTEMS COMMAND  
UNITED STATES AIR FORCE  
HANSCOM AIR FORCE BASE, MASSACHUSETTS 01731-5000

This technical report has been reviewed and is approved for publication.

  
ARTHUR JACKSON  
Contract Manager

  
DONALD A. CHISHOLM, Chief  
Atmospheric Prediction Branch

FOR THE COMMANDER

  
ROBERT A. McCLATCHEY, Director  
Atmospheric Sciences Division

This report has been reviewed by the ESD Public Affairs Office (PA) and is releasable to the National Technical Information Service (NTIS).

Qualified requestors may obtain additional copies from the Defense Technical Information Center. All others should apply to the National Technical Information Service.

If your address has changed, or if you wish to be removed from the mailing list, or if the addressee is no longer employed by your organization, please notify GL/IMA, Hanscom AFB, MA 01731. This will assist us in maintaining a current mailing list.

Do not return copies of this report unless contractual obligations or notices on a specific document require that it be returned.

Unclassified

SECURITY CLASSIFICATION OF THIS PAGE

REPORT DOCUMENTATION PAGE				Form Approved OMB No. 0704-0188	
1a REPORT SECURITY CLASSIFICATION <b>Unclassified</b>			1b RESTRICTIVE MARKINGS		
2a SECURITY CLASSIFICATION AUTHORITY			3 DISTRIBUTION / AVAILABILITY OF REPORT <b>Approved for public release; Distribution unlimited</b>		
2b DECLASSIFICATION / DOWNGRADING SCHEDULE					
4 PERFORMING ORGANIZATION REPORT NUMBER(S)			5 MONITORING ORGANIZATION REPORT NUMBER(S) <b>GL-TR-89-0288</b>		
6a NAME OF PERFORMING ORGANIZATION <b>Pennsylvania State University</b>		6b OFFICE SYMBOL (If applicable)	7a NAME OF MONITORING ORGANIZATION <b>Geophysics Laboratory</b>		
6c ADDRESS (City, State, and ZIP Code) <b>Department of Meteorology University Park, PA 16802</b>			7b ADDRESS (City, State, and ZIP Code) <b>Hanscom AFB Massachusetts 01731-5000</b>		
8a NAME OF FUNDING / SPONSORING ORGANIZATION		8b OFFICE SYMBOL (If applicable)	9 PROCUREMENT INSTRUMENT IDENTIFICATION NUMBER <b>F19628-86-C-0092</b>		
8c ADDRESS (City, State, and ZIP Code)			10 SOURCE OF FUNDING NUMBERS		
			PROGRAM ELEMENT NO <b>61102F</b>	PROJECT NO <b>2310</b>	TASK NO <b>G8</b>
					WORK UNIT ACCESSION NO <b>BE</b>
11. TITLE (Include Security Classification) <b>Analysis of Significant Weather on Meso-Alpha Scales Using Conventional and Remotely-Sensed Data - Further Studies</b>					
12 PERSONAL AUTHOR(S) <b>Gregory S. Forbes, Timothy Dye, Ming-Tzer Lee, Dennis W. Thomson, John J. Cahir, Scott R. Williams, Arthur A. Person</b>					
13a TYPE OF REPORT <b>FINAL REPORT</b>		13b TIME COVERED FROM <b>2/86</b> TO <b>2/88</b>		14 DATE OF REPORT (Year, Month, Day) <b>1990 August</b>	
15 PAGE COUNT <b>120</b>					
16 SUPPLEMENTARY NOTATION					
17. COSATI CODES			18 SUBJECT TERMS (Continue on reverse if necessary and identify by block number)		
FIELD	GROUP	SUB-GROUP			
			<b>Wind measurement Rainbands Fronts</b>		
			<b>Wind profilers Mesoscale meteorology</b>		
		<b>HYVCC</b>	<b>Cyclones Weather analysis &amp; forecasting</b>		
19 ABSTRACT (Continue on reverse if necessary and identify by block number) <b>This report summarizes the M.S. Thesis research of three Penn State graduate students under the supervision of Professors Greg Forbes and Dennis Thomson, and other wind profiler-related research. Chapter 2 summarizes the work of Ming-Tzer Lee, and examines the atmospheric structures accompanying some meso-alpha-scale cloud patterns and the surface weather affiliated with them, via detailed analyses of wind fields involving time-space conversion of hourly profiler-measured horizontal winds and rawinsonde winds and temperatures. Chapter 3 summarizes the research of Tim Dye, and is a study using profiler three-dimensional winds at 5-minute intervals (or less) to examine the structure of meso-beta-scale precipitation bands. Chapter 4 summarizes the research of Larry Knowlton, in which winds from 2- and 3-station wind profiler networks are used to examine the circulations associated with atmospheric fronts.)</b> <b>In the course of performing the above research, and during the preceding contract period, a number of analysis techniques were examined for use with wind profiler data.</b>					
20 DISTRIBUTION / AVAILABILITY OF ABSTRACT <input type="checkbox"/> UNCLASSIFIED/UNLIMITED <input type="checkbox"/> SAME AS RPT <input type="checkbox"/> DTIC USERS			21 ABSTRACT SECURITY CLASSIFICATION <b>Unclassified</b>		
22a NAME OF RESPONSIBLE INDIVIDUAL <b>Arthur Jackson</b>			22b TELEPHONE (Include Area Code)		22c OFFICE SYMBOL <b>GL/LYP</b>

Cont of Block 19:

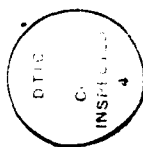
Some of the key techniques are:

Time-Height Sections of Total winds, Perturbation Winds and Relative Winds  
Horizontal charts of Total, Perturbation, and Relative Winds  
Horizontal Charts with Time-Space Conversion of Winds  
Measured, Kinematic, and Adiabatic Vertical Velocities  
Other Kinematic Quantities: Divergence, Vorticity, Deformation  
Thermal Wind-Assumed Temperature Gradients  
Q-Vector Forcing Streamfunctions

The deployment of a network of wind profilers across the Midwest will allow for real-time analysis improvements using the techniques described above, and these improved diagnoses should lead to improvements in nowcasting and very-short-term forecasting. Further, the insertion of time-height series of data from the profiler network into mesoscale numerical weather prediction models, via four-dimensional data assimilation, will allow for impressive improvements in mesoscale short-term forecasting.

Request For	
DIS ORA&I	<input checked="checked" type="checkbox"/>
DTIC TAB	<input type="checkbox"/>
Unannounced	<input type="checkbox"/>
Justification	
By	
Distribution/	
Availability Codes	
Dist	Avail and/or Special

A-1



## PREFACE

Between 1985 and 1989, two Air Force Geophysics Laboratory Contracts with the lead author supported research on the use of wind profiler data for meteorological analysis and forecasting. The first contract was F19628-85-K-0011, and dealt with the development and use of software for processing of wind profiler data for meteorological analysis and forecasting. Graduate students Cathy Carlson and Paul Neiman began their M.S. research under that contract. The final report of that contract (Forbes et al., 1989) describes the framework upon which the research of the second contract was based.

This manuscript is a somewhat delayed publication of the final report on the second contract, F19628-86-C-0092; delayed long enough for the graduate student research begun under the contract to reach completion. This second final report introduces a set of research topics which have been pursued in greater detail than in the course of the first contract; primarily the research of the lead author and graduate students Tim Dye and Ming-Tzer Lee, partially supported by AFGL. A complete reporting of their research is being made available concurrently, through submission of their M.S. Theses to AFGL. The second contract also supported the research of Larry Knowlton (1987) and the completion of the research of Cathy Carlson (1987a,b) and Paul Neiman (1987). Copies of each of these M.S. Theses are available from Greg Forbes at Penn State.

The topics treated by the M.S. Theses can be capsulized as follows:

Carlson Thesis: Calculations using a triangle of wind profilers

Neiman Thesis: Thermodynamic information estimated from single-station profiler winds

Knowlton Thesis: Frontal zone structure and circulations

Dye Thesis: Mesoscale precipitation bands

Lee Thesis: Time-space-conversion analysis of profiler and rawinsonde data

## TABLE OF CONTENTS

	PREFACE .....	111
1.	INTRODUCTION .....	1
2.	TIME-SPACE CONVERSION OF PROFILER WINDS AND RAWINSONDE DATA FOR DETAILED STUDIES OF CYCLONE SUBSTRUCTURES .....	3
3.	STUDIES OF MESO-BETA-SCALE PRECIPITATION BANDS .....	53
4.	STUDIES OF FRONTAL CIRCULATIONS .....	69
5.	CONCLUDING REMARKS .....	89
	ACKNOWLEDGEMENTS .....	92
	REFERENCES .....	92
	APPENDICES	
	1. PROJECT PERSONNEL .....	95
	2. REPORTS AND PUBLICATIONS PREPARED .....	96
	3. ACCURACY OF PROFILER MEASUREMENTS .....	98
	4. NOTES ON QUALITY CONTROL OF PROFILER DATA .....	103

## 1. INTRODUCTION

Meteorologists inspecting a satellite image cannot help but be amazed by the complexity of cloud patterns present, in terms of variety of shapes and scales of features. In many instances, particularly during (but not limited to) the "convective season", the patterns shown may bear little resemblance to the idealized cloud patterns which should accompany synoptic-scale, quasi-geostrophic travelling waves. Even during the winter, there can be significant mesoscale features in the satellite imagery which "distort" the otherwise-synoptic-scale cloud patterns. It is partly in this context that the research reported herein has been performed: as an effort to identify the character of the mesoscale circulations which accompany some of the travelling non-convective mesoscale features detectable in satellite imagery.

Weldon (1979) has described and documented the relationship between large-scale cloud patterns seen in satellite imagery and certain kinematic and dynamic properties of the atmosphere in which they occur. In particular, cloudy regions are often related nearly uniquely to regions experiencing positive vorticity advection (which is related to upward vertical velocity in quasi-geostrophic models of the atmosphere, for example). The western (upstream relative to the movement of the cloud pattern) limit of the cloud pattern is often found near the mid-tropospheric trough axis, where vorticity advection is nearly zero, and clear skies are usually found farther upwind where the vorticity advection is negative (and subsidence is occurring). The eastern (downwind) limit of the cloud pattern is often found near the mid-tropos-



pheric ridge axis.

When the atmosphere possesses a marked rotation (vorticity) center, the cloud pattern tends to spiral about that center into the shape of a comma. In the presence of a vorticity center that is dominated by contribution from lateral wind shear rather than curvature of the flow, the cloud pattern assumes the shape of a stretched "S", often termed a baroclinic leaf.

Sharp edges of cloud bands are often associated with regions where the wind field possesses a large deformation component. One such region of this type is on the northwest (northern-upstream) edge of a large-scale comma cloud or baroclinic leaf. Another region of this type is on the northwest (upstream with respect to the system translation) edge of the cloudy "tail" of the comma cloud. This is a confluence zone, and the cloud edge is associated with the axis of the jet stream. Carlson (1980) has shown that the clear and cloudy airstreams adjacent to the cloud edges have followed quite different trajectories. The cloudy airstream has ascended from a relatively warm, moist origin, while the clear airstream has had a history of previous descent and a colder, drier origin.

In this paper it is assumed that the reader is rather familiar with the principles described in the above-cited references, such that further discussion and illustration is unnecessary. What will be discussed in this paper are studies that have impact upon the application of these types of principles to day-to-day situations where (1) the shape of the cloud pattern may not be ideal, or (2) the features are of smaller scale. Chapter 2

(adapted from Forbes and Bankert, 1987 and Lee, 1990) examines the atmospheric structures accompanying some of the cloud patterns and the surface weather affiliated with them, via detailed analyses of wind fields involving time-space conversion of hourly profiler-measured horizontal winds and rawinsonde winds and temperatures. Chapter 3 is a related study (adapted from Dye, 1990), using profiler three-dimensional winds at 5-minute intervals (or less) to examine the structure of meso-beta-scale precipitation bands. In Chapter 4 (adapted from Knowlton, 1987), winds from 2- and 3-station wind profiler networks are used to examine the circulations associated with atmospheric fronts.

## 2. TIME-SPACE CONVERSION OF PROFILER WINDS AND RAWINSONDE DATA FOR DETAILED STUDIES OF CYCLONE SUBSTRUCTURES

### 2.1 Principles of Time-Space Conversion

Time-space conversion techniques have been used for many years to determine the approximate structure of weather systems that are too small to be sampled by simultaneous measurements from the available weather station networks. The object of the time-space conversion is to take advantage of the ability to make frequent measurements at a few locations while the weather system passes overhead. Temporal changes of a parameter  $P$  are transformed to spatial gradients via

$$\frac{\Delta P}{\Delta t} = - |\vec{C}| \frac{\Delta P}{\Delta s}, \quad (2.1)$$

where  $|\vec{C}|$  is the speed of movement of the weather system and  $\Delta s$

is a distance in the direction toward which the system is moving.

The underlying assumption of the time-space conversion technique (2.1) is that the weather system is in a steady state during the period in which time-space conversion is applied. During such a period, a derived "simultaneous" spatial analysis is obtained by plotting the observation of parameter P at a location displaced from where it was measured, by distance

$$\Delta s = |\vec{C}| \cdot \Delta t \quad , \quad (2.2)$$

where  $\Delta t$  is the time difference between the observation and the reference (analysis) time,  $t = t_{ref} - t_{obs}$ . For a weather system moving eastward, observations taken earlier than the reference time are plotted as if they were taken at a location east of the actual point of observation (c.f., Fujita, 1963). Observations taken later than the reference time are plotted as if they were taken at locations west of the actual point of observation.

Actually, it is often necessary to perform the time-space conversion more carefully than suggested by the simple explanation above. A rigorous treatment must consider that the observed quantities may be the combined results of a mesoscale weather system travelling within a synoptic-scale environment, and moving with a velocity different from the larger-scale weather system in which it is embedded. In a typical case, the large-scale environmental fields are either moving slower than the mesoscale system or are quasi-stationary. A rigorous procedure, then, must separate the mesoscale perturbation quantities from the prevailing large-scale fields, and apply the time-space conversion only to the perturbation quantities.

Most studies involving time-space conversion have been performed on mesoscale convective systems, most notably by Fujita (1955, 1963). For these systems, which evolve rapidly, the period of time-space conversion is necessarily short. During these short periods, the weather systems move relatively small distances with respect to the large-scale environment in which they are embedded. In addition, the large-scale gradients are usually quite weak and the large-scale wind speeds rather weak. This allows the simple displacement of observations as a reasonable approximation to the more complicated displacement of perturbation quantities. However, when the time-space conversion technique is used with respect to larger weather systems which can be considered steady state for longer periods, perturbation quantities must normally be used.

When time-space conversion periods are long, the moving weather system may travel through a sufficient distance that the background values of pressure, temperature, and humidity in the large-scale environment may change. Because of this, at first contemplation the perturbation concept may seem inconsistent with the steady-state assumption, and material advection of conserved quantities (as first indicated above) might seem to be correct. However, it must be remembered that even under adiabatic conditions the local change of temperature is controlled by a balance of horizontal advection, adiabatic warming or cooling, and mixing. The mixing ratio is, similarly, affected by horizontal and vertical advectons and mixing. Thus, because most mesoscale systems are characterized by appreciable vertical velocities and,

hence, adiabatic temperature changes and vertical fluxes, a steady-state mesoscale system (with a steady pattern of vertical velocities) must be treated as producing a perturbation on a large-scale background.

The concept of a moving perturbation (as opposed to advection of conserved values) also applies to air velocity, but with some subtleties owing to the vector character of this quantity. Figure 2.1 shows, by illustration, the manner in which perturbation velocity components must be computed and displaced. Because the large-scale flow pattern may contain curvature, mesoscale weather systems may change orientation perceptibly after a period of more than a few ( $\sim 3-6$ ) hours. Perturbation quantities  $u'$  and  $v'$  must, therefore, be computed in the natural system-oriented (or curved mean-flow) coordinate system, as opposed to a geographic (N-S-E-W) system. When the mesoscale system is characterized as inducing perturbations in the along-axis direction ( $n$ ) and the axis-normal direction ( $s$ ), the perturbation quantities in this frame of reference will tend to be conserved. If the system is steered by the mean flow, the  $s$  and  $n$  directions can be thought of as being along and normal to the system movement, respectively.

The time-space converted winds were obtained in the following manner. (1) Large-scale wind fields ( $U$ ,  $V$ ) were obtained at multiple levels in the manner discussed in the next paragraph. (2) Since the axis of the pressure trough associated with the comma cloud system was oriented approximately normal to the mean flow, perturbation velocities with respect to the curved mean-

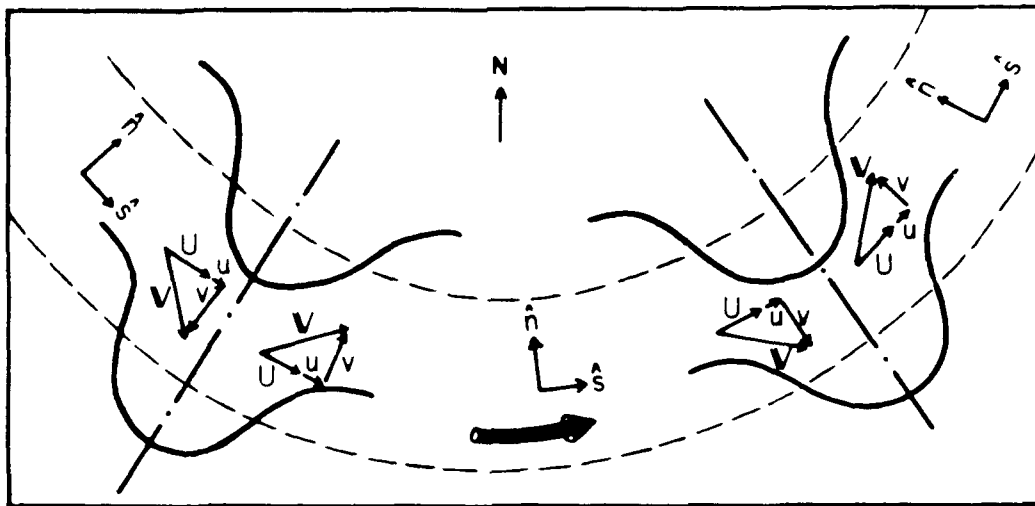


Figure 2.1. Schematic diagram depicting the movement of a sinusoidal disturbance through a curved prevailing mean flow (dashed). Total streamlines (heavy lines) represent the total velocity field at two times, composed of prevailing mean flow  $U$ , and along-movement and along-axis perturbations,  $u$  and  $v$ .

wind ( $s$ ,  $n$ ) reference system were computed for individual observations. (3) Velocity of the moving weather system,  $\vec{C}$ , (the comma cloud in the example which follows) was obtained from satellite imagery. (4) The time-space converted total wind velocities at the reference time were obtained by displacing the perturbations to their appropriate locations using (2.2) and then performing the addition

$$\vec{V}_{total} = (u' + U)\hat{s} + v'\hat{n} \quad , \quad (2.3)$$

where  $\vec{V}_{total}$  is the vector velocity at the displaced location,  $u'$  and  $v'$  are the perturbation quantities,  $U$  is the large-scale mean velocity at the displaced location, and  $\hat{s}$  and  $\hat{n}$  are oriented along and normal to the mean flow at the displaced location.

The large-scale prevailing fields can be obtained either by spatial averaging of simultaneous data over distances comparable

to the scale (wavelength or diameter) of the mesoscale system or by temporal averaging of data over an interval comparable to the period (time required for passage of the entire mesoscale system) of the moving system. The latter technique was used in this research to obtain mean fields, while both temporal and spatial averaging was used to obtain the large-scale steering velocities.

The procedure described above was developed by Forbes and used to examine the case of 19-20 January 1987 (Forbes and Bankert, 1987). That case study was performed via hand calculations and analyses of the mean and perturbation quantities. Once this "pilot project" showed considerable prospects for future applications of the technique, a computer-based scheme was developed by Lee (1990), involving only a modest amount of forecaster interaction. This interaction involved the selection of the appropriate translation velocity of the weather system under consideration. Several options were investigated, including (1) the insertion of a constant value at all locations of the domain; (2) the use of the mean winds in a "steering layer" (5-6 km) and spatially averaged (1000 km radius; to represent the synoptic-scale steering flow), which varied from location to location, as a surrogate for a translation velocity; (3) an adjusted "steering" wind, which varied from location to location and consisted of the "steering layer" wind multiplied by a constant and rotated by a constant. These constants were determined by comparing the subjectively computed (satellite-based) translation speed and direction with the "steering layer" wind speed at the location of the center of the feature under examination. Thus, if the feature was moving

faster than and to the right of the mean wind, for example, then the translation speed was taken to be the mean "steering layer" speed multiplied by a constant (greater than 1) and the translation direction was taken to be the mean "steering layer" direction augmented by a constant. The latter scheme generally gave results most consistent with the findings of Weldon (1979) and, therefore, was considered best.

## 2.2 Time-Space Conversion Applied to Analysis of a Cyclone with Embedded Mesoscale Snow Bands

In the analyses that follow, temporal averaging was performed using rawinsonde and wind profiler data for a 36-hour period. This represented four 12-hourly rawinsonde observations and 37 hourly wind profiler observations between 0000 UTC on 19 January 1987 and 1200 UTC 20 January 1987, inclusively. Perturbation quantities were computed from the rawinsonde observations at 1200 /19 and 0000/20, and from wind profiler observations between 1200 /19 and 0500/20. The reference time for the analyses was selected as 1930 UTC by Forbes and Bankert (1987), which was at a time approximately midway between two brief heavy snow events which occurred within the profiler network in Pennsylvania. Lee (1990) performed the time-space conversions for an analysis time of 1800 UTC on 19 January 1987. In order to facilitate the use of wind profiler data without estimation of the heights of the pressure surfaces, analyses were performed at constant altitudes.

Figure 2.2 shows the large-scale mean flow at 4.6 km MSL, hand-computed by Forbes and Bankert (1987). The large-scale flow



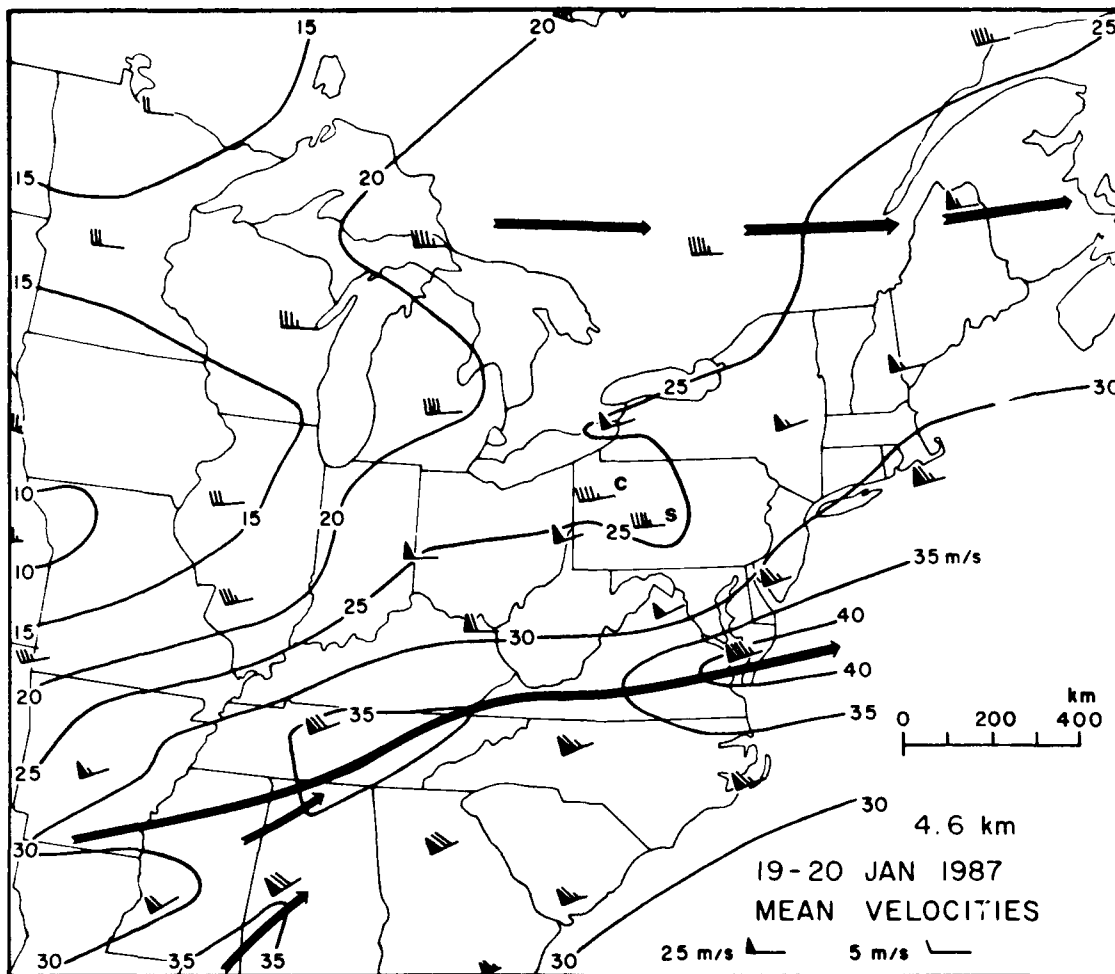


Figure 2.2. 36-hour mean velocity at 4.6 km on 19-20 January 1987. All winds are from rawinsondes except for the two sites in Pennsylvania showing speeds of about 22.5 m/s, which are from VHF (about 50 MHz) Doppler radar wind profilers: (c) Crown, PA; (s) "Shantytown" or McAlevys Fort, PA.

is characterized as having a jet stream extending from Mississippi to Virginia, and much weaker winds in the central Midwest. A weak long-wave trough axis is suggested (from wind shifts) across Missouri to eastern Ohio, to east of James Bay. The wind profiler mean winds (37 observations) blend in well with the rawinsonde mean winds (4 observations), to within the accuracy expected from the rawinsonde values. Objective mean wind fields computed by Lee (1990) are very similar.

Figure 2.3 is a sequence of satellite images that shows the presence of a well-developed comma cloud system, having a head and tail easily identified in the imagery. The mid- and upper-tropospheric rotation center is only partly surrounded by clouds, but can be detected over extreme southeastern Missouri at 1201 UTC (Fig. 2.3a), extreme western Kentucky at 1501 UTC (b), southeastern Indiana at 1801 UTC (c), and over southeastern Ohio at 2101 UTC (d).

Figs. 2.3e and f give enlarged visible imagery views of a portion of the comma cloud, revealing two abrupt cloud edges (or walls). One runs nearly south-north from northwestern Georgia to the western tip of Lake Erie at 1431 UTC (Fig. 2.3e) and from central North Carolina through central Pennsylvania and a bit farther northward at 1931 UTC (Fig. 2.3f). This cloud edge is affiliated with the warm conveyor belt (Carlson, 1980), having sharp west edge co-located with the axis of the upper-level jet stream. The second cloud edge, curving from western Ohio into southeastern Missouri at 1431 UTC (e) and from northwestern Pennsylvania to Lake Erie to northwestern Ohio at 1931 UTC (f), is associated with the cold (easterly) conveyor belt (Carlson, 1980).

Beneath the comma cloud, a significant winter storm was occurring, with many locations receiving moderate to heavy snow. Figure 2.4 is the surface chart for 1800 UTC, and reveals a distorted cyclone center stretching from central Ohio toward the southwestern corner of Pennsylvania, and then into West Virginia. A cold front extends from the cyclone center along the

Appalachians into Georgia. However, the coldest air is found farther west, to the rear of a trough line that stretches across southern Indiana and Illinois, and the air behind the indicated cold front is actually warmer than the air ahead of the cyclone.

Cold air damming (e.g., Forbes et. al, 1987) is in progress

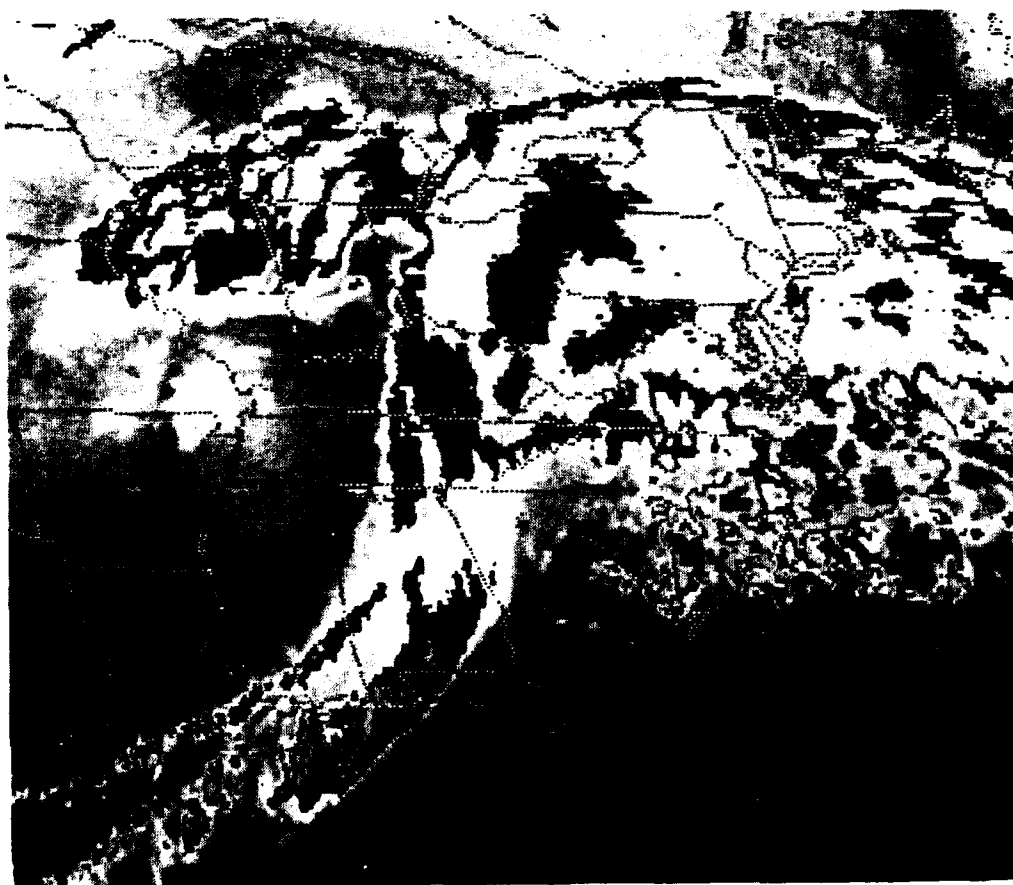
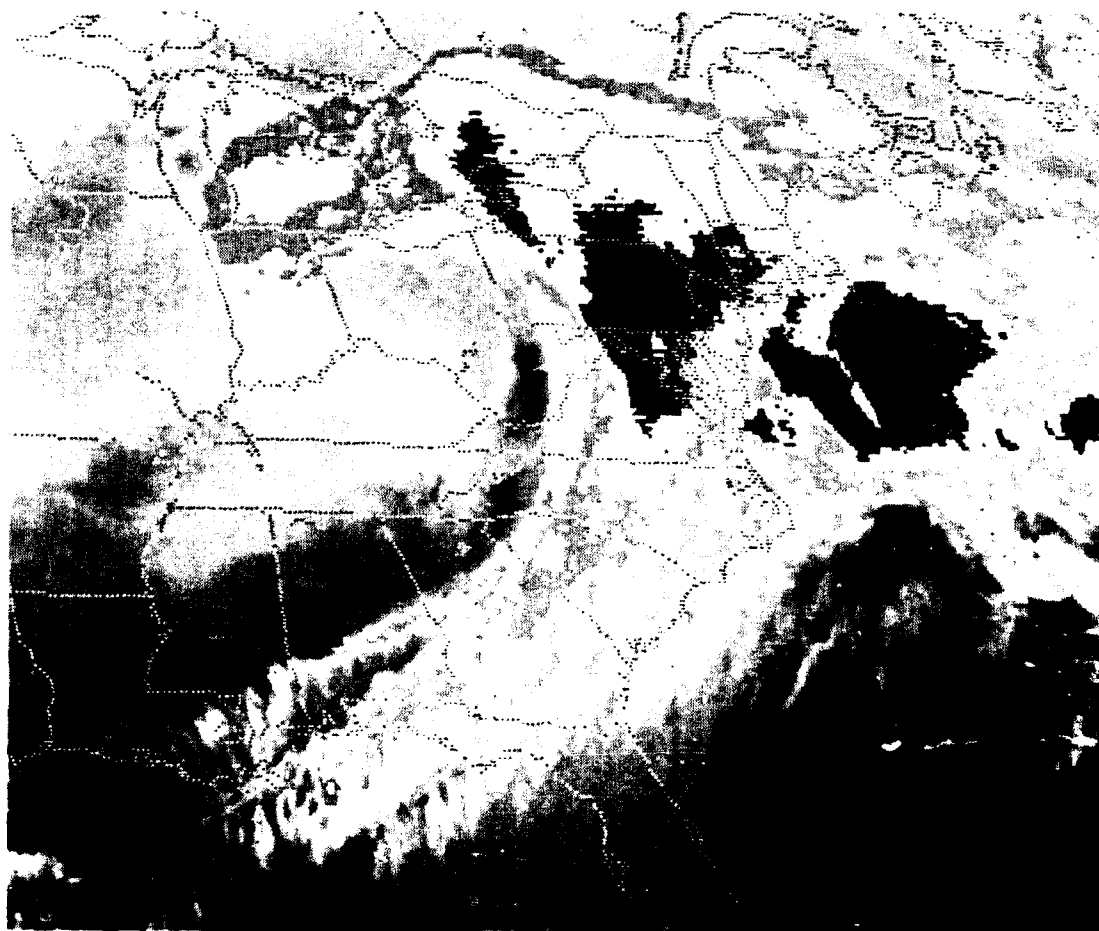


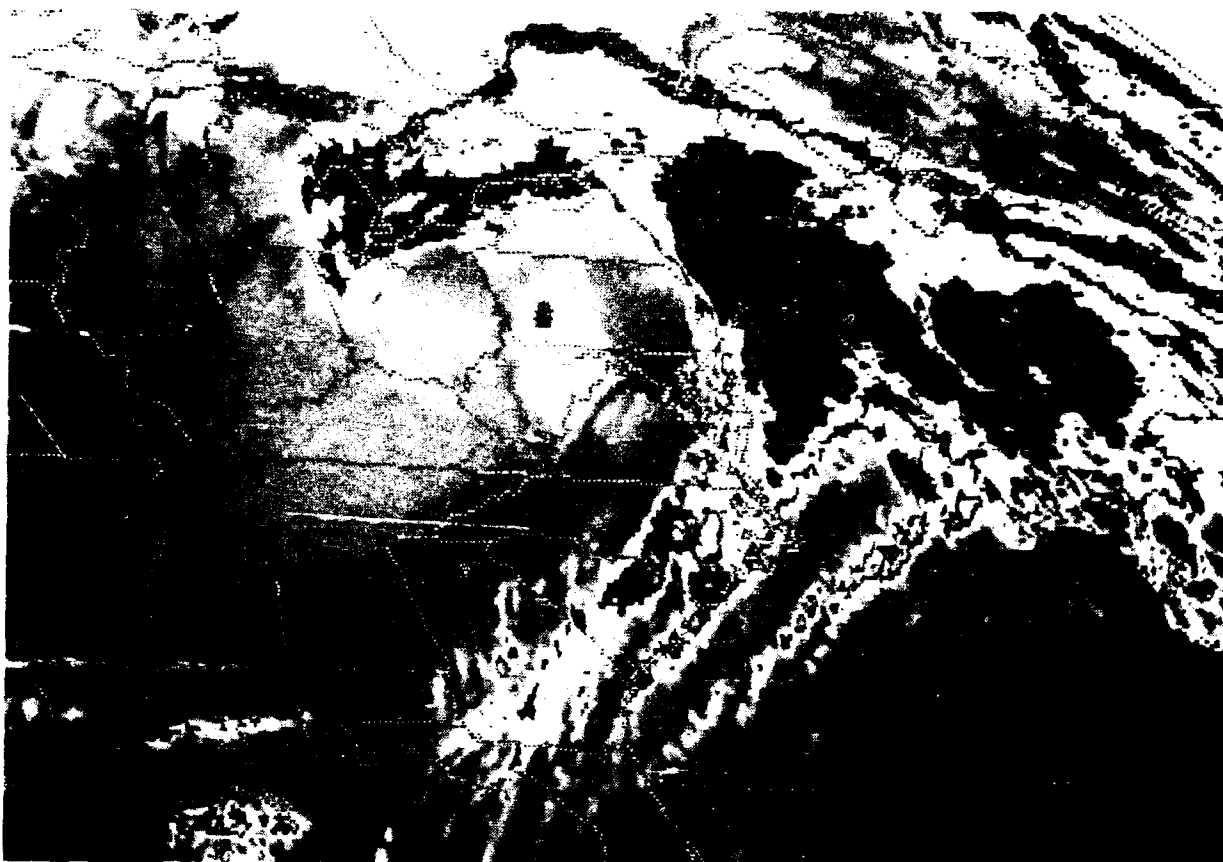
Figure 2.3. Satellite images of the comma cloud of 19 January 1987. Enhanced infrared images at (a) 1200 UTC, (b) 1500 UTC, (c) 1800 UTC, (d) 2100 UTC. Visible images at (e) 1431 UTC, (f) 1931 UTC.



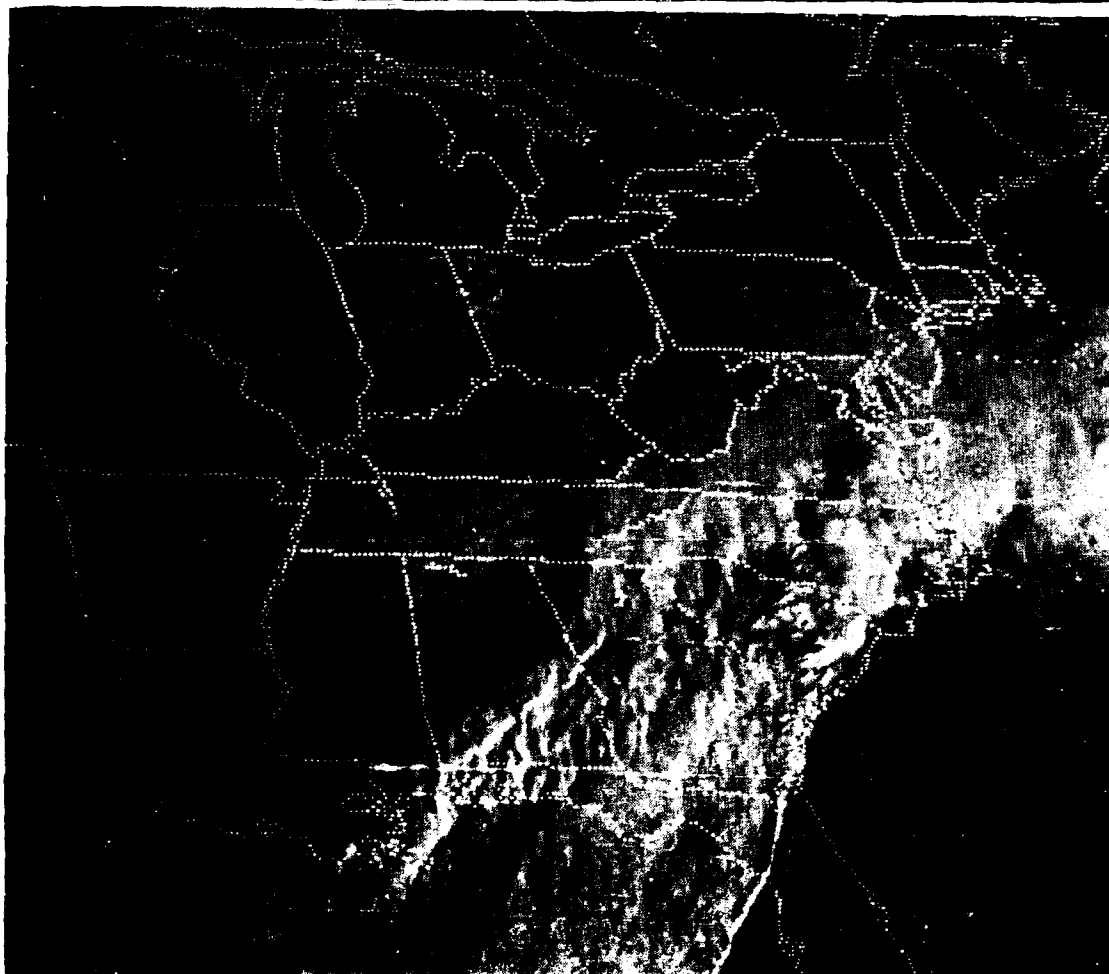
b



c

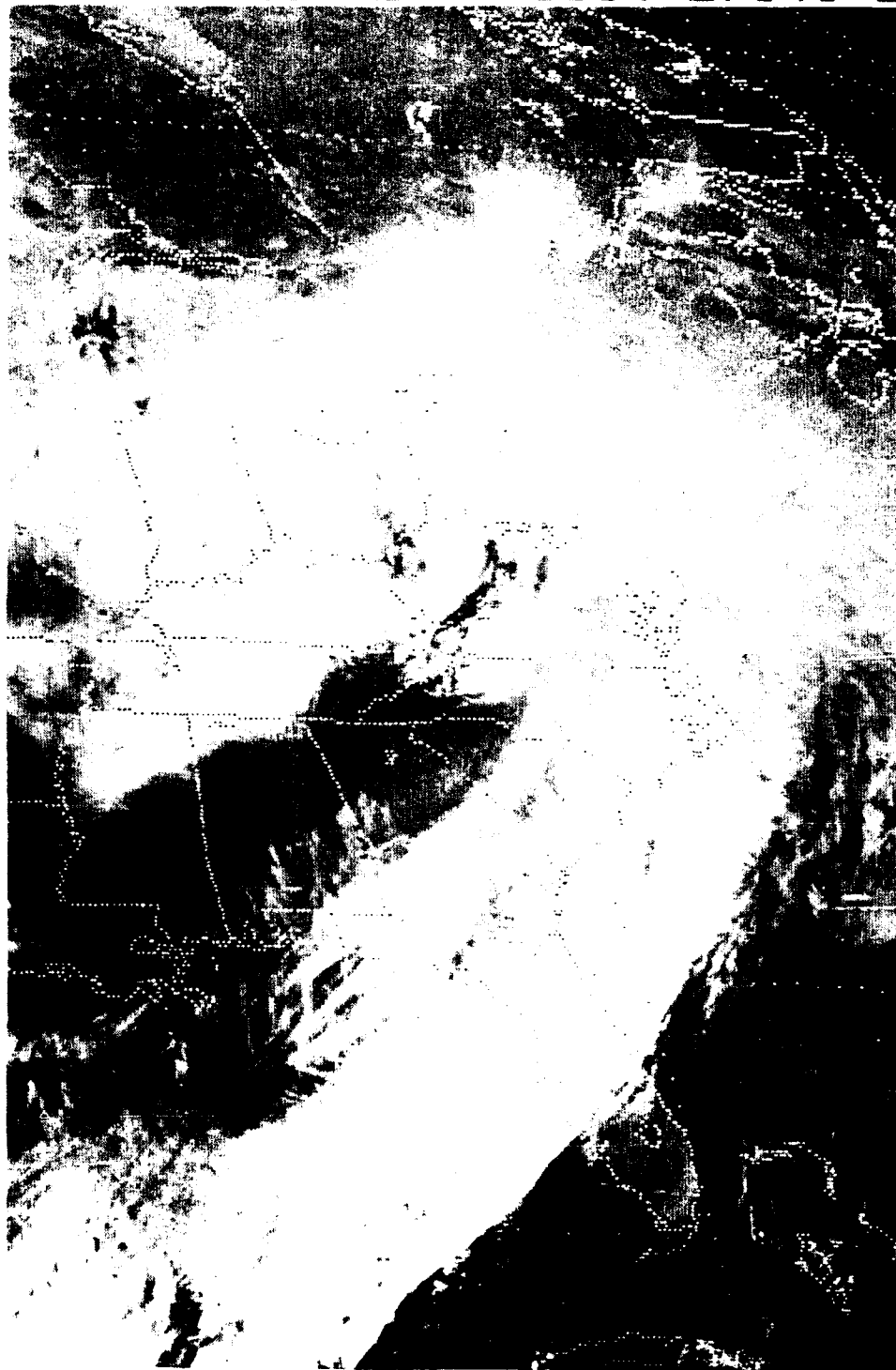


d



e

19JA87 18A-2 01534 27341 D



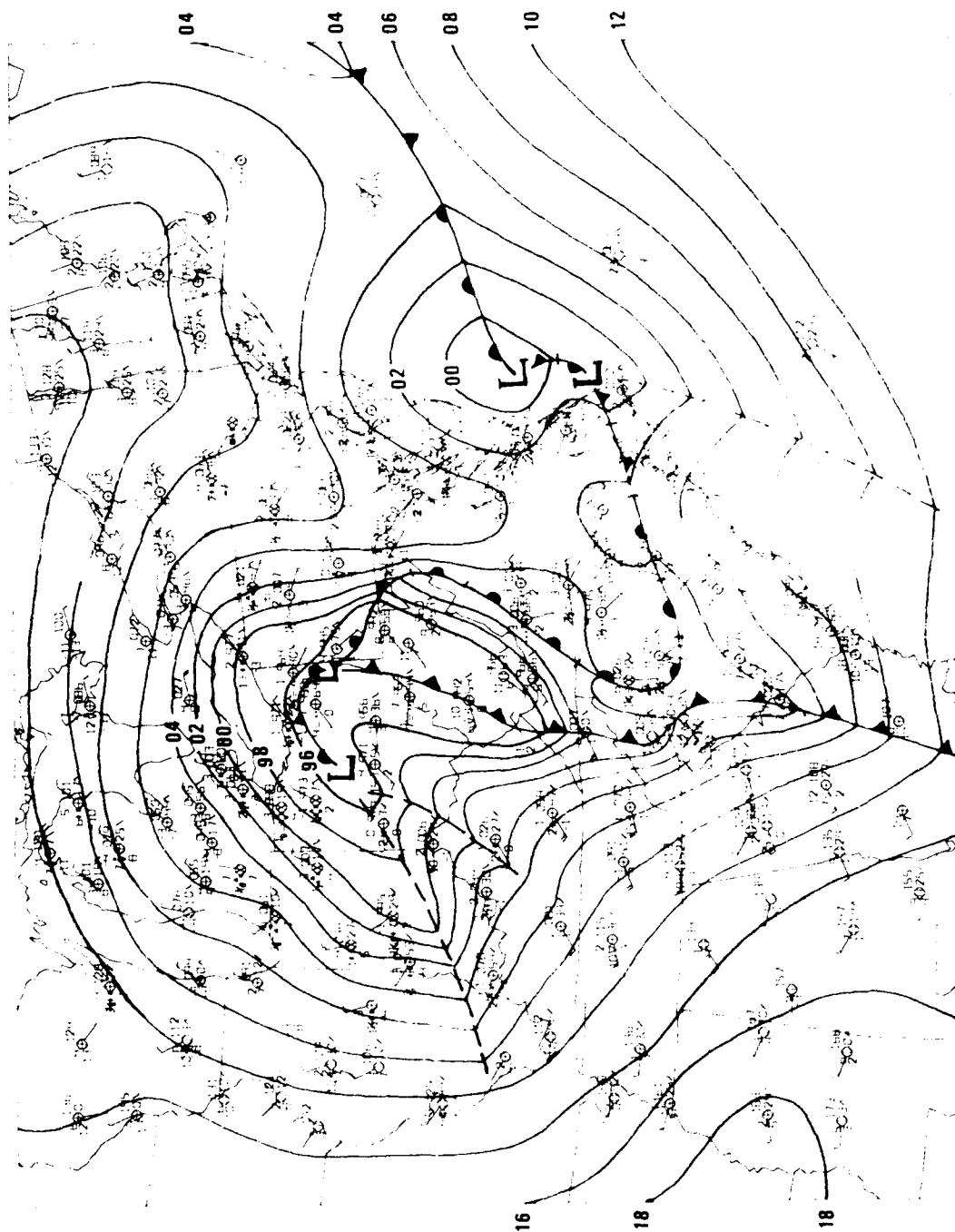


Figure 2.4. Surface weather map for 1800 UTC on 19 January 1987. Temperatures and dew points are in Celsius, plotted conventionally in the station model. Isobars are drawn at 4mb intervals. Each full wind barb represents 5 m/s.

over the area east of the Appalachians, and has impeded the northward progress of the warm front, which has barely crossed the mountains into western Virginia on the western fringe of the damming region and has stalled over North Carolina near the axis of the high-pressure ridge. A coastal cyclone has formed offshore of Virginia, and the northerly flow to its rear is enhancing the confluence and frontogenesis along the damming-stalled "warm" front over North Carolina.

Despite the proximity to the surface pressure ridge, moderate snow is occurring in a NW-SE band from Bradford, PA to Williamsport, PA and toward Harrisburg, PA, where the precipitation has turned to moderate rain. This is the first of the two meso-scale snow bands that passed over the Pennsylvania wind profiler network, and is occurring just east of the warm conveyor belt cloud edge shown in Fig. 2.3c. This band yielded the first snow event over the State College area and over the McAlevy's Fort ("Shantytown") wind profiler from about 1630 to 1900 UTC, during which time snow fell at a rate in excess of 5 cm/h.

The second period of enhanced snowfall occurred for about an hour at State College, centered at about 2200 UTC, and accompanied the developing patch of clouds that was over southwestern PA at 2100 (Fig. 2.3d). Incidentally, there is a larger, meso-alpha-scale region of moderate-heavy snowfall extending across southwestern Ontario, southeastern Michigan, and northwestern Ohio that does show up on the surface chart of Fig. 2.4. Movement of the weather system was from slightly south of west, so that this portion of the storm did not traverse the Penn State



wind profilers. This latter snow area was in a region of low-level convergence in the northwestern sector of the cyclone, where the synoptic-scale conditions are generally favorable for heaviest snows, and is in a geographic location where the effects of Lakes Huron and Erie may have made some contribution toward the enhanced precipitation.

Figure 2.5 shows time-height sections of the observed wind velocities measured at the Crown, PA (Fig. 2.5a) and McAlevy's Fort ("Shantytown"), PA (Fig. 2.5b) sites. A very striking feature of each of these diagrams is the rapid progression from a wind speed maximum (about 1900 UTC at Crown and 2000 UTC at McAlevy's Fort) to a wind speed minimum (about 0030 UTC/20) which occurred in the region between the warm conveyor belt cloud edge and the mid- and upper-tropospheric vortex center.

Figure 2.6a shows the wind velocity perturbations accompanying the comma cloud at the 4.6 km level (approximately the 600 mb pressure level), hand-computed by Forbes and Bankert (1987). A broad view shows that there is a cyclonic perturbation wind circulation of approximately 20 m/s tangential velocity and radius ~300-500 km accompanying the comma cloud. Even more obvious are some mesoscale details, notably five mesoscale jets. The easternmost of these, across east-central Pennsylvania, had been associated with the first short-duration (about 2-hour) moderate-heavy snow event that had moved across the wind profiler network a few hours earlier. Similar southerly and southeasterly perturbation "jets" detected by the profilers, typically coming from warmer and moister areas, have--in fact--been associated with

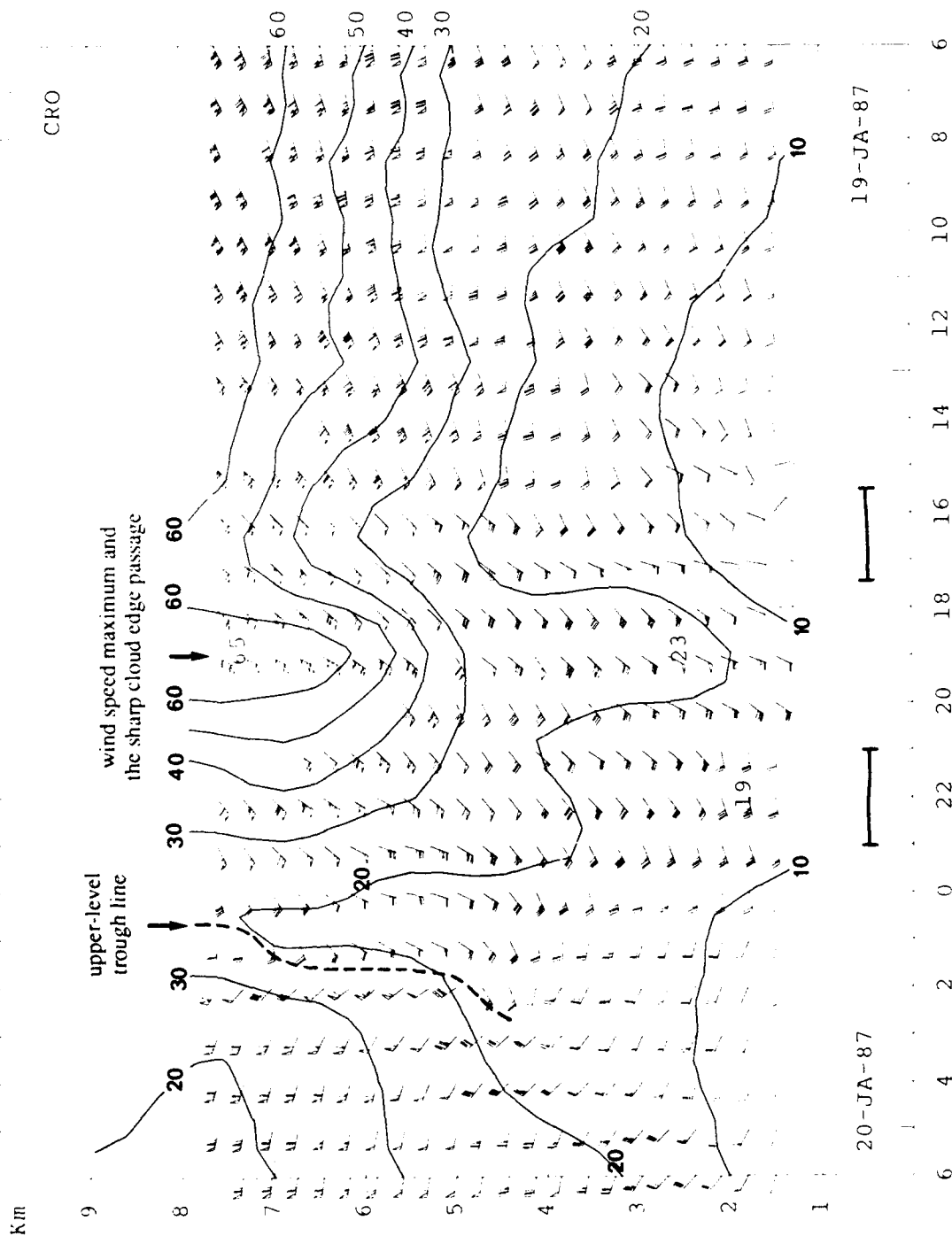


Figure 2.5a. Time-height sections of the profiler-measured winds during the period from 0600 UTC 19 January to 0600 UTC 20 January 1987 at the Crown profiler site. Note that the profiler winds are plotted at the time positions corresponding to the end of the hour-long measuring period. For example, the data for the hour ending at 0600 is plotted at the 0600 UTC position, rather than at 0530 UTC. Brackets indicate times of heaviest precipitation. Very light precipitation fell throughout most of the 24h period.

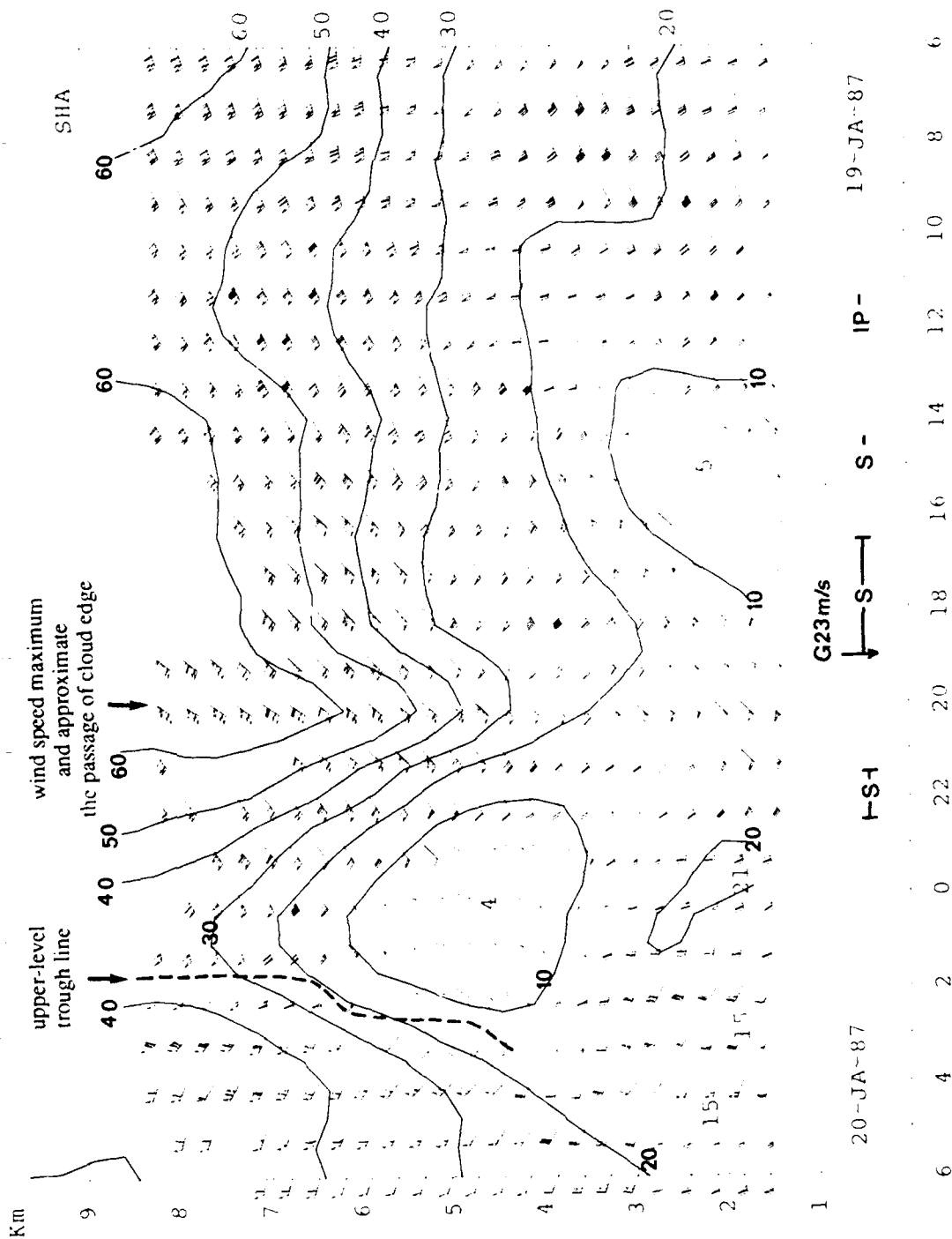


Figure 2.5b. Time-height sections of the profiler-measured winds during the period from 0600 UTC 19 January to 0600 UTC 20 January 1987 at the "Shantytown"/McAleveys Fort profiler site. Note that the profiler winds are plotted at the time positions corresponding to the end of the hour-long measuring period. For example, the data for the hour ending at 0600 is plotted at the 0600 UTC position, rather than at 0530 UTC. Brackets indicate times of heaviest precipitation. Very light precipitation fell throughout most of the 24h period.

precipitation events on most occasions, but having much weaker speeds. At the analysis time, the slot of dry air in Fig. 2.3 had begun to work its way into the central Pennsylvania, accompanied by ceasing precipitation and brightening skies. As the northwestern portion of the next wind maximum drifted across PA from its location in southeastern Ohio in Fig. 2.6a, however, the second brief heavy snow event occurred.

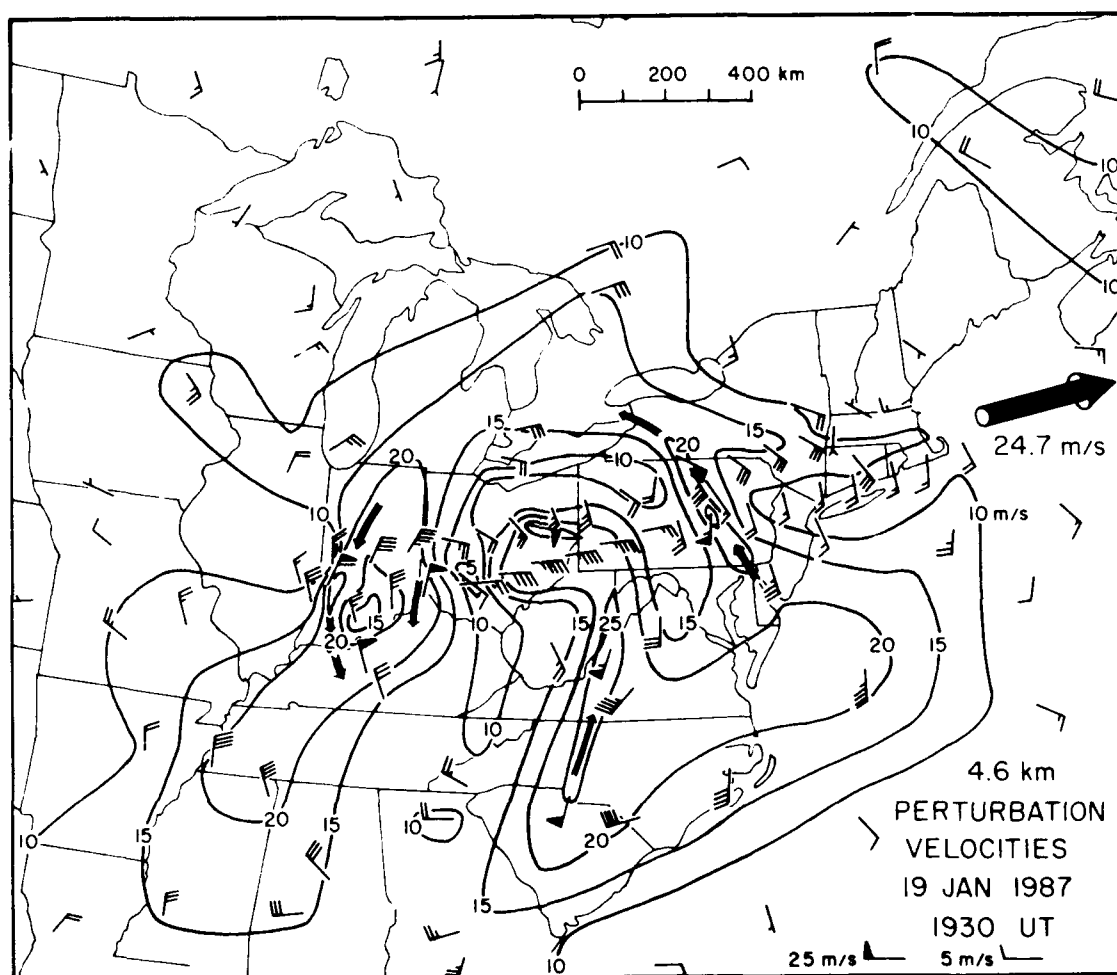


Figure 2.6a. Time-space converted mapping of the perturbation velocities at 4.6 km, positioned relative to the comma cloud at 1930 UTC. Five belts of wind maxima are evident: in east-central Pennsylvania; across central South and North Carolina, western Virginia, and into eastern West Virginia; in eastern Ohio; in southwestern Indiana; and near the Ohio-Indiana-Kentucky border. Each contains a perturbation wind speed of about 25 m/s or greater.

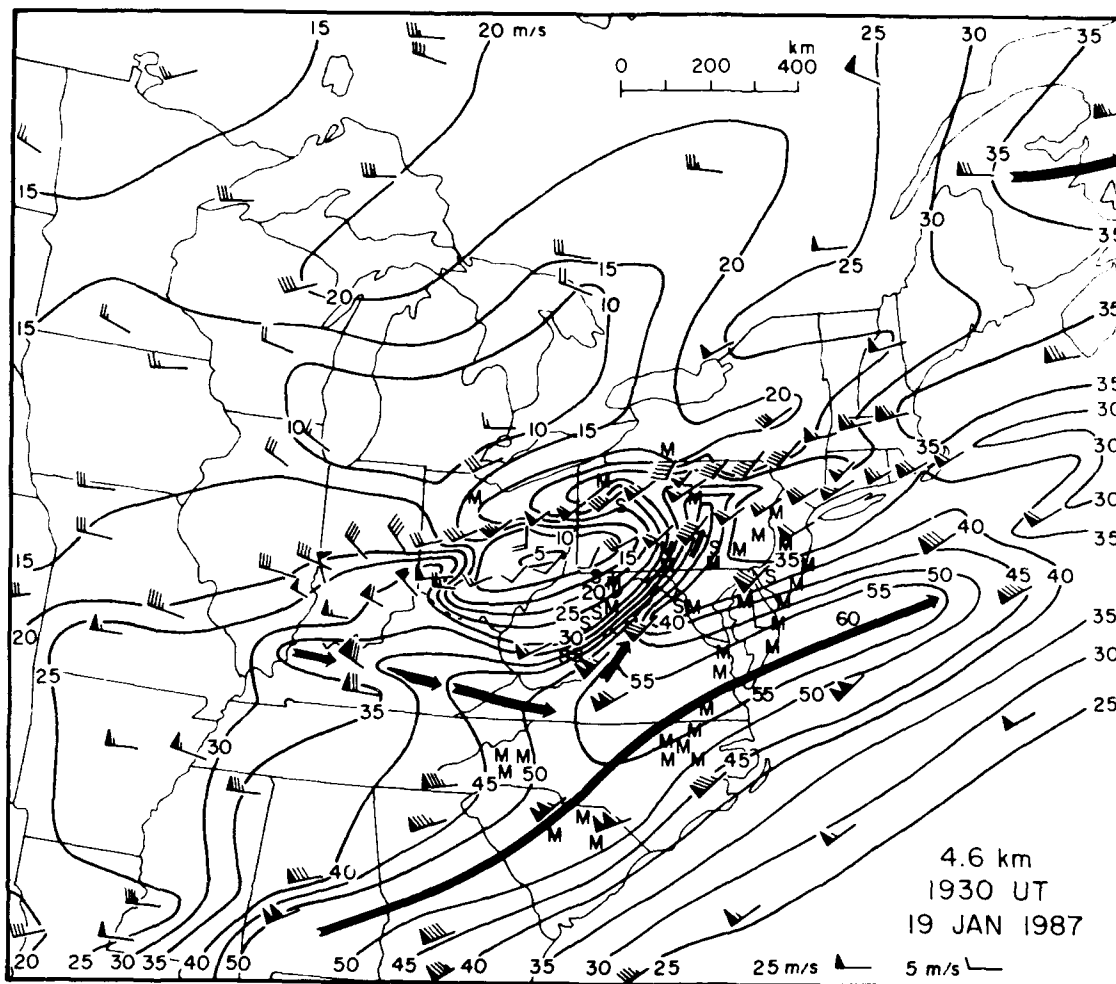


Figure 2.6b. Total time-space converted wind velocity field at 4.6 km pertaining to 1930 UTC on 19 January 1987.

The elongated perturbation wind maximum stretching from South Carolina (or northeastern Georgia) to the Virginia-West Virginia border relates almost perfectly to the sharp cloud edge of Fig. 2.3b. It will subsequently be seen that the relationship between this edge and the perturbation wind maximum was far better than that between the total mid- and upper-level wind speeds and the cloud edge on this occasion.

Also evident by comparing Figs. 2.6a and 2.3f is that the sharp cloud edge across northern Ohio is occurring very nearly

coincident with a belt of minimum perturbation velocities, appearing to separate strong easterlies and southeasterlies to its south from moderate easterlies to its north. The cloud edge appears to occur at a line of convergence of these perturbation velocities. Since the true cold conveyor belt lies to the north of the cloud edge, the easterlies and southeasterlies to its south are somewhat anomalous. They are probably affiliated with the development of a secondary pressure center over western West Virginia, and perhaps with a mesoscale area of enhanced mid-tropospheric positive vorticity advection, and with the development of the second mesoscale snow band.

Figure 2.6b shows the total time-space converted wind field at 4.6 km for 1930 UTC, calculated by hand by Forbes and Bankert (1987). The jet stream associated with the warm conveyor belt is readily apparent. Also apparent is a zone of northwesterly flow to the rear of the head of the comma cloud. This flow sets up a deformation (confluence) zone across northern Ohio and Lake Erie, with a southwesterly or southerly flow across eastern Ohio. A tongue of relatively strong southwesterlies extends westward beneath or just south of the cloud edge.

Because the weather system was moving into a region of strong prevailing southwesterly flow, with mean speeds ranging from 20 to in excess of 40 m/s, the total winds do not show a closed circular wind circulation at this time. Similarly, no pressure level above 850 mb at 0000 UTC on 20 January showed easterly winds, whereas all levels showed weak easterly wind components at 1200 UTC on 19 January.

Simple interpretation of the total observed winds--specifically, the disappearance of the easterlies--would erroneously suggest that the circulation with this system was weakening. In fact, it was slowly intensifying, and intensified even more when it reached the vicinity of the mean jet stream. Preparation of a perturbation chart such as Fig. 2.6a, or a chart of system relative winds such as those used by Carlson (1980), allows for the detection of perturbation (or relative) easterly winds, which indicate that the comma cloud will be maintained or intensify. Conversion of model-output and observed winds into cyclone-relative winds on a regular basis would allow forecasters to make more realistic assessments of the status of the evolution of the comma cloud system and its substructures.

Time-space-conversion analyses have been prepared objectively by Lee (1990) for a number of levels. Figure 2.7 shows the steering velocity field used in this case study. As discussed previously, to determine a steering field for disturbances embedded in a baroclinic weather system such as this one, the 36h temporal-mean winds are first averaged over a scale comparable to the wavelength of the synoptic-scale weather system (1000 km radius in this case). Then these winds, at various levels and for various layers, are examined objectively to find steering velocities which best match a set of velocities entered interactively that represent the movement of various storm features seen in satellite imagery. In this case, the 5 km level was objectively chosen as most representative, but nevertheless showed small speed and direction biases. A 4-degree azimuth adjustment was

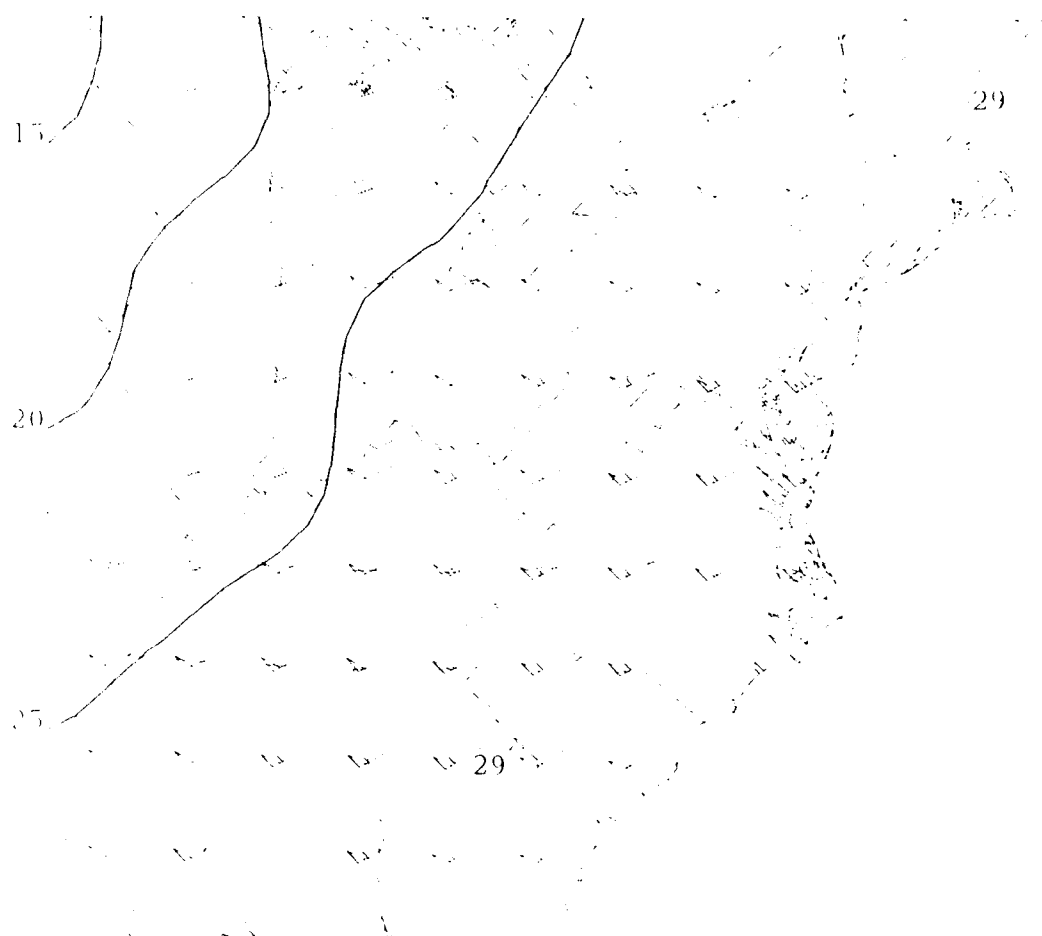


Figure 2.7. Steering winds used in the time-space conversion of the case of 19 January 1987, by Lee (1990). Isotachs are in m/s.

applied to correct for the direction mismatch, and a 5% speed adjustment was made to adjust for the speed mismatch. The perturbation quantities at all levels are displaced using this velocity field.

Figure 2.8 shows the analyses at the 3 km level. Fig. 2.8a displays the perturbation winds, while Fig. 2.8b displays the total time-space-converted wind field. The cold conveyor belt perturbation east-southeasterlies can be seen stretching from northeastern PA to southern MI. This corresponds quite well to the northwestern cloud shield of Fig. 2.3. Strong perturbation southerlies stretch from GA to southern PA, corresponding well to the



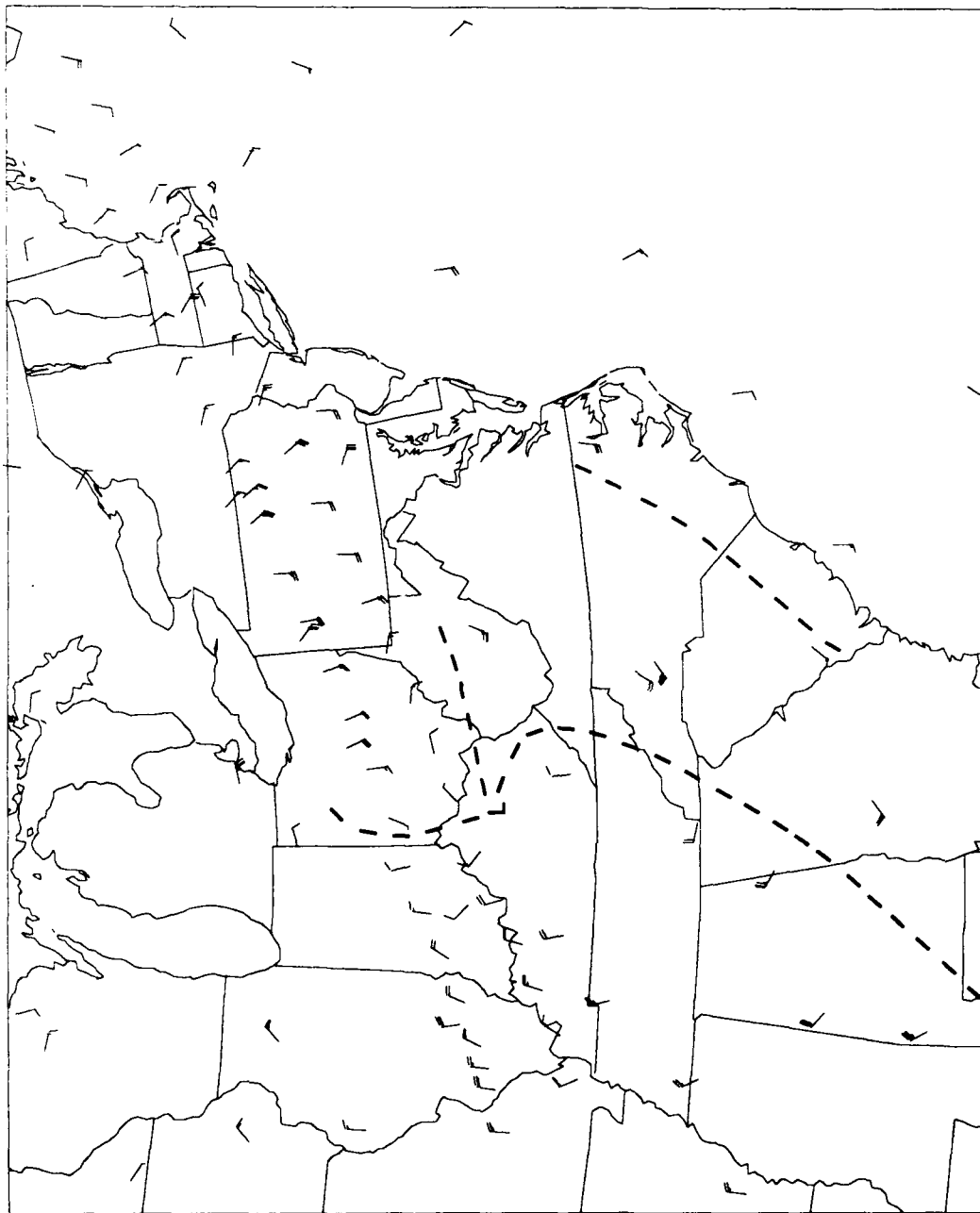


Figure 2.8a. Time-space converted perturbation velocities at the 3.0 km level at 1800 UTC on 19 January 1987.



Figure 2.8b. Time-space converted total wind velocities at the 3.0 km level at 1800 UTC on 19 January 1987. In this figure, rather than showing data points, winds have been interpolated to a 30x40 grid. Total velocity vectors are displayed for about every third grid point.

warm conveyor belt clouds of Fig. 2.3. A line of perturbation cyclonic wind shifts from eastern AL to WV marks the cold front position. A line of cyclonic wind shifts from extreme southwestern VA (near the KY border) to northwestern OH marks the trough line of the extended or multi-centered low-pressure system at this altitude. This position and orientation indicates a reasonable slope between the surface pressure trough of Fig. 2.4 and the 4.6 km circulation center of Fig. 2.8a, with a bit more extension of the trough to the northwest. The total 3.0 km winds of Fig. 2.8b are generally not as revealing, although they emphasize the strength of the winds (up to 45 m/s) in the warm conveyor belt from GA to the NC-VA border.

Figure 2.9 shows the objectively computed perturbation and total time-space-converted wind analyses at the 5.0 km level. These analyses are rather similar to those at 4.6 km, Fig. 2.6. The strength and orientation of the jet stream from AL to VA in Fig. 2.9b is impressive, as is the split branch of the jet that turns northward into southwestern PA. This feature is also a bit sharper than at 4.6 km.

Figure 2.10 shows the objectively computed perturbation and total time-space-converted wind analyses at the 7.0 km level. Fig. 2.10a suggests that the branch of the jet entering southwestern PA from VA has become more jet streak-like at this altitude. The hand-calculated total velocities at 9.1 km (Fig. 2.10c; from Forbes and Bankert, 1987) show a similar pattern.

Lee (1990) has also computed the system-relative winds for this and several other cases. The distinction between the sys-

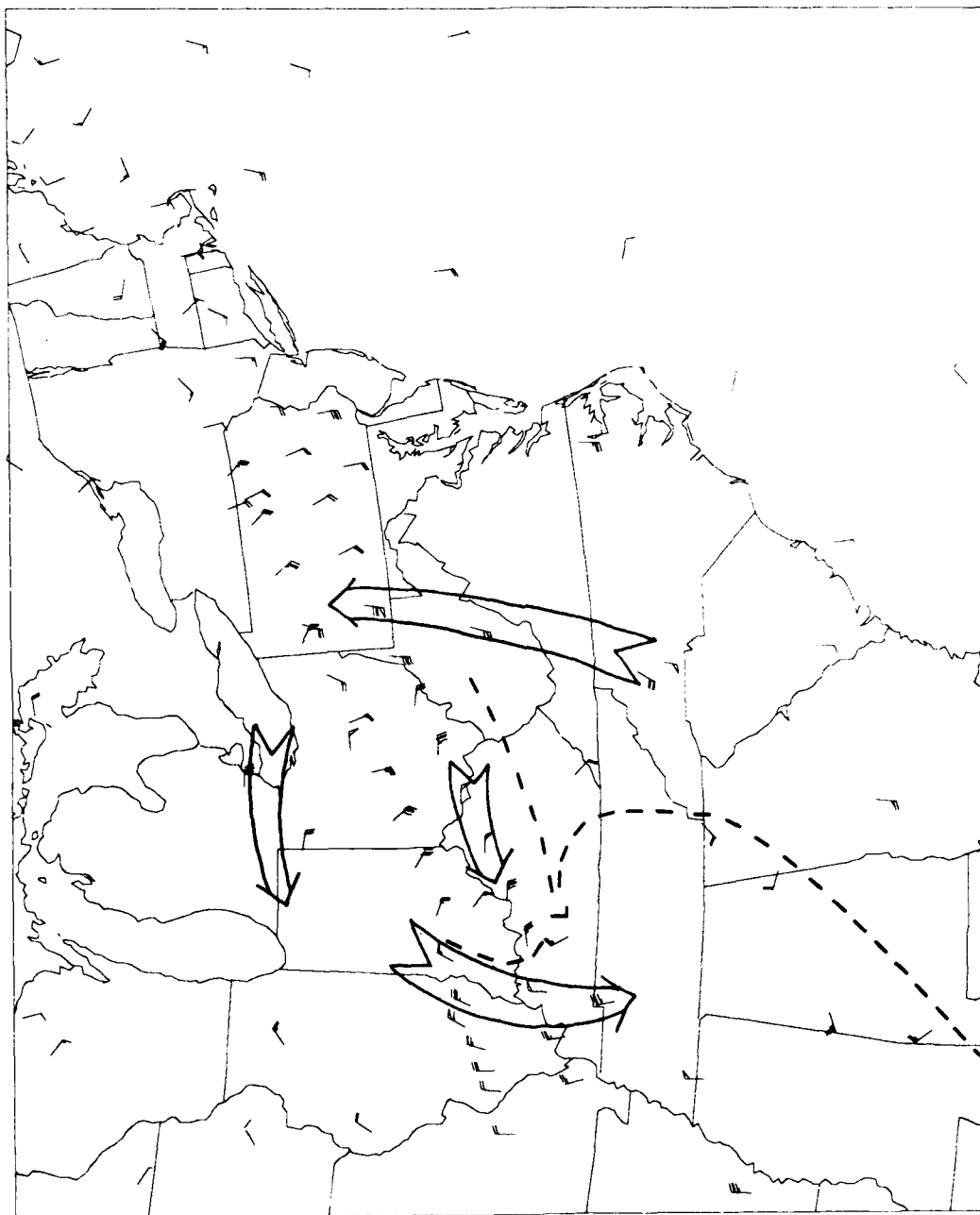


Figure 2.9a. Time-space converted perturbation velocities at the 5.0 km level at 1800 UTC on 19 January 1987.

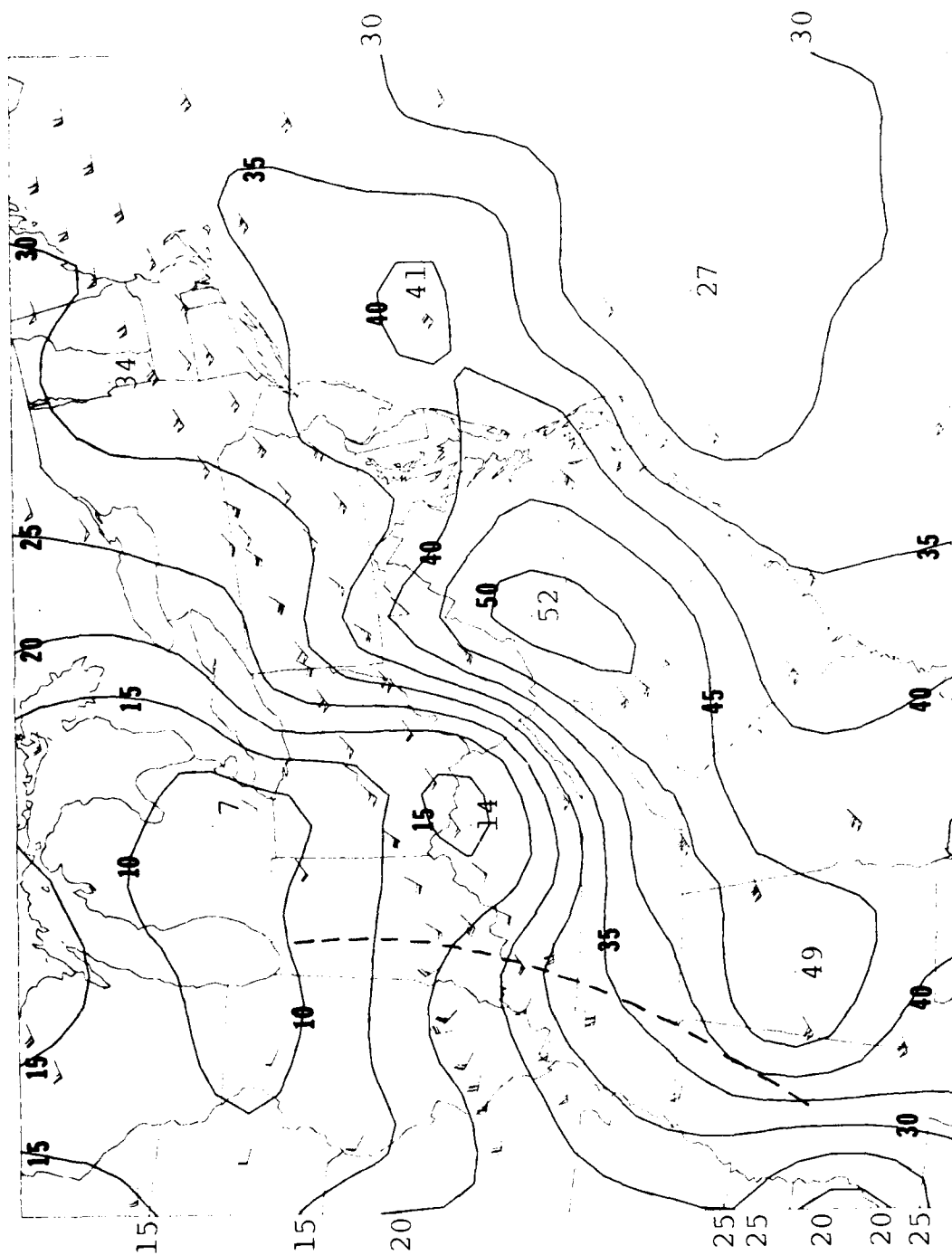


Figure 2.9b. Time-space converted total wind velocities at the 5.0 km level at 1800 UTC on 19 January 1987.

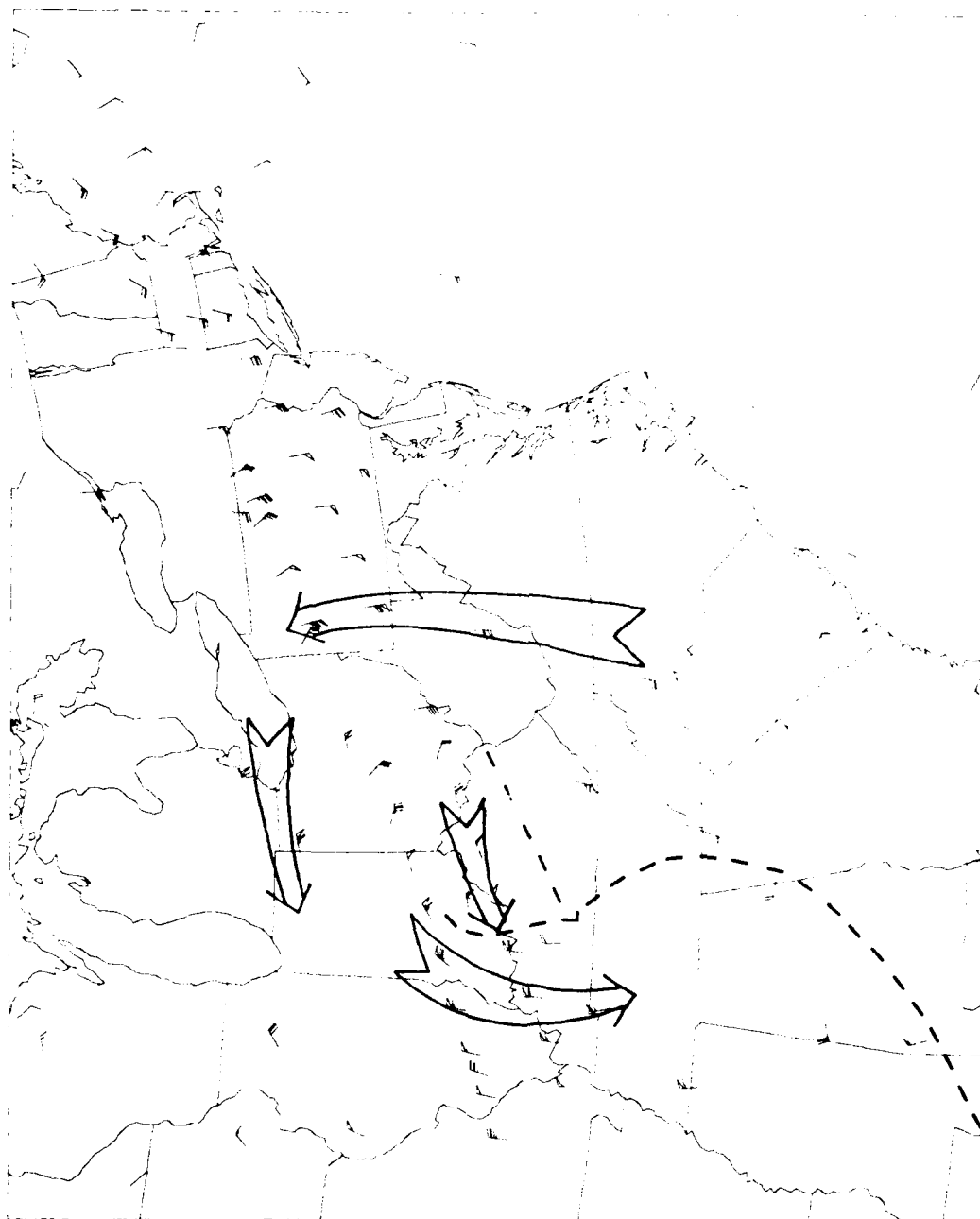


Figure 2.10a. Time-space converted perturbation velocities at the 7.0 km level at 1800 UTC on 19 January 1987.

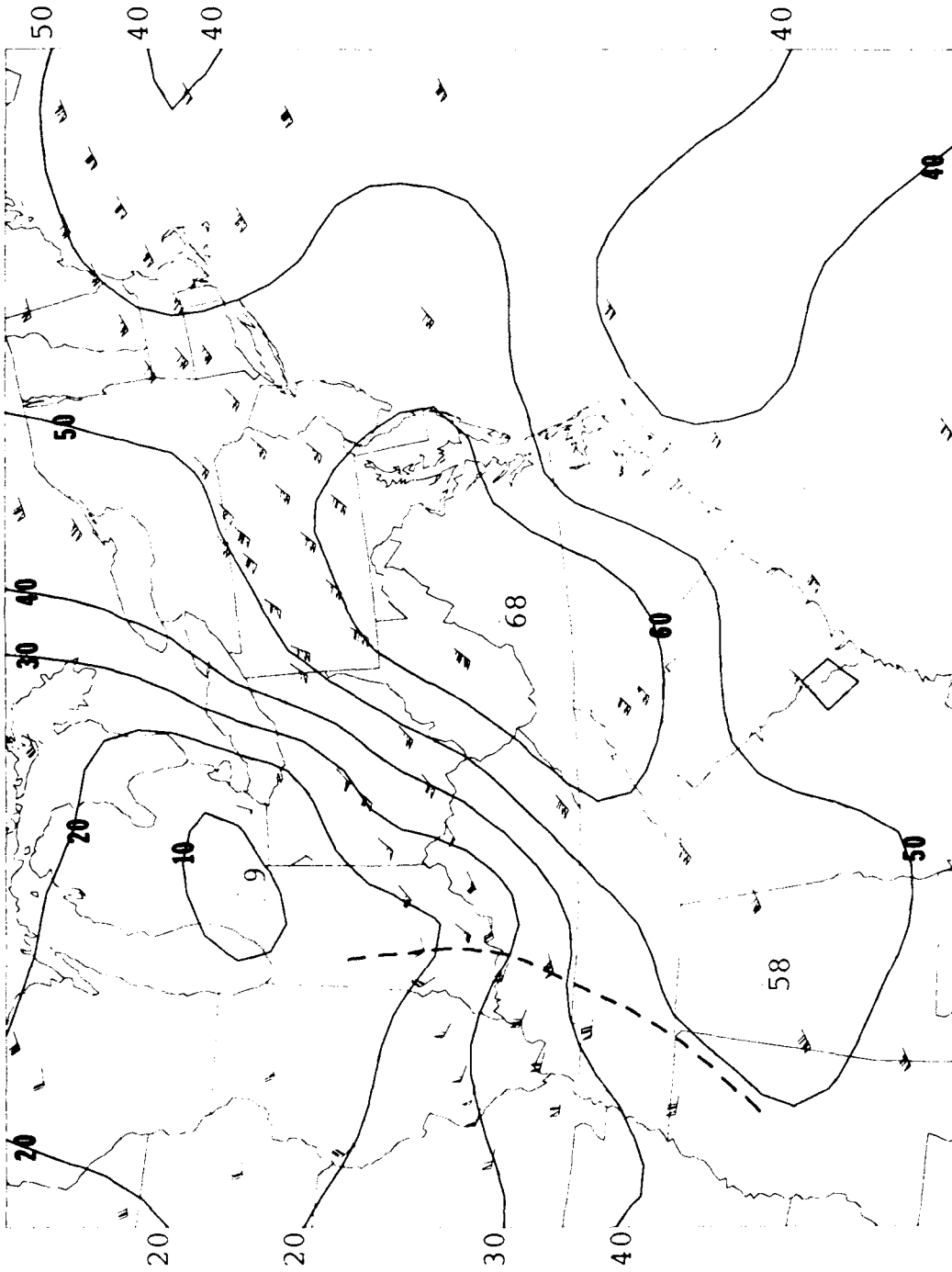


Figure 2.10b. Time-space converted total wind velocities at the 7.0 km level at 1800 UTC on 19 January 1987.

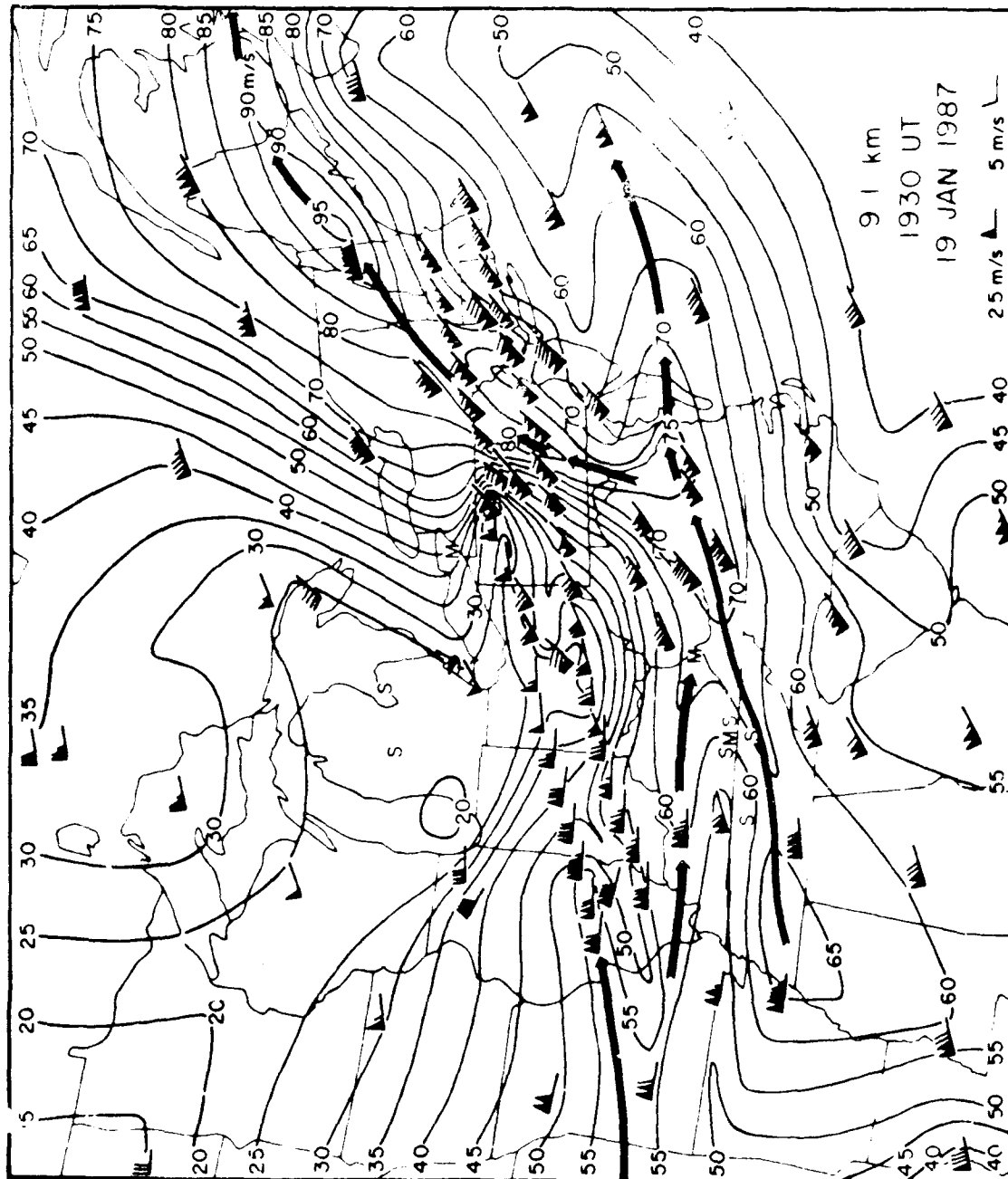


Figure 2.10c. Total time-space converted wind velocity field at 9.1 km pertaining to 1930 UTC on 19 January 1987. Hand-computed, from Forbes and Bankert (1987).



tem-relative winds and the perturbation winds is that a single velocity vector constant (the velocity of the center of the comma cloud system, from 250 degrees of azimuth at 24.7 m/s) has been subtracted from the observed winds to obtain the relative winds, whereas a mean wind field (e.g., Fig. 2.2 for the 4.6 km level) was subtracted from the observed winds to obtain the perturbation winds. The latter mean winds generally show a change of direction and speed from one geographic location to another. The velocity of the center of the comma cloud system was computed from a series of satellite images, by tracking the position of the apparent circulation center. In practice, the relative winds were obtained as a follow-on step, subsequent to the computation of the total time-space converted wind field. Thus, the time-space converted relative winds are consistent with the total and perturbation winds, and will be almost identical to the perturbation winds near the center of the cyclone at mid-tropospheric levels.

Figure 2.11 shows the time-height sections of the relative velocities at the Crown and McAlevys Fort, PA profiler sites. By intercomparison with Fig. 2.5, note that there are far more winds with easterly components once the west-southwesterly phase velocity has been subtracted. Note also that the mean vertical wind shear becomes more evident, in the form of a prevalent pattern of low-level east-southeasterlies and upper-level southwesterlies or northwesterlies.

Figure 2.12 shows the relative velocities and streamlines at the 3.0 km level. The cyclonic circulation affiliated with the synoptic-scale comma cloud of Fig. 2.3 is extremely well por-

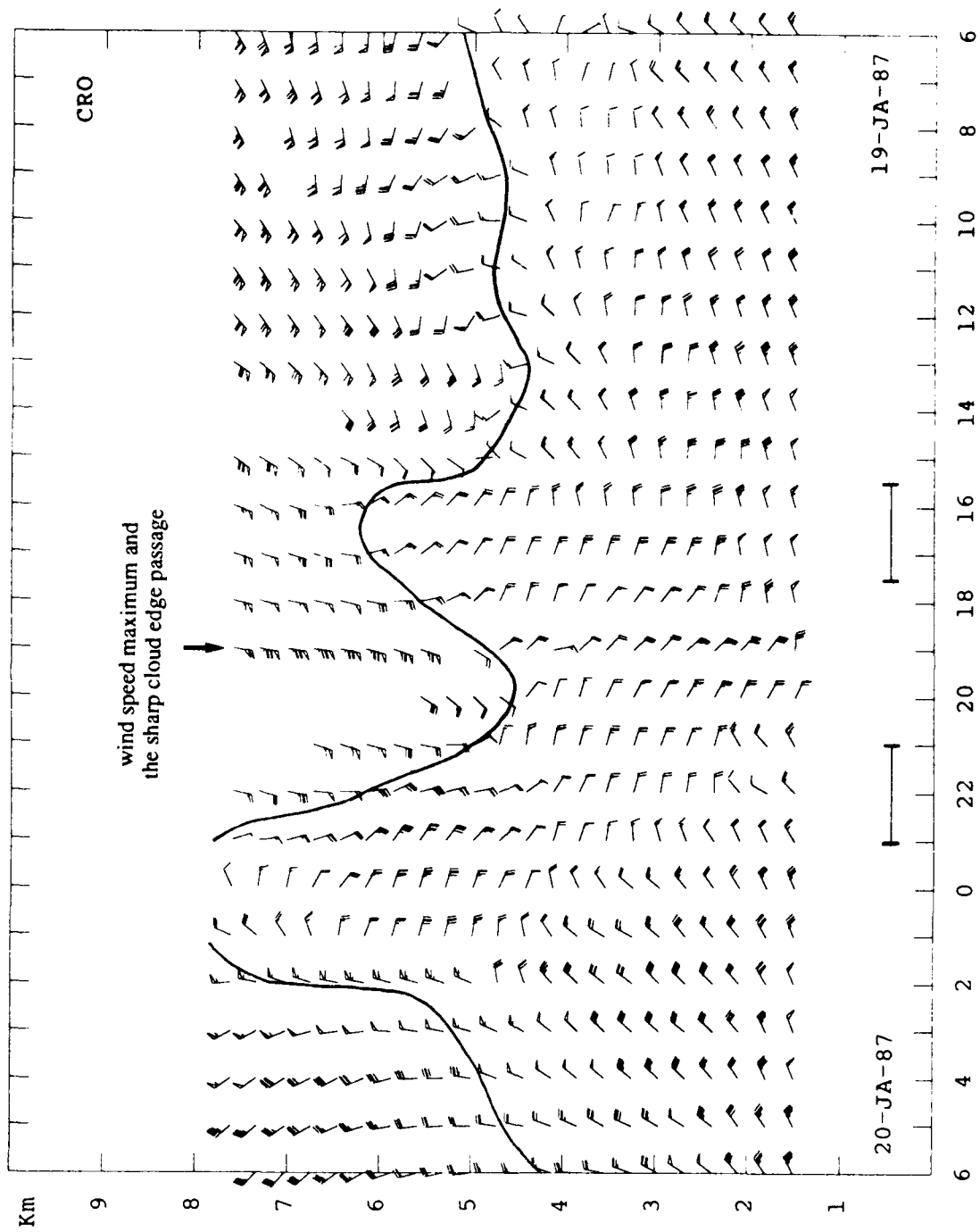


Figure 2.11a. Time-height sections of the relative winds at Crown, PA. Conventions as in Fig. 2.5a.

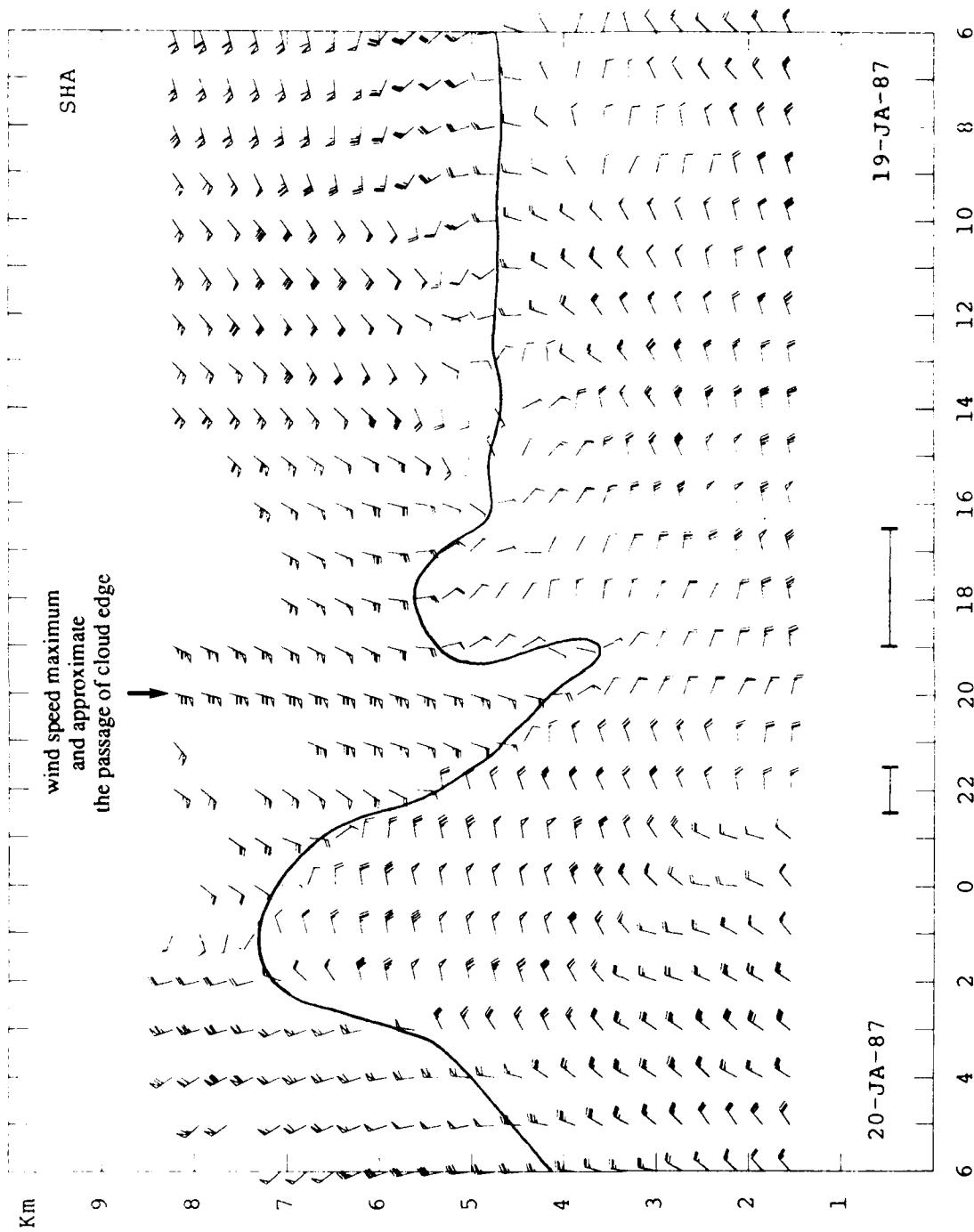


Figure 2.11b. Time-height sections of the relative winds at "Shantytown"/McAlevys Fort, PA. Conventions as in Fig. 2.5b.

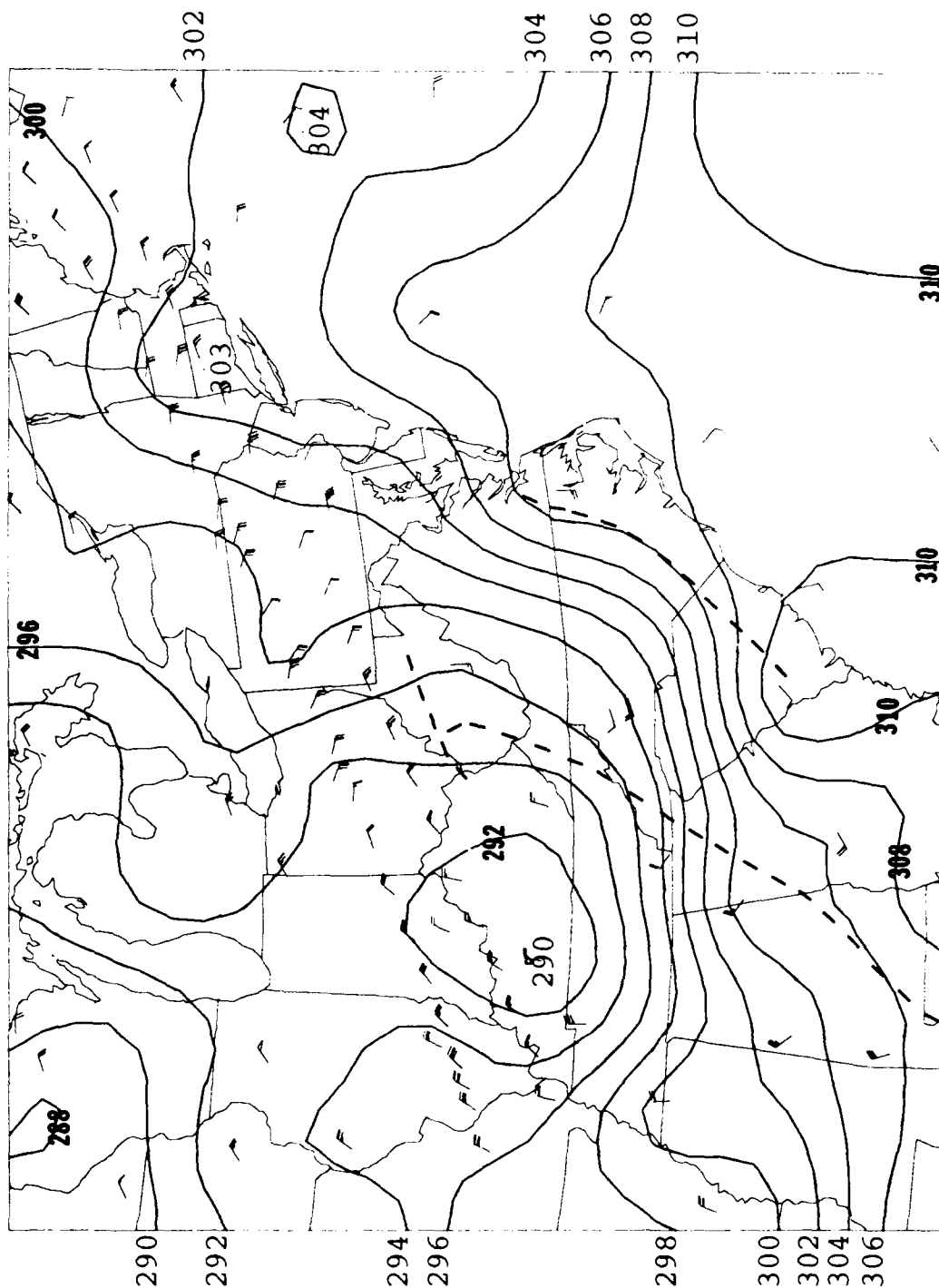


Figure 2.12a. Time-space converted relative winds at the 3.0 km level at 1800 UTC on 19 January 1987, and isopleths of the potential temperatures at that level.

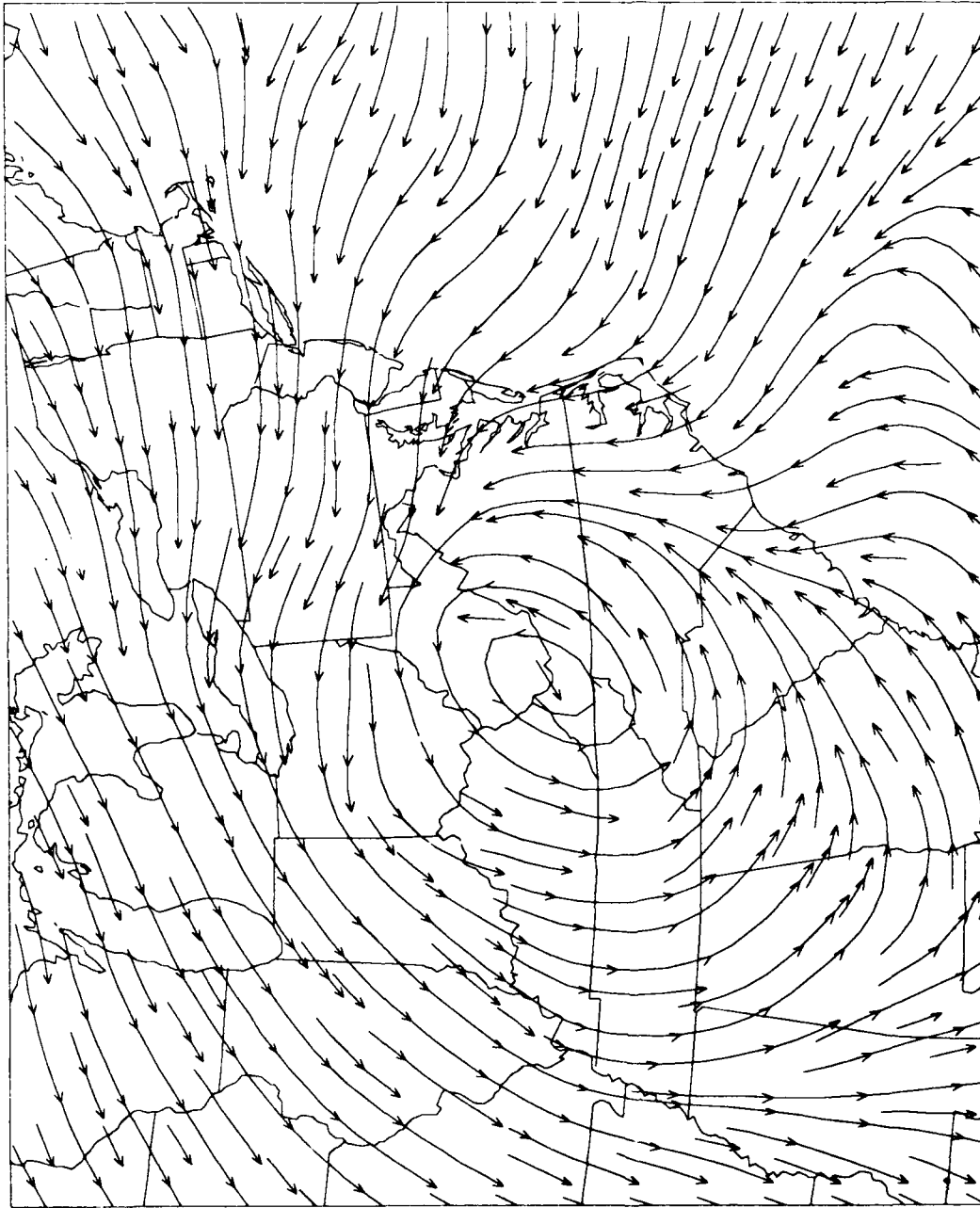


Figure 2.12b. Streamlines of the relative winds at the 3.0 km level at 1800 UTC on 19 January 1987.

trayed. The circulation has one single center near the intersection of the KY, VA, and WV borders, whereas the perturbation winds (Fig. 2.8a) suggested a more elongated trough axis oriented northwestward. The streamlines actually diverge slightly away from the center. These two observations are likely to be partly a consequence of comparably sparse data there, in contrast to where rawinsonde data has been augmented by wind profiler data, allowing too much latitude for the streamline program. In addition, at this altitude the weather system still has a distinct frontal zone to the southeast of the circulation center, so that most of the convergence is likely to be occurring there, over the Appalachian Mountains of North Carolina, Virginia, and West Virginia. It is likely that the front sharply separates two air-streams: warm relative-motion southwesterlies and cold relative-motion northerlies. However, the streamlines are unrealistically continuous across this region, which contributes to the lack of apparent convergence with the cyclone at this level.

Two confluence zones can be seen at 3.0 km near and east of the Appalachians. One connects to the circulation center and extends southward into northern Georgia and then into southeastern Alabama. The other is over central North Carolina and eastern South Carolina, where the warm conveyor belt is located. The confluence zone in the perturbation winds focused on the latter feature, which was not as important in terms of the affiliated clouds and precipitation.

While it is tempting to call the western confluence zone the cold front, it must be kept in mind that the trough line and cold

front can become separated farther aloft. The mid-tropospheric trough line sometimes coincides with the coldest temperatures rather than the leading edge of the zone of temperature gradient (which, by definition, is the location of the cold front).

Also shown on Fig. 2.12a are the time-space-converted potential temperatures at the 3.0 km level, based upon the rawinsonde data. In paragraphs below, the advection of potential temperature by the relative wind, as shown in Fig. 2.12a, will be used to compute a thermodynamic vertical velocity. Cold pockets are present west of the circulation center, which is displaced somewhat toward the cold side of a baroclinic zone oriented along the Appalachians.

The positioning of the strongest baroclinic zone over central North Carolina is interesting, since the main trough lies farther west, as discussed above. It is likely that the real front was sharper, and positioned a bit farther west, than shown by the potential temperature analysis. Virginia and central NC, for example, are devoid of time-space converted rawinsonde observations, so that the gradient is smeared over the entire east-west lengths of these States. However, as was also discussed above, it is not at all inconsistent for the southwesterly relative winds over western North Carolina to lie rearward of the largest temperature gradient. The true cold front at this level could be found very near, but just east, of these wind sites.

A final step has been added to the time-space conversion procedure for potential temperatures by Lee (1990) that has helped reduce the "gradient-smearing" problem, in the following

manner. When a rawinsonde site shows minimal temperature change between the two soundings used in the time-space conversion (one prior to and one after the analysis time), then all time-space converted locations in between will be assigned the same potential temperature, thereby filling gaps in the data which allow for the fictitious spreading of gradients into data-void regions.

The presence of the eastern confluence zone apparently ahead of the cold front may signify the transition of this cyclone to a katafront type, in which the air sinks down the cold frontal surface aloft, and the cold front passage is "dry". The surface analysis (Fig. 2.4) also shows a tendency for this, as there is a trough and confluence line across southeastern Georgia and central South Carolina, and a gradual temperature decrease to its west. Some of the low-level cold air may have been retained west of the Appalachians, while streaming eastward aloft. The cold front may be re-forming at the surface in the lee of the Appalachians as the cold air aloft is mixed down to the surface. This type of occurrence is well known in the lee of the Alps, and has been cited by Petterssen (1941) as occurring over the Carolinas. One of the authors (Forbes) noticed during the GALE field project that cold air was slow to move into South Carolina at the surface, and that this region was a frequent site for secondary trough formation (with fronts lagging behind there, presumably in response to the orographically retarded low-level cold advection).

Another confluence zone at 3.0 km is also clearly evident in Fig. 2.12b, with airstreams contracting near Lake Erie from a



broader source region along the East Coast from near the Chesapeake Bay to Long Island. This corresponds to the cold conveyor belt, and is somewhat more clearly portrayed than in the perturbation winds (Fig. 2.8a).

The relative velocities and streamlines at the 5.0 km level are shown in Figure 2.13. The cold pocket in the potential temperature pattern in eastern KY, combined with the sharp trough in the streamline pattern, gives a very strong signal that a short-wave trough is present there. There is strong evidence of this meso-alpha-scale feature in the satellite imagery (Fig. 2.3), and it was this feature which subsequently triggered the second period of enhanced snowfall in PA.

Figure 2.14 shows the relative velocities and streamlines at 7.0 km. At this level there is no sign of the short wave trough over eastern KY, indicating that the feature was not only meso-scale in horizontal extent, but also limited in vertical depth.

For these meso-alpha-scale features, the errors of profiler-measured vertical velocity were likely to be non-trivial percentages of the true values and contaminated by the presence of smaller-scale features and turbulence, and were not used. (However, Dye [1990], undertook the painstaking quality control procedures [see Appendix 4] needed to use profiler-measured vertical velocities in the work described in section 3.) Meso-alpha-scale vertical velocities were computed through use of the thermodynamic (adiabatic) omega equation. In this method, the motion is assumed to be adiabatic, such that the observed temperature change is due to horizontal temperature advection, to adiabatic warming

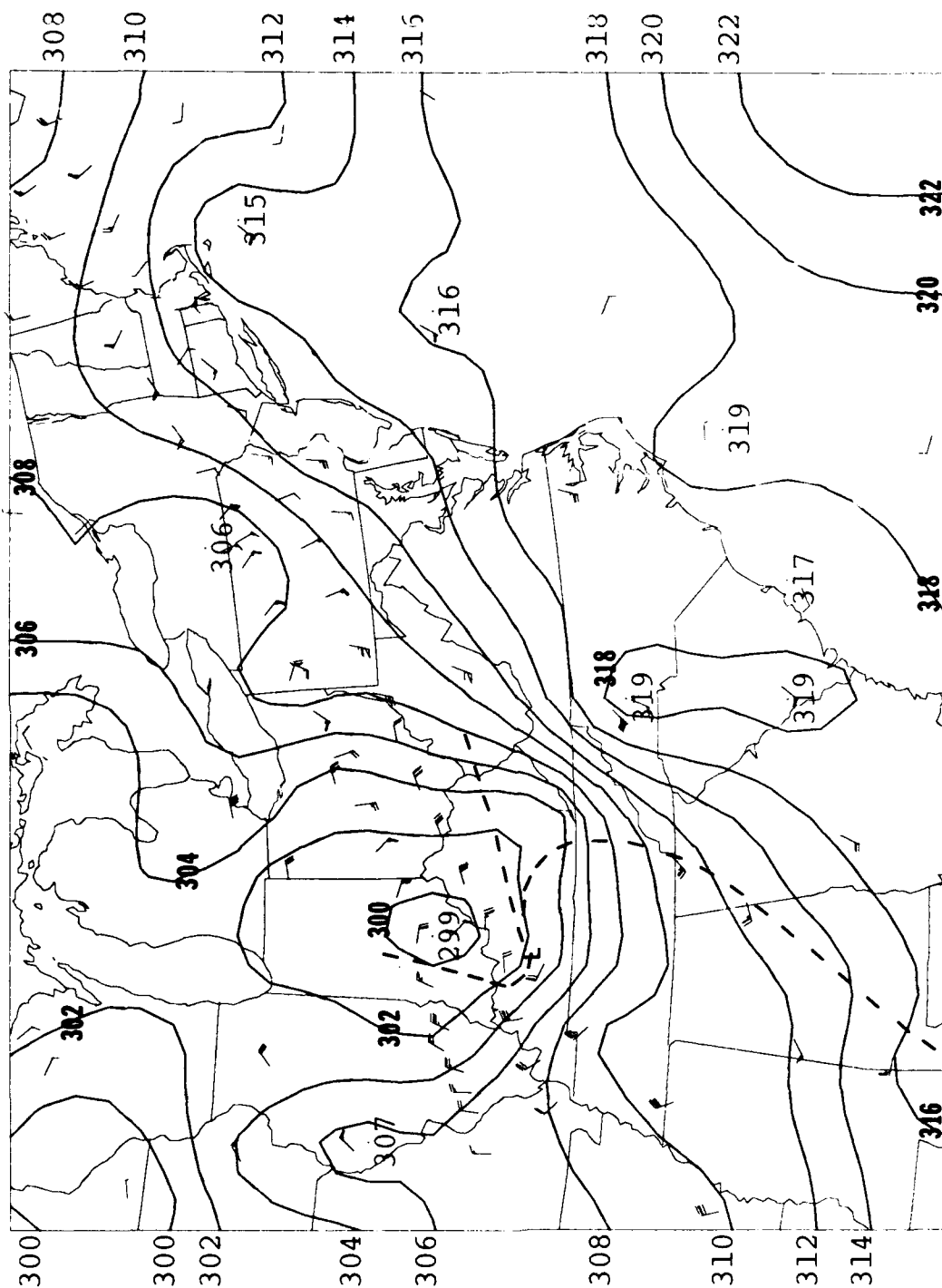


Figure 2.13a. Time-space converted relative winds at the 5.0 km level at 1800 UTC on 19 January 1987, and isopleths of the potential temperatures at that level.

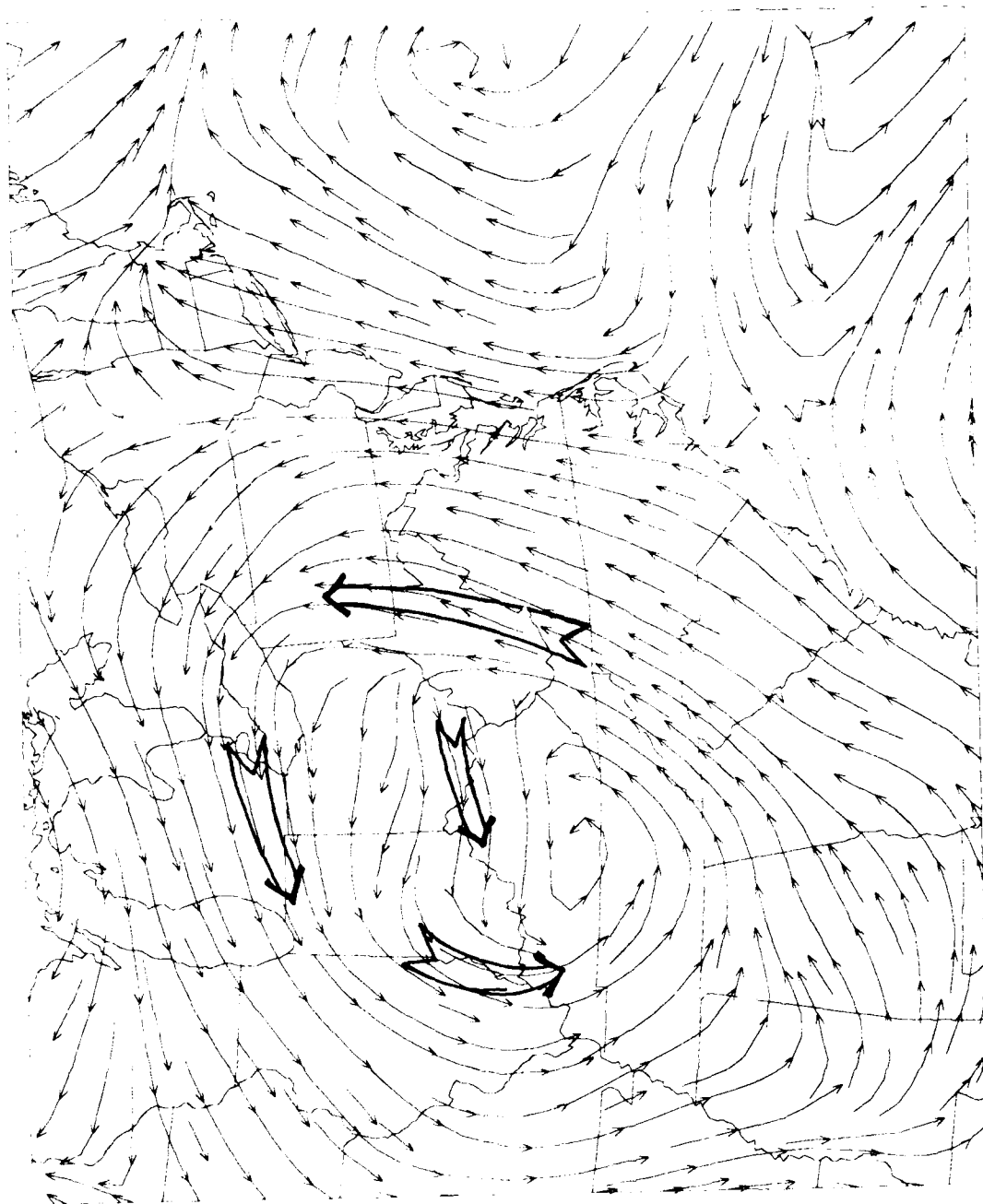


Figure 2.13b. Streamlines of the relative winds at the 5.0 km level at 1800 UTC on 19 January 1987.

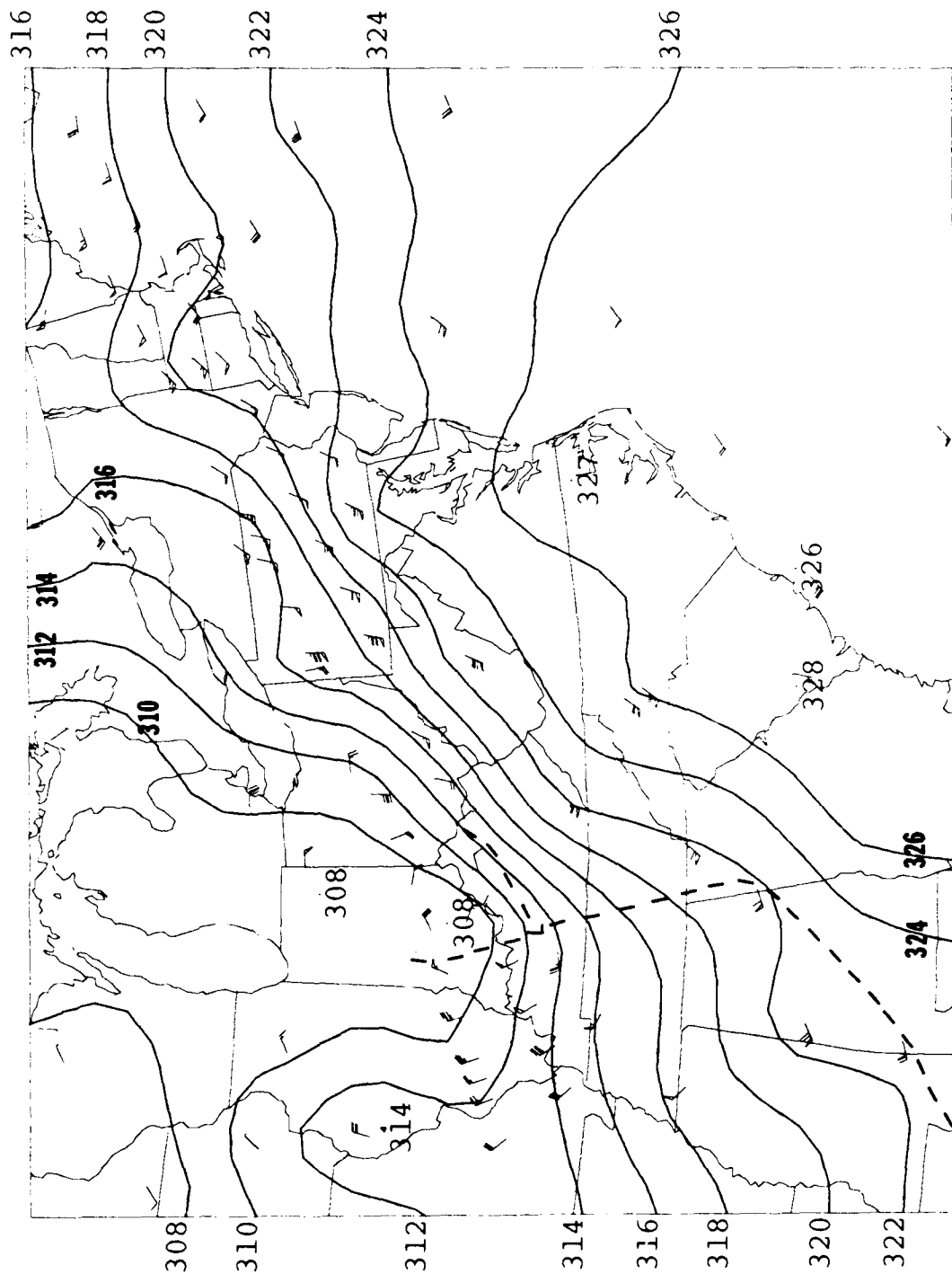


Figure 2.14a Time-space converted relative winds at the 7.0 km level at 1800 UTC on 19 January 1987, and isopleths of the potential temperatures at that level.

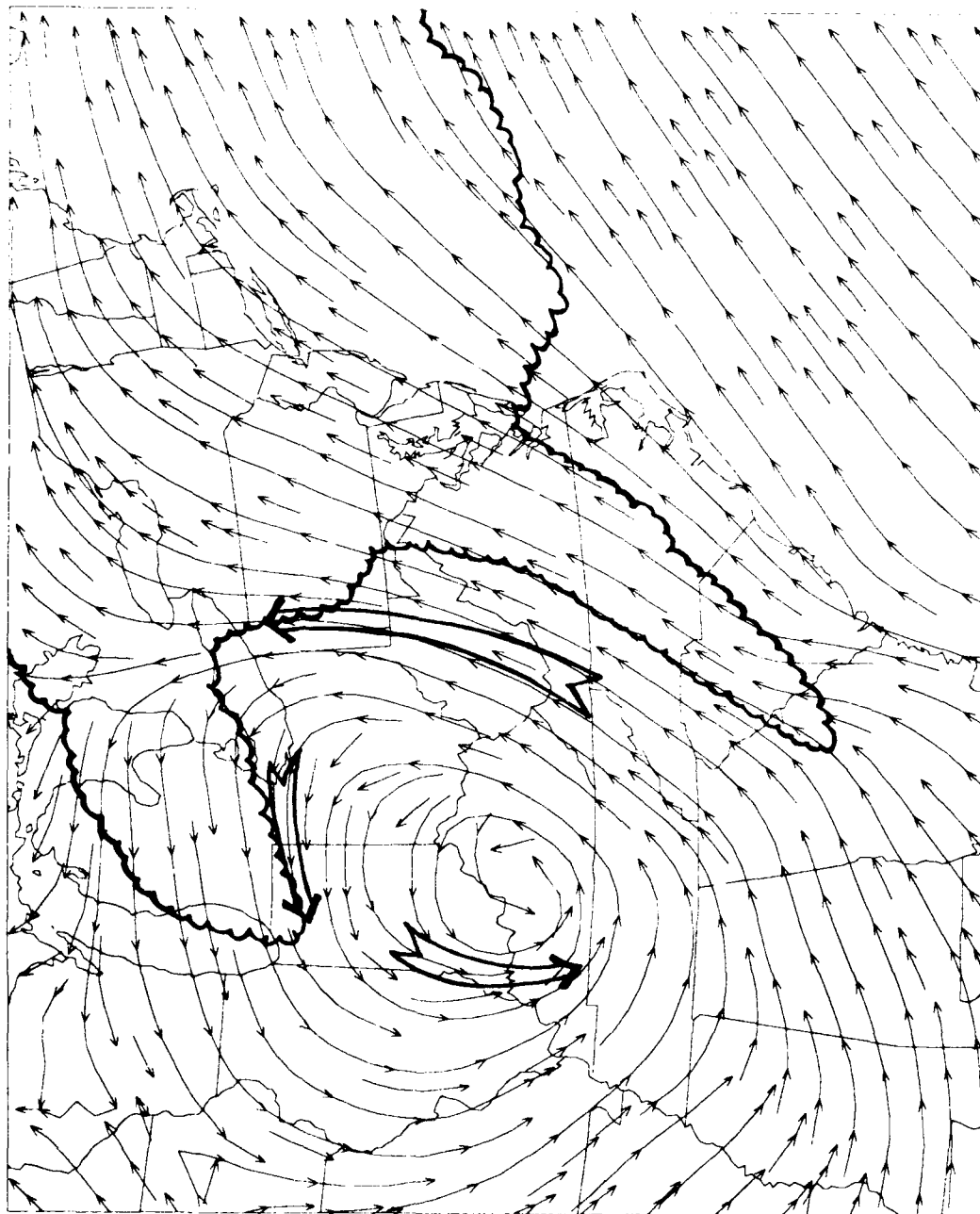


Figure 2.14b. Streamlines of the relative winds at the 7.0 km level at 1800 UTC on 19 January 1987.

or cooling during descent or ascent, and to the translation of a steady state weather system over the observing location. With these assumptions, the vertical velocity becomes

$$w = -(\vec{V}_h - \vec{C}) \cdot \nabla \theta \left( \frac{\partial \theta}{\partial z} \right)^{-1} \quad (2.4)$$

Thus, the vertical velocity computed by this method depends only upon the airflow relative to the moving pattern of adiabats and upon the ambient static stability  $\partial \theta / \partial z$ .

Kinematic vertical velocities were not calculated as part of the research by Lee (1990) because, for the cases studied, many of the rawinsonde winds were not reported above 400 mb (data lost at low elevation angles because balloons were carried by the jet stream), so that upper-level divergences could not be computed. The profilers were typically able to measure the winds up to the tropopause level until the axis of the jet stream passed the profiler sites. Thereafter, the winds became noisy in the upper-troposphere once the dry air west of the jet stream axis began to advect over central Pennsylvania.

Figure 2.15 shows the thermodynamic vertical velocities at the 3.0 km level, based upon Fig. 2.12. Bands of weak ascent can be seen beneath the warm conveyor belt and under its intersection with the cold conveyor belt. Strong descent is diagnosed over southern TN, within the dry slot of the synoptic-scale comma cloud.

Figure 2.16 shows the thermodynamic vertical velocities at the 5.0 km level, based upon Fig. 2.13. Strong ascent can be seen over NC, VA, and PA in affiliation with the warm conveyor



Figure 2.15. Thermodynamic vertical velocity (cm/s) at the 3.0 km level at 1800 UTC on 19 January 1987, derived from the relative winds and potential temperatures of Fig. 2.12a.

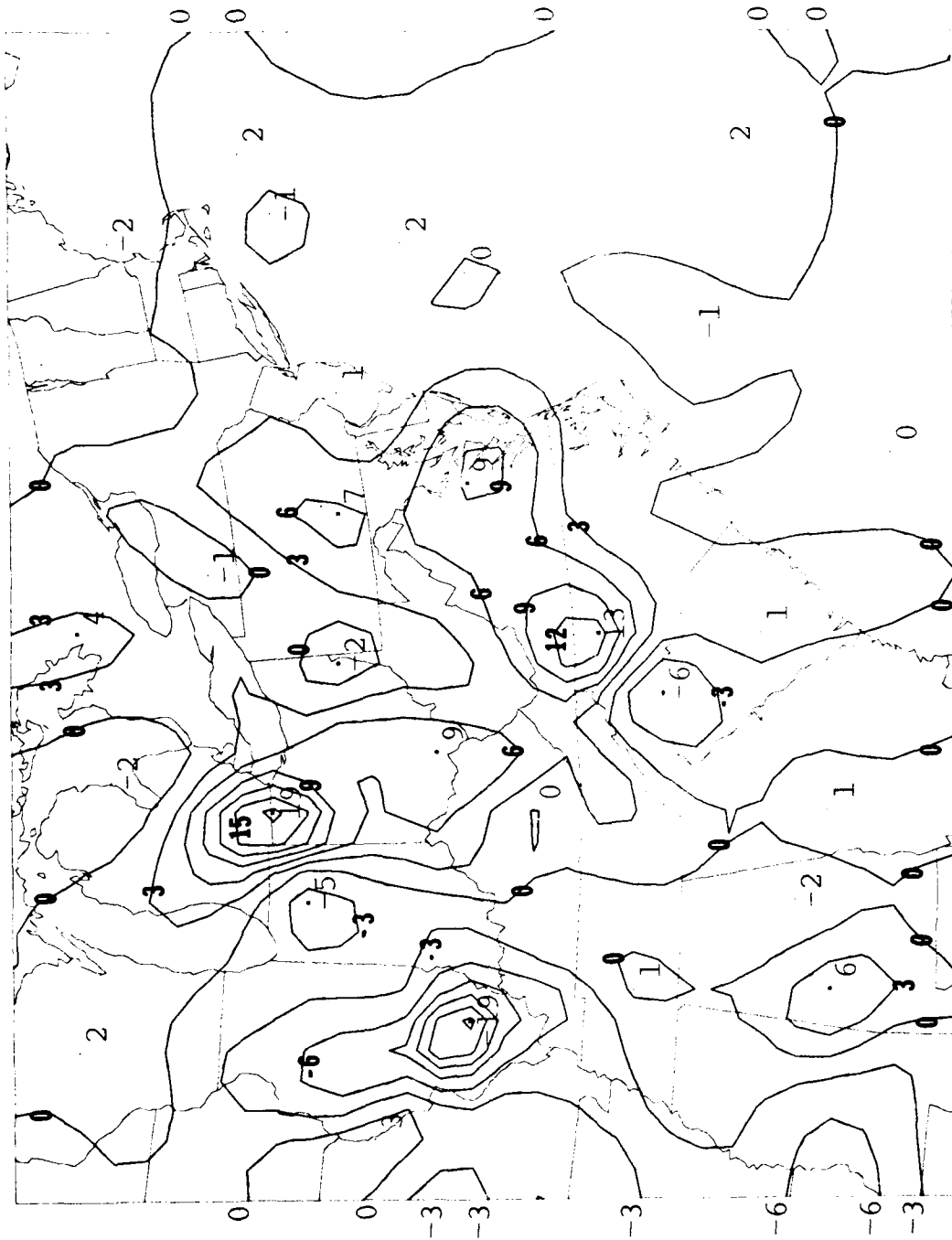


Figure 2.16. Thermodynamic vertical velocity (cm/s) at the 5.0 km level at 1800 UTC on 19 January 1987, derived from the relative winds and potential temperatures of Fig. 2.13a.



belt. Pockets of ascent over OH and eastern TN appear to be affiliated with the short-wave trough discussed in the context of Fig. 2.13. However, the number of quasi-circular maxima and minima in this analysis suggest that there is some noise in the wind and temperature fields, which may be partially eliminated by the planned changes in the potential temperature analysis scheme discussed above.

Figure 2.17 shows the thermodynamic vertical velocities at the 7.0 km level, based upon Fig. 2.14. The "bullseye" over southwestern PA appears to be another manifestation of noisy wind and potential temperature analyses, but the overall patterns of ascent and descent seem reasonable.

Lee (1990) has expanded the time-space conversion studies to include several additional cases. Meteorological features examined include other short-wave troughs, upper-level jet streaks, and their accompanying lower-level wind perturbations and jet streaks.

The results presented above certainly lend optimism to the prospects of producing enhanced synoptic or meso-alpha-scale diagnostic analyses using time-space converted rawinsonde and wind profiler data. When the analyses are performed by time-space converting the perturbations that are superimposed on a larger-scale, quasi-stationary pattern, the ensuing analyses performed to date do not show large sensitivities to the steady-state assumption invoked in this method. The total wind fields obtained in this manner are generally not as diagnostically useful as are the perturbation winds and the relative winds, each of which can

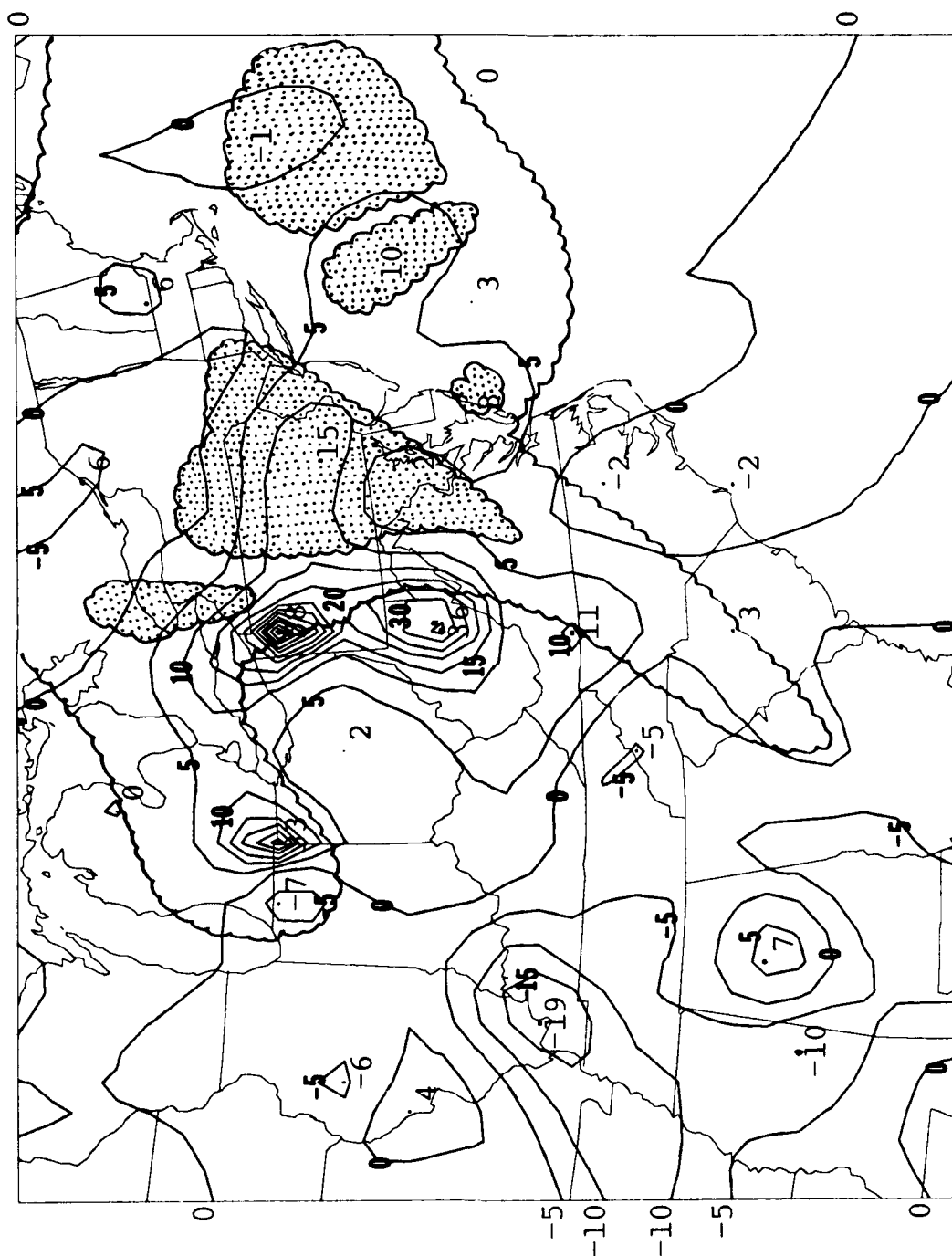


Figure 2.17. Thermodynamic vertical velocity (cm/s) at the 7.0 km level at 1800 UTC on 19 January 1987, derived from the relative winds and potential temperatures of Fig. 2.14a.

give different perspectives on the character of the weather system under examination. The thermodynamic vertical velocities computed in a similar manner seem diagnostically useful, though this field is rather sensitive to the presence of noise in the wind and temperature fields.

The most difficult aspect of the application of the time-space conversion procedure proved to be the determination of the appropriate layer to be used in the first-guess computation of steering velocity. For meteorological features on meso-alpha scales and linked to the baroclinicity of a travelling cyclone system (i.e., a deep-tropospheric trough system), the mid-tropospheric-layer spatially averaged wind described above worked well. For shallower features, such as those affiliated with an upper-level jet streak, the mid-tropospheric steering velocity did not work as well, and a steering layer at a higher level was used.

Actually, the use of time-height sections of profiler perturbation winds (departures from temporal means, layer by layer) can help make the selection of the appropriate steering layer less subjective. Because the organized pattern of significant wind perturbations is often confined to a particular layer, that layer tends to be the best one to use to compute the steering velocity of the perturbation pattern.

### 3. STUDIES OF MESO-BETA-SCALE PRECIPITATION BANDS

Dye (1990) used time-space conversion techniques to examine the structure of meso-beta-scale precipitation bands. Since these were of considerably smaller scale than the features studied by Lee (1990), it was necessary to use profiler winds averaged for periods considerably shorter than an hour; say, 5 minutes or less. Also, since vertical velocities were expected to be larger in the precipitation bands than in the meso-alpha-scale features, profiler-measured vertical velocities were used directly, rather than deduced from the thermodynamic omega equation. Quality control measures used in obtaining vertical velocities are presented in Appendix 4.

Since the precipitation bands could not always be seen in satellite imagery, Dye collected radar imagery from the Penn State WSR-74C radar and from NWS radars during the passage of a number of precipitation bands across Central Pennsylvania. In addition, he obtained precipitation data from a raingauge placed at the McAlevy's Fort profiler site, from conventional hourly surface stations and from a network operated by PEMA. This enabled the definition of the time and space locations of the precipitation bands.

Profiler-measured horizontal wind velocities were broken into components along and perpendicular to the precipitation band, and combined with profiler-measured vertical velocities to obtain airflow trajectories. Typical values of precipitation terminal velocities were then used to determine precipitation trajectories affiliated with the precipitation bands.

Like Lee (1990), Dye found that the computation of relative winds was rather sensitive to the layer selected for steering the precipitation bands. Again, the use of the time-height sections of profiler perturbation winds helped isolate the appropriate steering layer. Choice of an improper steering velocity resulted in a pattern of relative winds that gave precipitation trajectories which did not correspond to the near-surface locations of the radar and raingauge-detected precipitation.

Examples from two cases examined by Dye (1990) are presented here. One case is from a warm sector rainband of 16-17 November 1988 and the other is from a wide coldfront rainband on 10-11 October 1988.

### 3.1 Case of 16-17 November 1988

Figure 3.1 shows the radar echo pattern at 0330 UTC on 16 November 1988. The rear edge of a rainband is over the McAlevy's Fort wind profiler (SHA, "Shantytown") at this time, and is moving slowly eastward.

Figure 3.2 is a time-height section of the hourly winds at the "Shantytown"/McAlevys Fort, PA site. Brackets indicate the intensive observation period (IOP), when high-time-resolution wind profiles were obtained. Two rainbands occurred during the IOP, with the second one examined in more detail below. A surface cold front passed at 0615 UTC. Figure 3.3 shows surface analyses during the IOP.

Figure 3.4 shows the perturbation winds during the passage of this rainband, computed level by level as the vector depar-

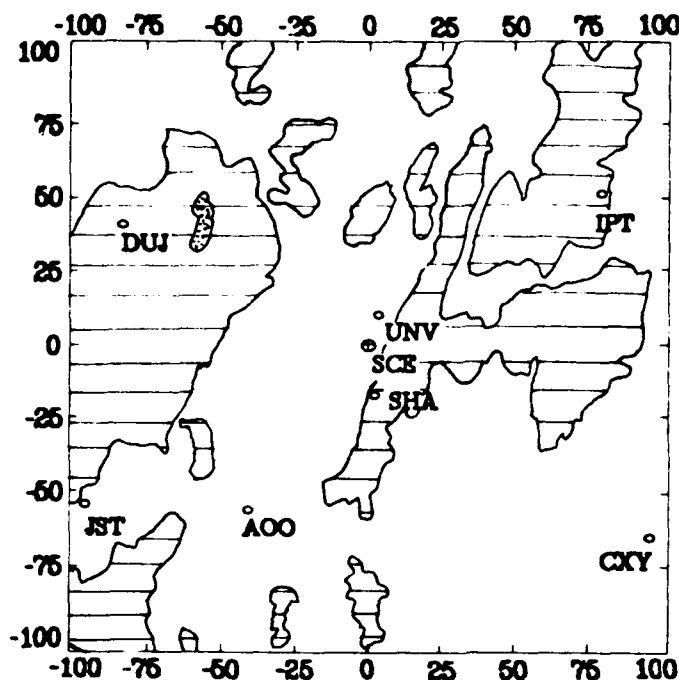


Figure 3.1. Outline of the radar echo detected on the Penn State WSR-74C weather radar at 0330 UTC on 16 November 1988. Dots show the locations of companion weather data: DUJ, AOO, UNV, CXY, and IPT refer to Dubois, Altoona, University Park, Harrisburg, and Williamsport, PA airports where surface weather data are collected at least hourly; SCE refers to the Borough of State College, PA, where the Penn State radar is located on the University Park Campus; SHA refers to the McAlevy's Fort ("Shantytown") VHF Doppler wind profiler site. Numbers show distances relative to the WSR-74C radar.

tures from an 11-hour mean encompassing the entire precipitation period. Below 3 km, perturbation winds had been westerly, shifted to southerly just prior to the arrival of the rainband, and remained southerly during the rainband. The layer from 3-6 km had easterly winds throughout. Farther aloft, winds shifted from northerly to westerly during the passage of the rainband.

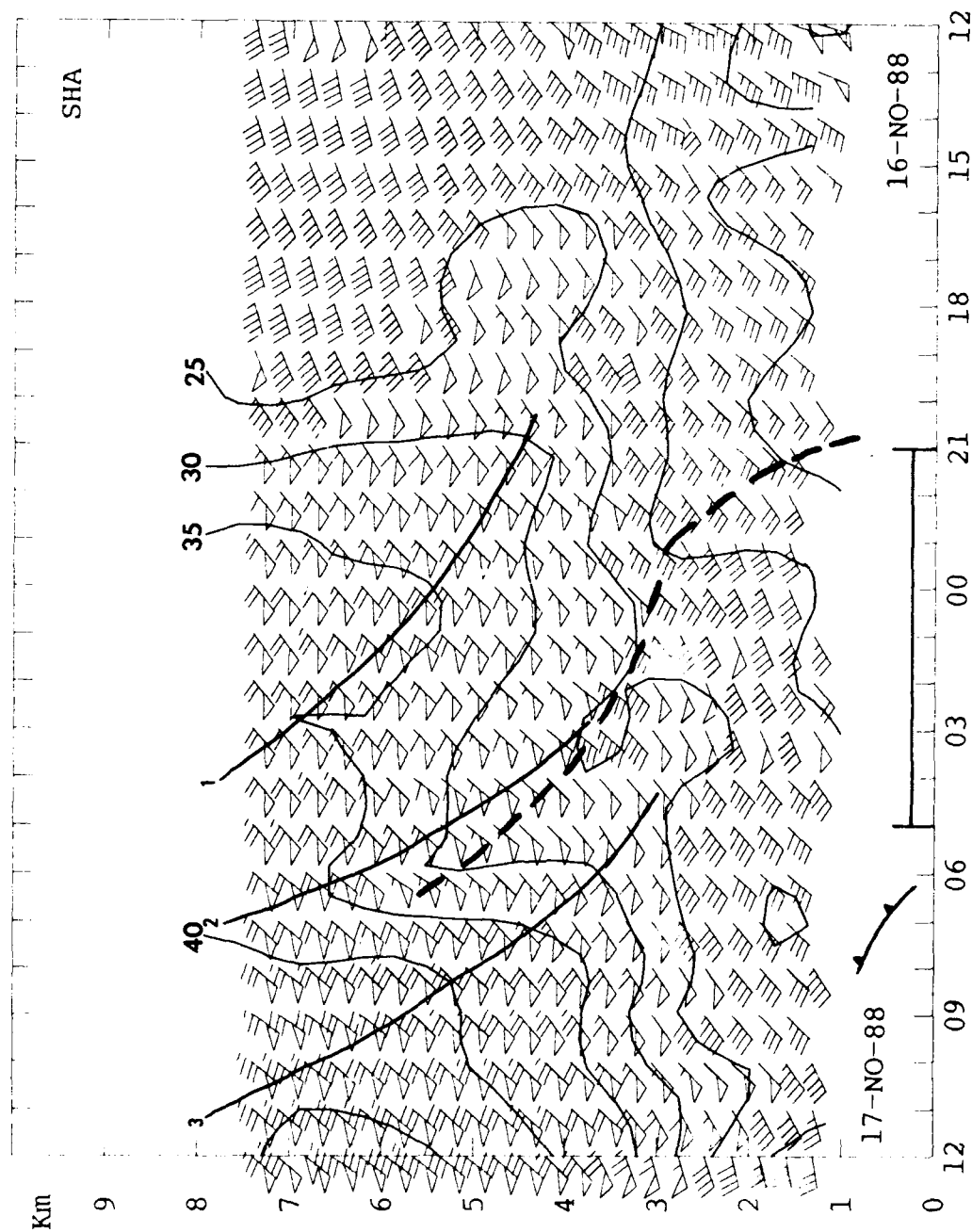


Figure 3.2 Time-height section of hourly horizontal winds measured by the "Shantytown"/McAleveys Fort, PA wind profiler from 1200 UTC 16 November 1988 to 1200 UTC 17 November 1988. A flag represents 25 m/s; a barb represents 5 m/s. Isotachs are in m/s. Bracketed time period indicates the intensive observing period, during which two rainbands occurred. Dashed line indicates a trough axis; solid lines indicate axes of windspeed maxima and minima. Surface cold front passage at 0615 UTC.

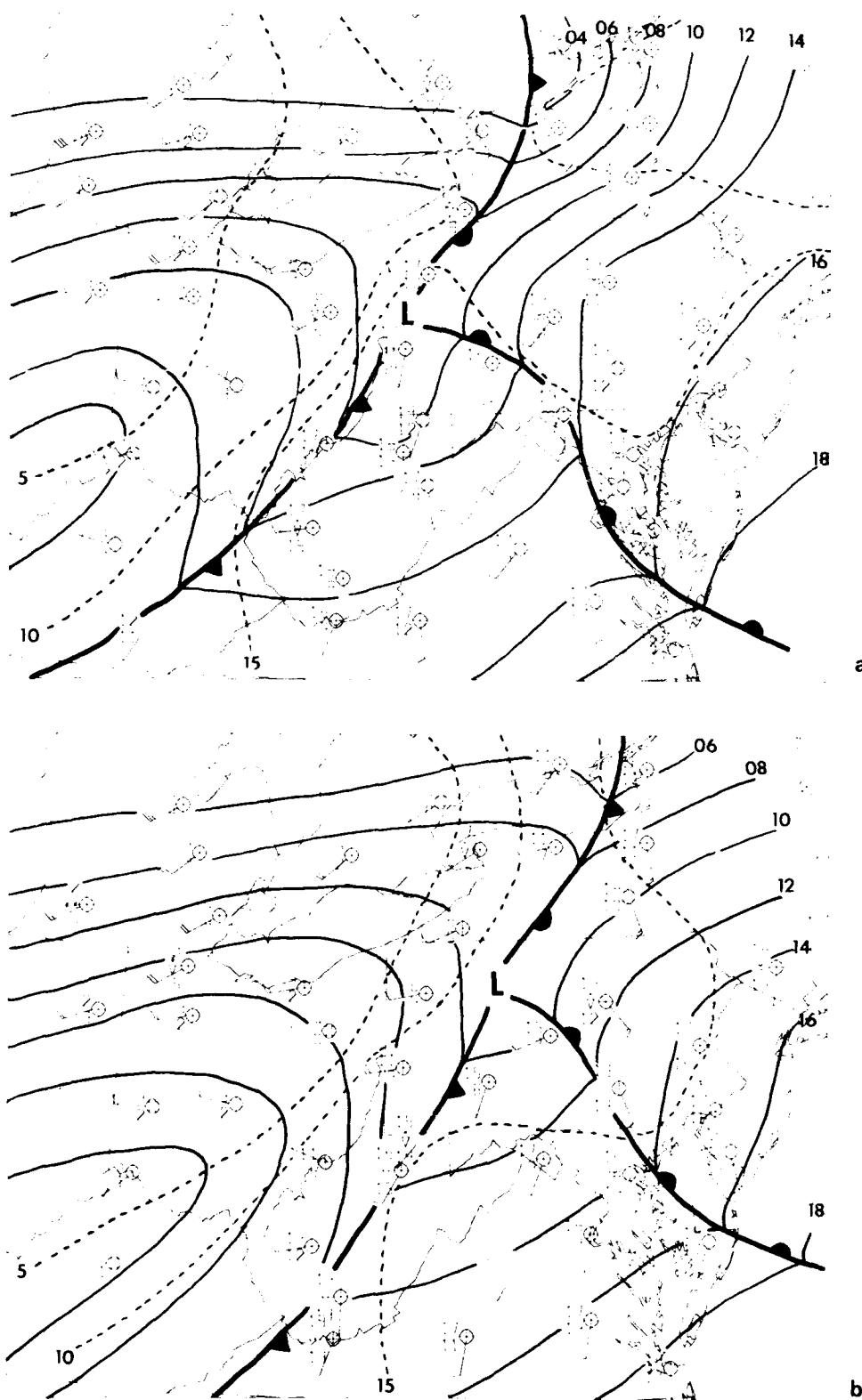


Figure 3.3. Surface analyses at (a) 0000 UTC and (b) 0300 UTC 17 November 1988 during the IOP of Fig. 3.2. Isobars (solid) at 2 mb intervals; isotherms (dashed) at 5 C intervals.



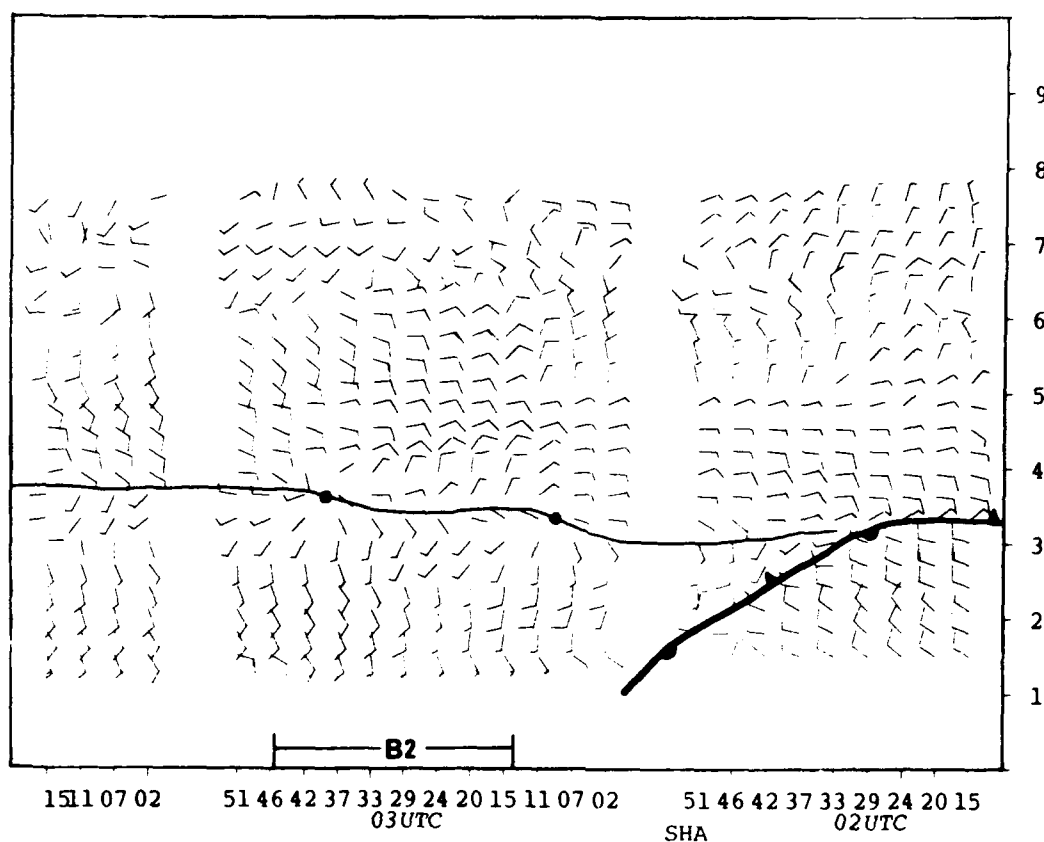


Figure 3.4. Time-height section of horizontal perturbation wind velocities at McAlevy's Fort, computed as vector departures from the 11-hour mean (level by level) over the period encompassing the rain event. A full wind barb denotes 5 m/s, and an arrow pointing toward the top of the diagram represents a southerly wind. The time-height section covers the time period from 0210 UTC (right) through 0420 UTC (left) on 17 November 1988.

Figure 3.5 shows the velocities relative to the travelling rainband. Streamlines in Fig. 3.5a depict the 2-dimensional velocity in the vertical plane of the time-height section, oriented across the rainband. Speeds of the rearward flow at the 4 km level were about 5 m/s. Isotachs denote flow normal to the plane of the section, having direction along the band, with positive values toward the NNE (leftward). Vertical velocities are shown in Fig. 3.5b, and stippling denotes upward motion. The

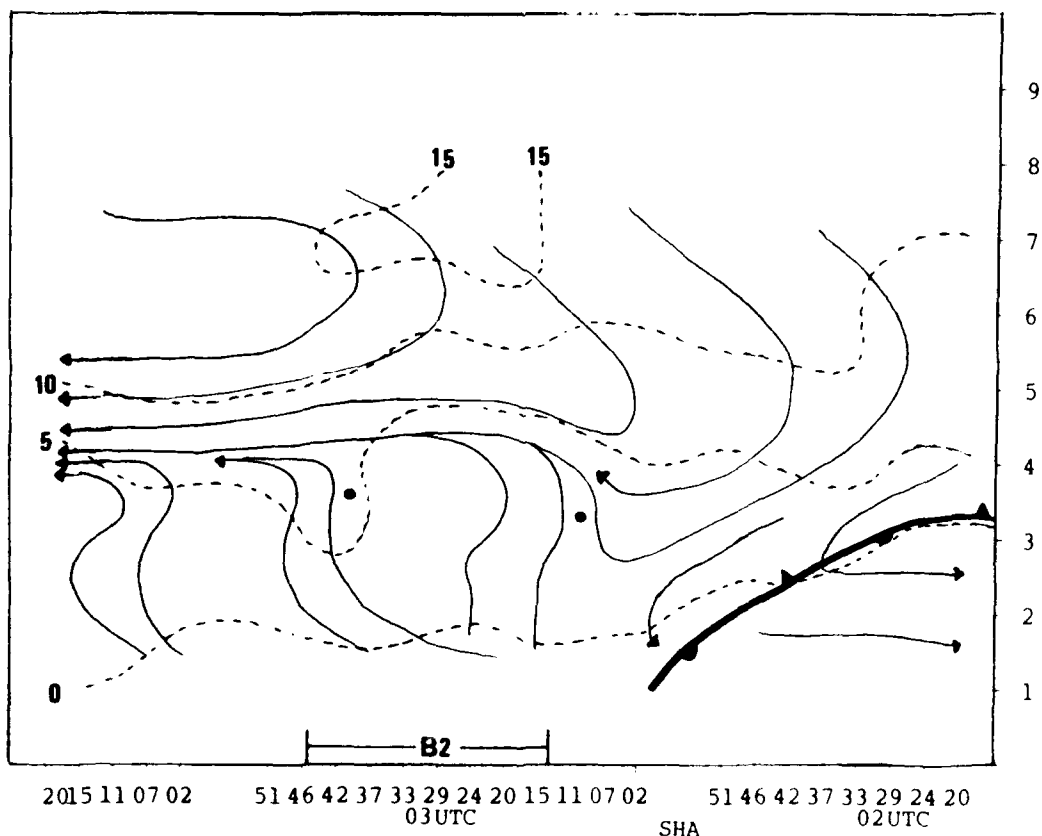
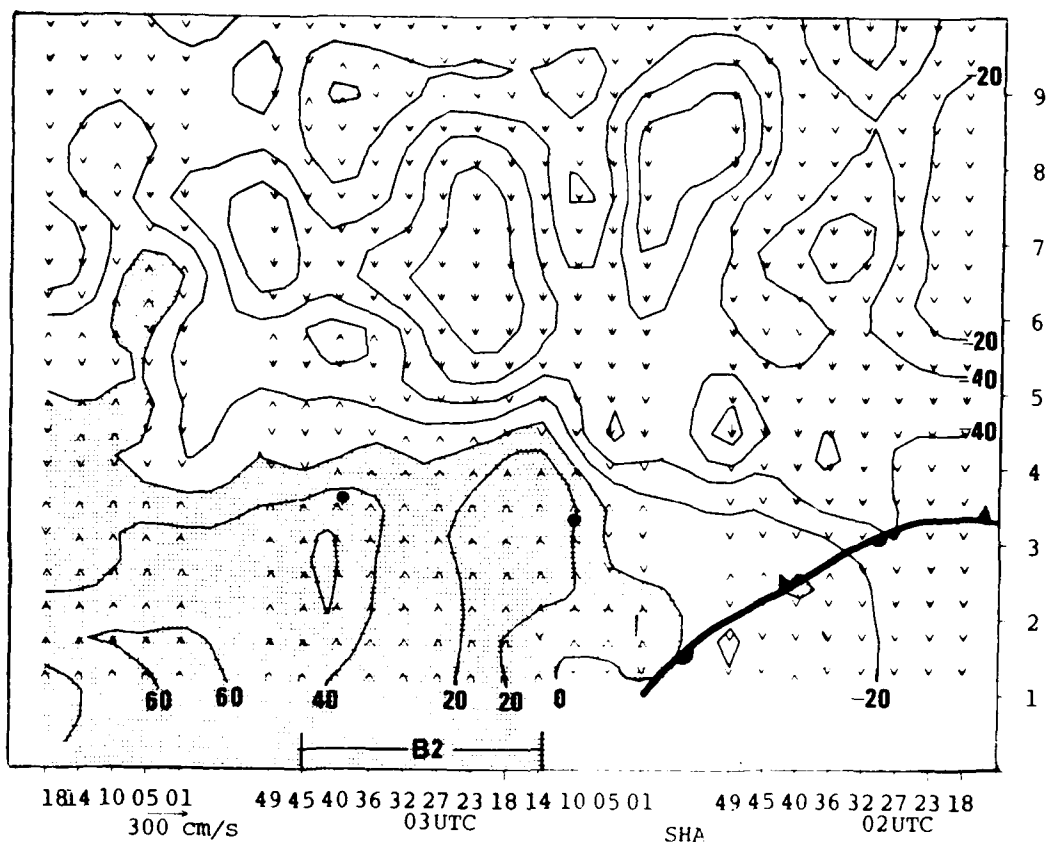


Figure 3.5. Time-height section of the relative winds in the  $x$ - $z$  plane through McAlevy's Fort, where  $x$  is the cross-front direction. (a) Streamlines (thin lines with arrows) of the cross-band flow and isotachs (solid; m/s) of the band-parallel flow. Positive values indicate flow into the page (toward NNE). (b) Vertical velocities (cm/s); upward where stippled.

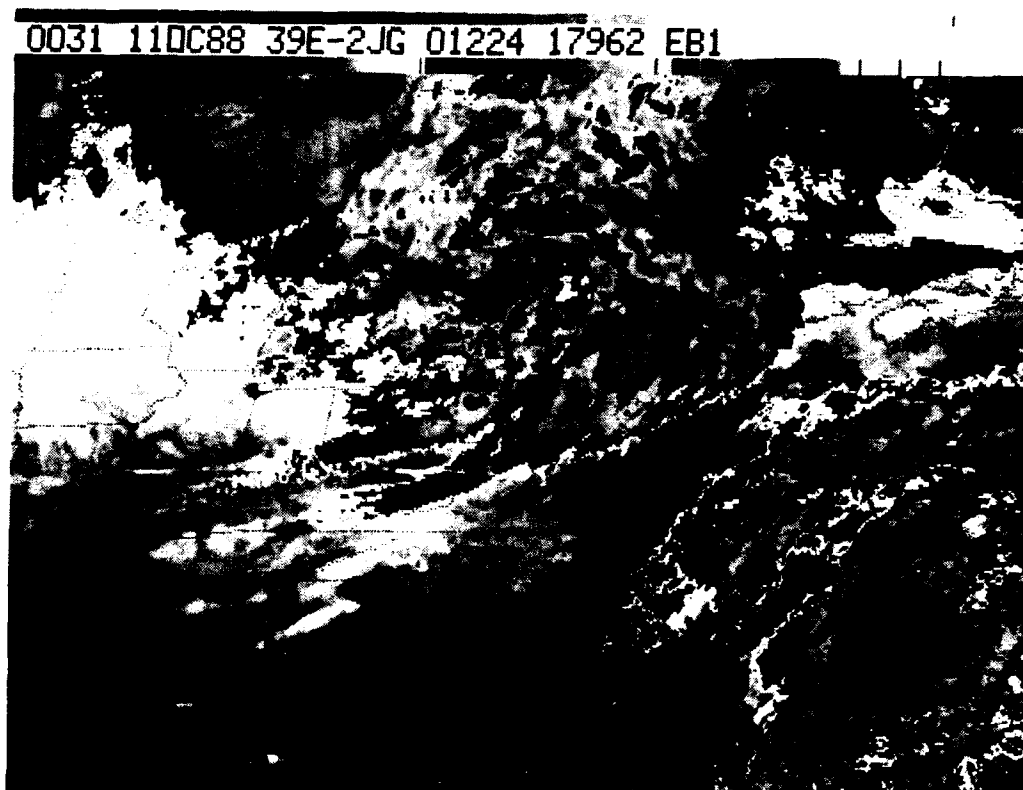


Figure 3.6. Enhanced infrared satellite image of the cloud bands passing over Pennsylvania at 0031 UTC on 11 October 1988.

rainband was accompanied by upward vertical velocities through about 5 km. A shallow layer of strong relative easterly flow, shown in Fig. 3.4, separated the ascent from a belt of descent further aloft. This warm sector rainband was nearly vertical, perhaps suggesting its origin due to static instability rather than conditional symmetric instability.

### 3.2 Case of 10-11 October 1988

Figure 3.6 shows an enhanced infrared satellite image of the clouds associated with the case of 10-11 October 1988. At this time, 0031 UTC on 11 October, at least two rainbands have passed the McAlevy's Fort wind profiler site (beneath the cloud band across east-central PA), and a third is approaching. Figure 3.7

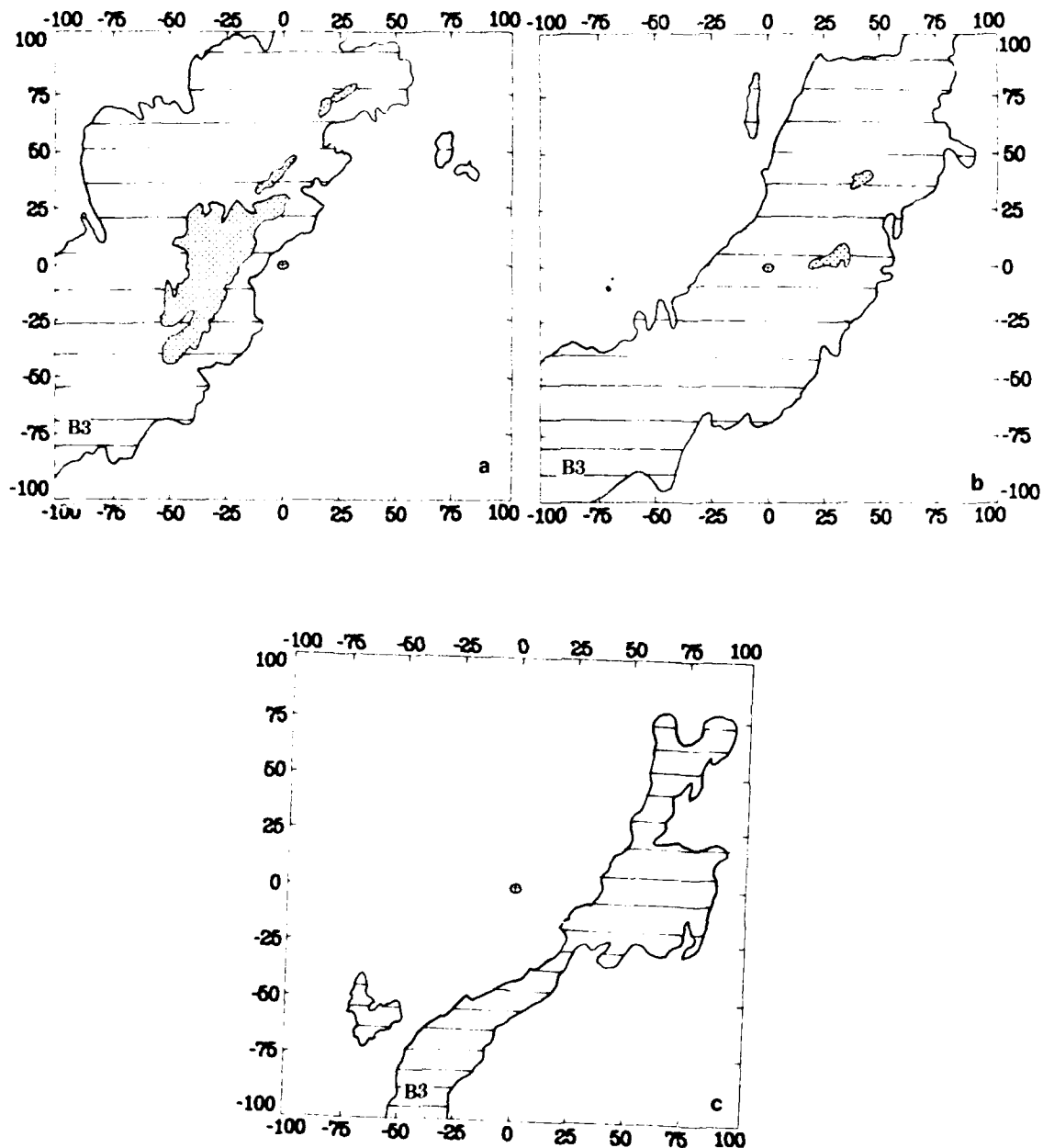


Figure 3.7. Sequence of radar echoes from the Penn State WSR-74C weather radar, at 0200, 0300, and 0400 UTC on 11 October 1988. The dot at  $x=y=0$  refers to the WSR-74C radar site.

shows a sequence of radar schematics during the passage of this rainband over the "Shantytown"/McAlevys Fort, PA profiler site. The latter radar-detected rainband is affiliated with the cloud band over northwestern PA in Fig. 3.6.

Figure 3.8 shows a time-height section of the hourly winds measured by the profiler, depicting the large-scale setting of the IOP, which is indicated by brackets. The third rainband, examined in detail below, coincided with the passage of the front.

Figure 3.9 shows time-height sections of the high-resolution total (a) and perturbation velocities (b) during the passage of the wide cold frontal rainband between 0200 UTC and 0400 UTC on 11 October 1988, the third rainband of the IOP. There was evidence that the front passed at 1 km prior to its passage at the surface. In Fig. 3.9b, a sloping zone of vertical wind shear, near 2 km at about 0100 UTC, near 4 km at 0230 UTC, and near 7 km at 0300 UTC, also has front-like characteristics, and may have been the remnant inversion of an old front that had previously moved offshore. The slope of this front-like feature and the low-level front were about 1:50. The passage of the rainband was associated with the steepest slope.

Figure 3.10 shows streamlines of the relative winds (a) and (b) vertical velocities during the passage of the rainband. Upward velocities are stippled. Strongest ascent began just prior to the onset of precipitation at the surface, shown near 4 km at 0200 UTC, and sloped upward above the frontal surface. A deeper layer of ascent occurred toward the rear of the band at about 0301 UTC. Precipitation continued for a while after the ascent

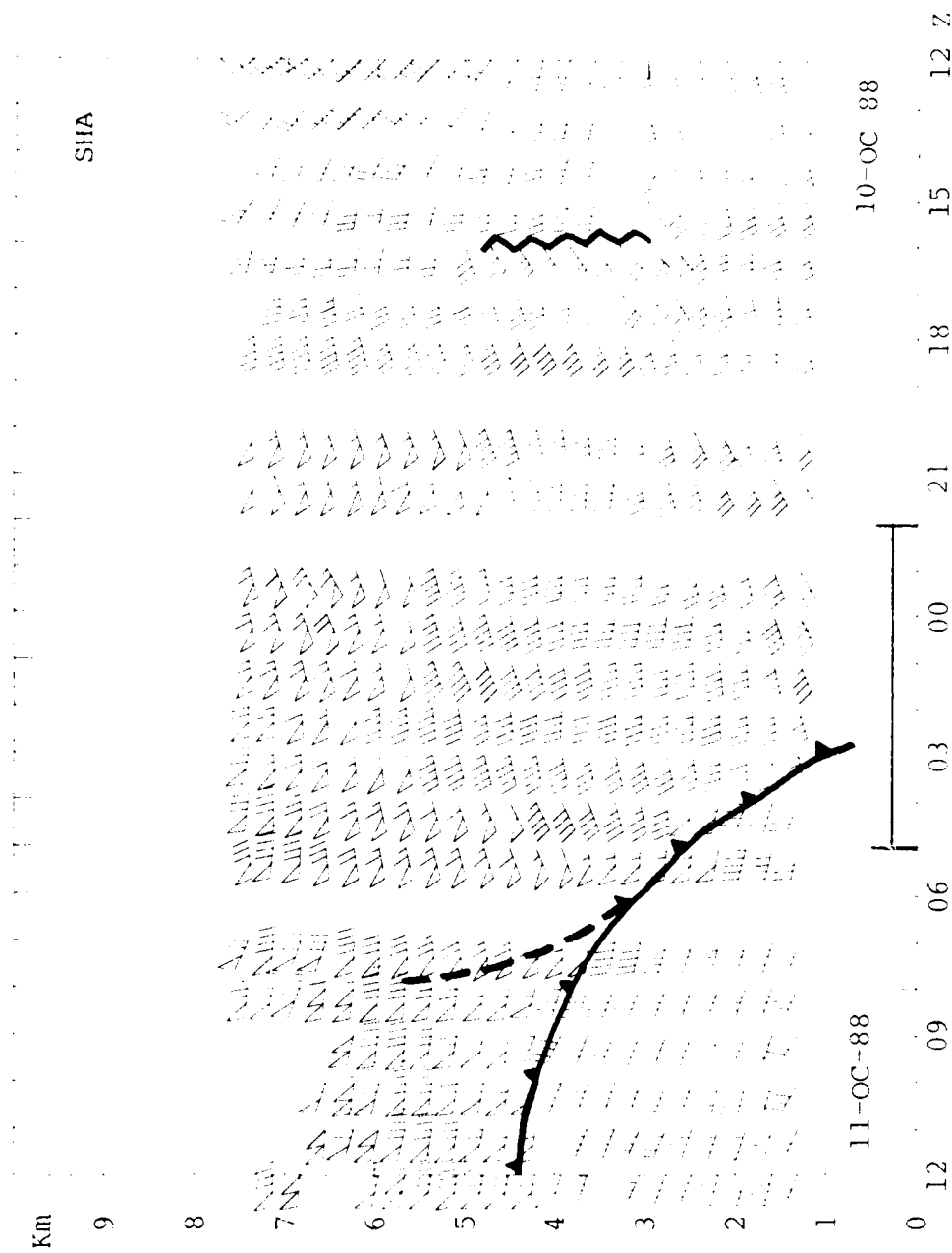


Figure 3.8. Time-height section of the hourly horizontal winds measured by the "Shantytown"/McAleys Fort, PA wind profiler on 10-11 October 1988. Conventions as in Fig. 3.2. Three rainbands occurred during the bracked IOP, with the third one straddling the cold front.

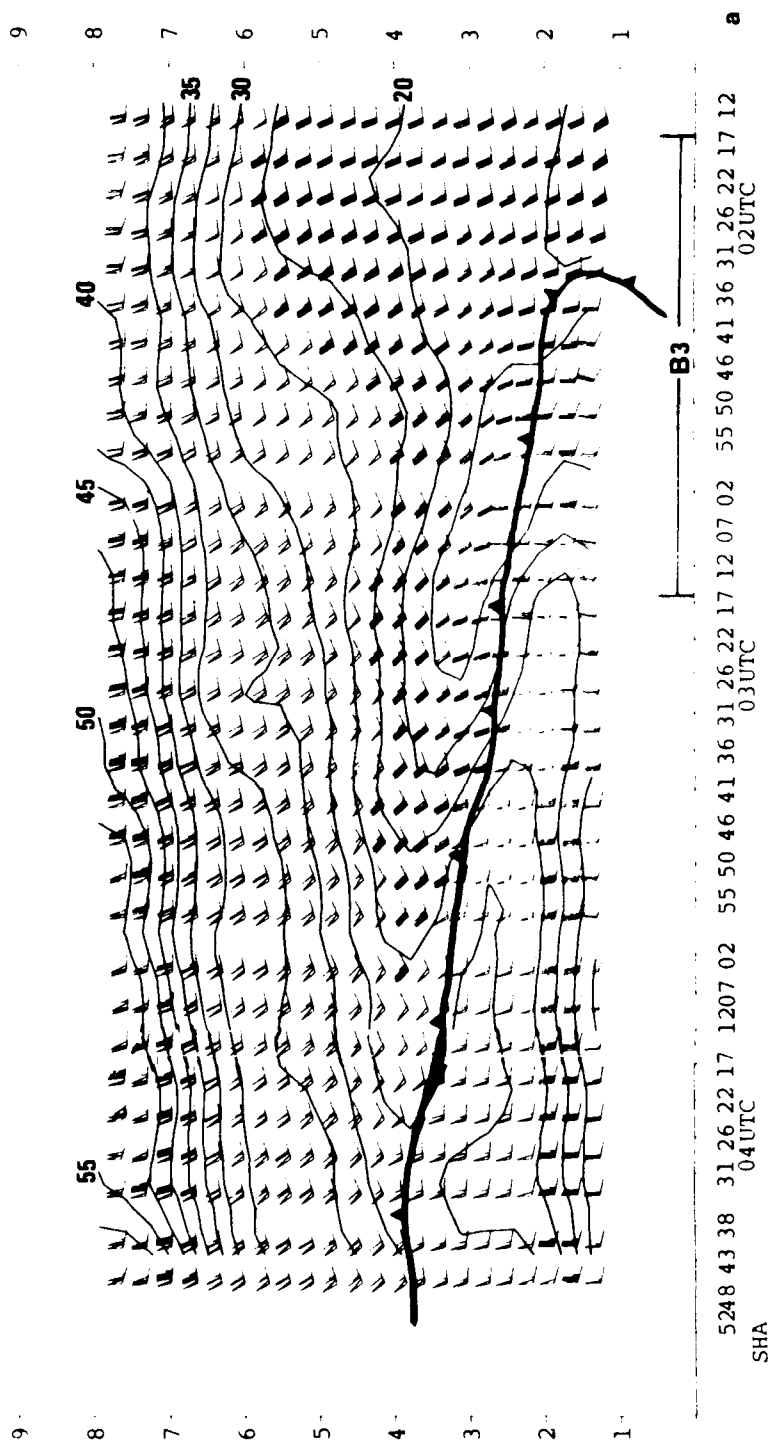


Figure 3.9. Time-height section of (a) total horizontal and (b) perturbation winds at McAlevy's Fort, computed as vector departures from the 11-hour mean winds over the period encompassing the precipitation event. Data on the section comprises the period from 0212 UTC to 0443 UTC on 11 October 1988. A full barb represents 5 m/s.

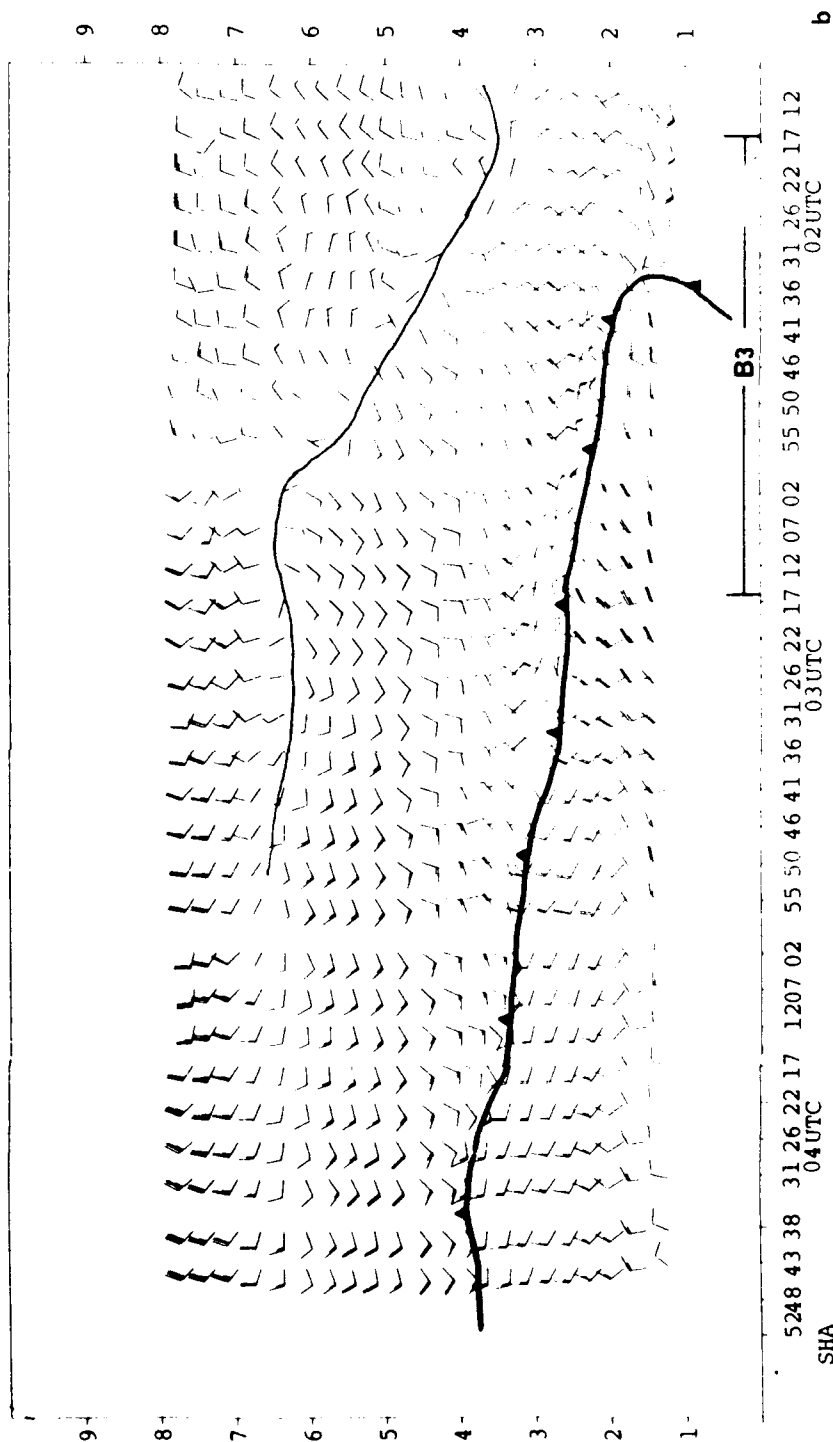


Figure 3.9b Time-height section of perturbation winds in the x-z plane through McAlevy's Fort (vectors and streamlines), where x is the cross-front direction. Isotachs (m/s) and stippling refer to the along-front wind component, and stippled areas have flow out of the plane toward the reader.



at altitudes below 4 km had apparently ceased. The latter period appears to be partly related to the time necessary for the precipitation generated aloft to reach the ground. Passage of the low-level cold front was marked by a shift from a flow along the band in a northward direction to flow along the band in a southward direction, as shown by the isotachs of band-parallel flow in Fig. 3.10a. Band-normal flow also reversed direction from rearward prior to the front passage to forward in the cold air.

There were several subtle differences in the nature of the two rainbands presented in this chapter. One was that the for-

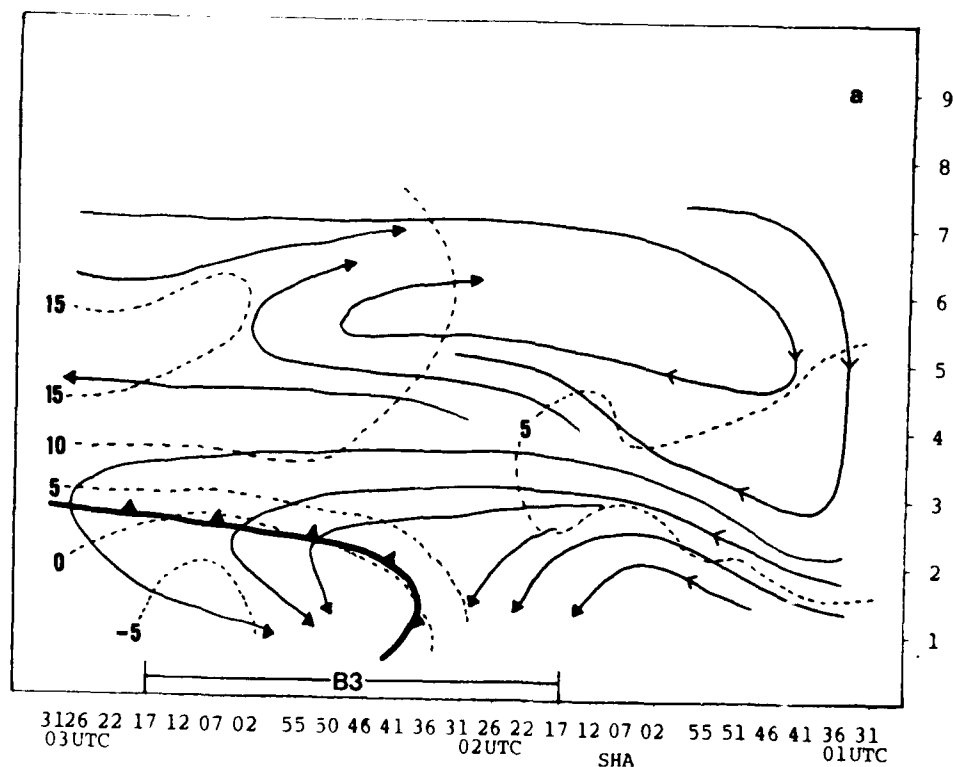


Figure 3.10. Time-height section of the relative winds in the  $x$ - $z$  plane through McAlevy's Fort, where  $x$  is the cross-band direction. (a) Streamlines of the cross-band velocity and isotachs (dashed, m/s) of the band-parallel flow, with positive values toward the north. (b) Vertical velocities (cm/s); stippling represents upward motion.

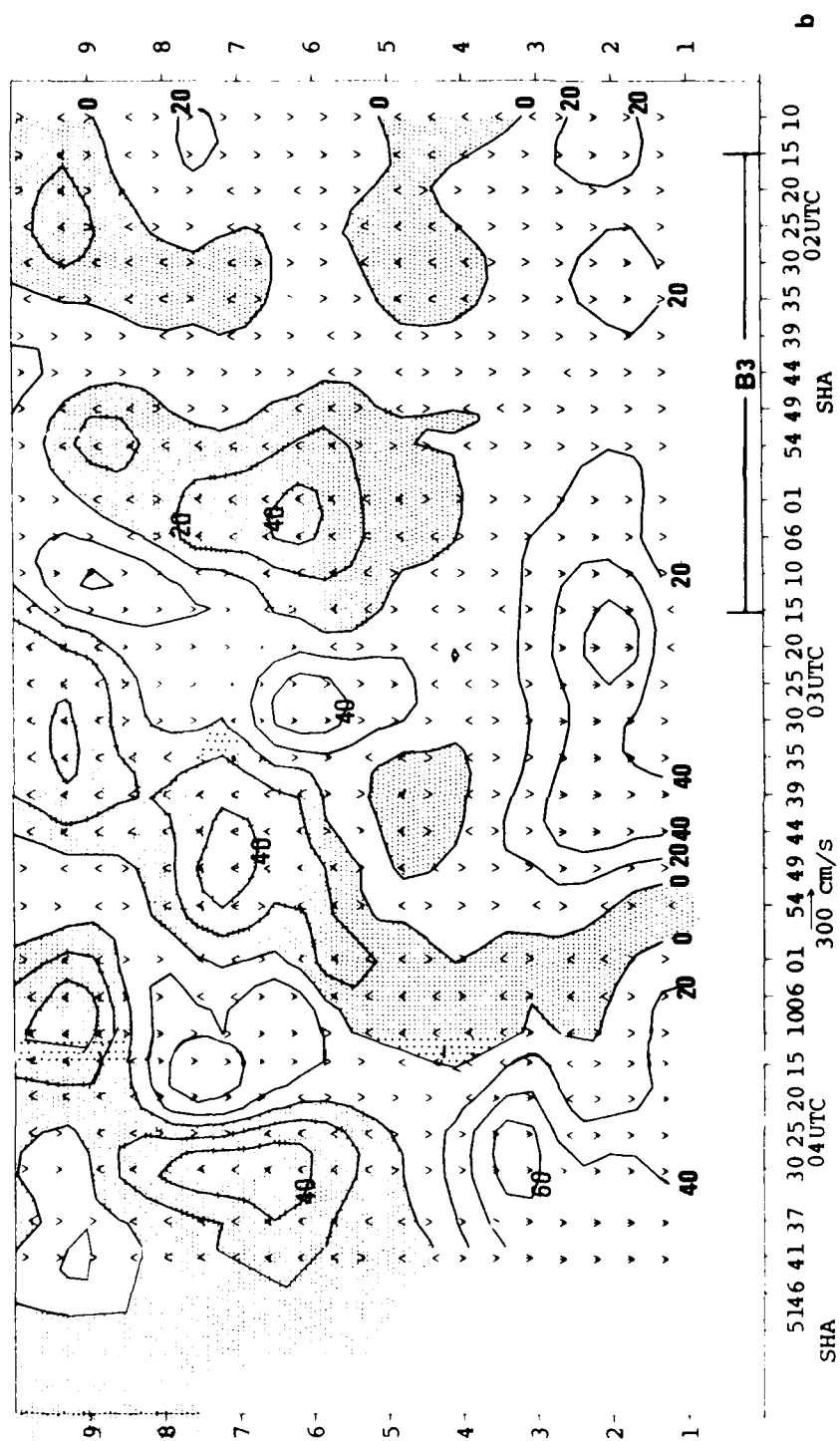


Fig. 3.10b. Time-height section of the relative winds in the x-z plane through McAlevy's Fort, where x is the cross-band direction. Vertical velocities (cm/s); stippling represents upward motion.

ward relative flow across the rainband was quite weak in the narrow warm sector band of November 16, whereas there was a stronger forward relative flow in the case of the wide cold frontal band of 11 October. Rearward flows existed in both cases, but the rearward flow appeared at the top of the rainband in the former case, but appeared to be directly affiliated with the updraft of the latter. In the former case, upward velocities were almost co-located with the rainband, because precipitation was generated and fell almost straight to the ground. In the latter case, precipitation was generated in the sloping updraft on the front (east) side of the rainband and swept rearward relative to the band during its descent to the ground by the strong relative flow.

Additional information about rainband character, both through studies of additional rainbands during these cases, and through studies of additional cases, is presented by Dye (1990). It should be noted that neither of the rainbands presented in this chapter exhibited a well-defined roll circulation in the cross-band vertical plane, as might have been expected. Other rainbands studied by Dye did have this character.

#### 4. STUDIES OF FRONTAL CIRCULATIONS

Knowlton (1987) used wind data obtained from two-station and three-station VHF wind profiler networks to examine two cases of atmospheric fronts in Pennsylvania and Colorado, respectively. The first case study, of a snow and rain event on 11-12 November 1986, used the wind profilers at Crown and McAlevys Fort, PA, and considered only cross-front variations. The second case study, of a Colorado snowstorm on 28-29 September 1985, used wind profiler data from a triangle of Colorado sites. The latter study also examined the differences in results obtained through use of 2 versus 3 wind profilers, wherein along-front variations could also be incorporated into the calculations. Figure 4.1 illustrates the locations of the 2-station and 3-station profiler networks used in the studies.

In the studies, a variety of quantities were computed, including kinematic vertical velocities and kinematic quantities relating to frontogenesis/frontolysis, front movement, and Q-vector forcing of frontal circulations. The inferences derived from these analyses were evaluated in light of the observed weather.

The adiabatic form of Miller's (1948) equation for frontal intensification is often used to evaluate processes which can change the intensity of the cross-front (x-direction) temperature gradient:

$$\frac{d}{dt}\left(\frac{\partial\theta}{\partial x}\right) = -\frac{\partial u}{\partial x}\left(\frac{\partial\theta}{\partial x}\right) - \frac{\partial v}{\partial x}\left(\frac{\partial\theta}{\partial y}\right) - \frac{\partial w}{\partial x}\left(\frac{\partial\theta}{\partial z}\right) . \quad (4.1)$$

This equation is fairly amenable for use with 3-profiler-network data, but less so in the case of a 2-profiler network. Because a triangle of wind profilers enables the computation of the geo-

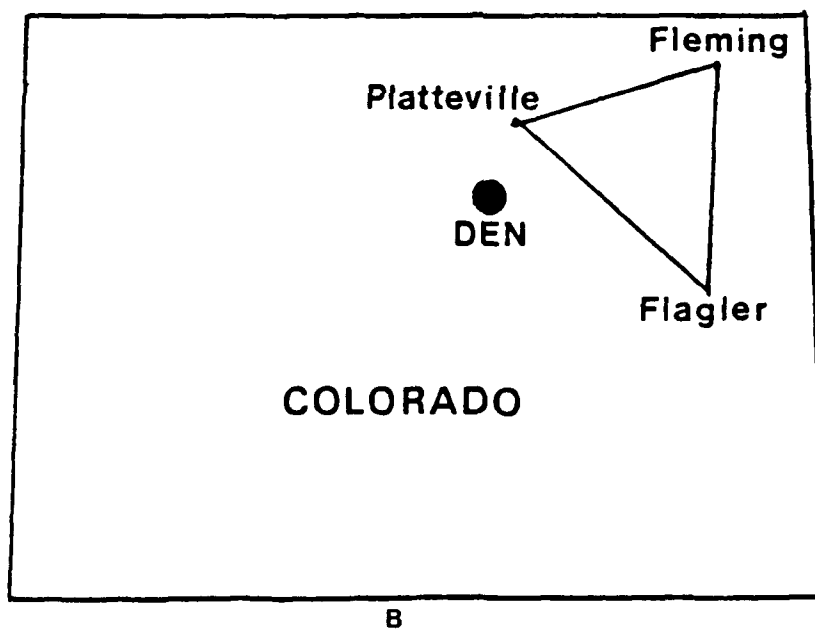
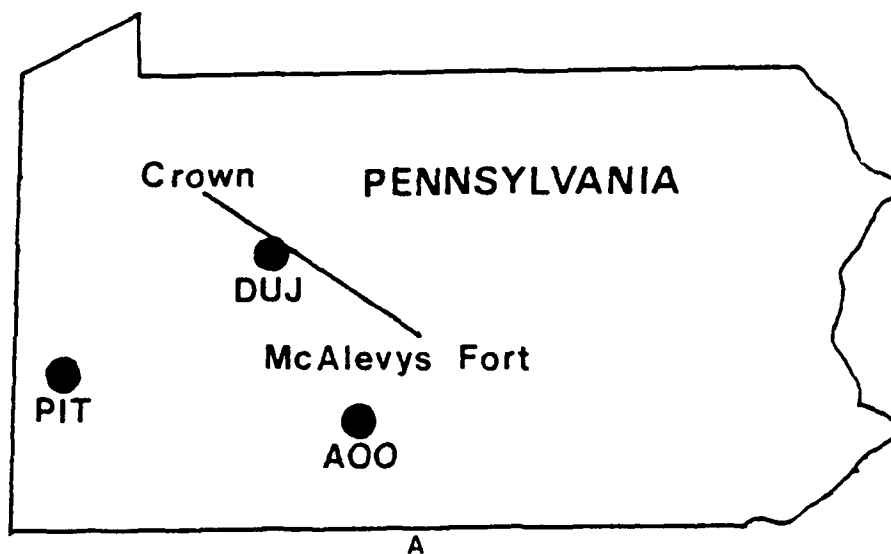


**Figure 4.1.** The Pennsylvania and Colorado profiler networks. (A) Crown-McAlevys Fort baseline located in western Pennsylvania, and (B) Platteville-Flagler-Fleming triangle located in northeastern Colorado. (FAA observing stations: DUJ - Dubois, AOO - Altoona, PIT - Pittsburgh, DEN - Denver)

strophic winds,

$$u_g = \bar{u} - u_{ag}, \quad u_{ag} = -\frac{1}{f} \left( \frac{\partial \bar{v}}{\partial t} + \bar{u} \frac{\partial \bar{v}}{\partial x} + \bar{v} \frac{\partial \bar{v}}{\partial y} + \bar{w} \frac{\partial \bar{v}}{\partial z} \right),$$

$$v_g = \bar{v} - v_{ag}, \quad v_{ag} = \frac{1}{f} \left( \frac{\partial \bar{u}}{\partial t} + \bar{u} \frac{\partial \bar{u}}{\partial x} + \bar{v} \frac{\partial \bar{u}}{\partial y} + \bar{w} \frac{\partial \bar{u}}{\partial z} \right), \quad (4.2)$$

the two horizontal temperature gradient terms can be evaluated in terms of the vertical wind shears of the geostrophic wind components, through use of the thermal wind relationship. The geostrophic wind can be calculated only approximately using a two-profiler network, because variations of the winds normal to the baseline must be ignored:

$$u_g = \bar{u} - u_{ag}, \quad u_{ag} = -\frac{1}{f} \left( \frac{\partial \bar{v}}{\partial t} + \bar{u} \frac{\partial \bar{v}}{\partial x} + \bar{w} \frac{\partial \bar{v}}{\partial z} \right),$$

$$v_g = \bar{v} - v_{ag}, \quad v_{ag} = -\frac{1}{f} \left( \frac{\partial \bar{u}}{\partial t} + \bar{u} \frac{\partial \bar{u}}{\partial x} + \bar{w} \frac{\partial \bar{u}}{\partial z} \right). \quad (4.3)$$

This discourages use of (4.1), as does the difficulty in assessing the third term on the right-hand side.

The adiabatic and inviscid form of the Sawyer-Eliassen equation was used (after Keyser and Carlson, 1984) to examine frontal circulations,

$$-\left(\frac{g}{f\theta_0}\right) \left(\frac{\partial \theta}{\partial z}\right) \frac{\partial^2 \psi}{\partial x^2} + 2 \left(\frac{\partial v}{\partial z}\right) \frac{\partial^2 \psi}{\partial x \partial z} - \left(f + \frac{\partial v}{\partial x}\right) \frac{\partial^2 \psi}{\partial z^2} = 2 \left( \frac{\partial v}{\partial x} \frac{\partial u}{\partial z} - \frac{\partial u}{\partial x} \frac{\partial v}{\partial z} \right), \quad (4.4)$$

where  $\psi$  is a streamfunction in the  $x, z$  plane and  $x$  is in the cross-front direction. The terms on the right-hand side of (4.4), sometimes referred to as the  $Q$ -vector forcing terms, are shearing and stretching deformations of the geostrophic winds, and are similar to the horizontal terms in (4.1). These terms force ageostrophic circulations  $u_{ag}$  and  $w$ , equal in magnitude to the vertical gradient and negative  $x$ -direction gradient of the streamfunction, respectively. By using profiler winds to evaluate the forcing terms, and defining the  $x$ -direction normal to the front, the corresponding ageostrophic circulations were deduced in a

qualitative sense.

Kinematic vertical velocities, ageostrophic velocities, and thermal wind-derived temperature gradients were also calculated. The kinematic vertical velocities in the 2- and 3-profiler cases were computed from

$$w(z_n) = w(z_0) - \sum_{i=1}^n \left( \frac{\partial u}{\partial x} \right)_i \Delta z_i, \quad (4.5)$$

$$w(z_n) = w(z_0) - \sum_{i=1}^n \left( \frac{\partial u}{\partial x} + \frac{\partial v}{\partial y} \right)_i \Delta z_i, \quad (4.6)$$

respectively.

The frontal circulation diagnoses obtained from both the two and three-station calculations generally compared favorably to the observed weather. Periods of precipitation coincided with those time periods during which the low- and middle-level geostrophic forcing suggested upward motion in the ageostrophic response. The heaviest precipitation occurred during the period diagnosed to have the most intense rising motion. Non-precipitating and decreasing-precipitation periods coincided with diagnosed low- and middle-level sinking. Upper-level ageostrophic circulations were diagnosed in association with jet streak features revealed in the profiler time-height wind profiles.

Some examples of these diagnostic products are illustrated below, and in more detail by Knowlton (1987). The general weather situation during the Pennsylvania snow and rain event of 11-12 November 1986 is depicted in the cross-section of Figure 4.2 and in the surface analyses of Figure 4.3. A mid- and upper-level front passed over the 2-profiler network near 700 mb at 1200 UTC 11 November and is seen at the surface near Cape Hatteras, NC. Another surface front is approaching Flint, MI (72637) at

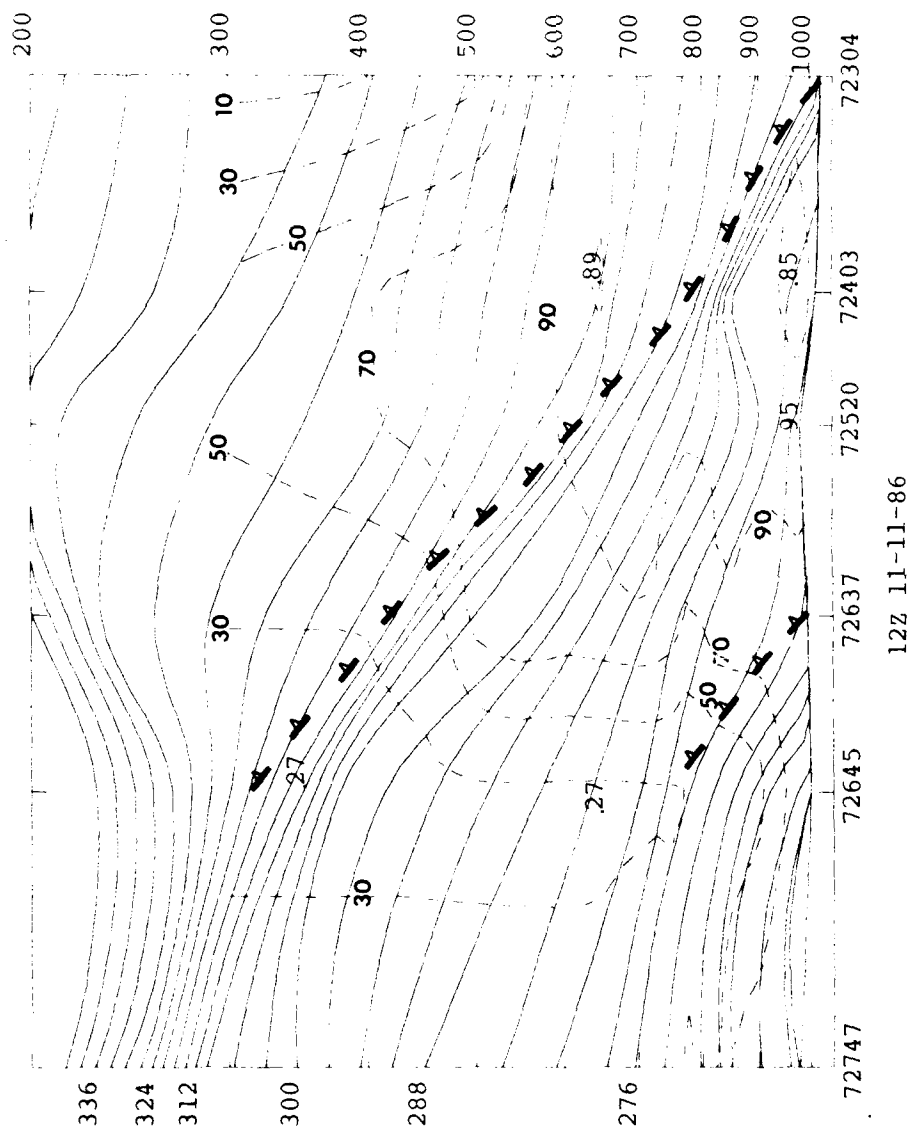


Figure 4.2. Northwest-southeast cross-section of potential temperature (solid) and relative humidity (dashed) from 1200 UTC on 11 November 1986. Observation sites are located by WMO numbers, with the '72' omitted: International Falls, MN--72747; Green Bay, WI -- 72645; Flint, MI -- 72637; Pittsburgh, PA -- 72520; Dulles International Airport, Washington, DC -- 72403; Cape Hatteras, NC -- 72304.



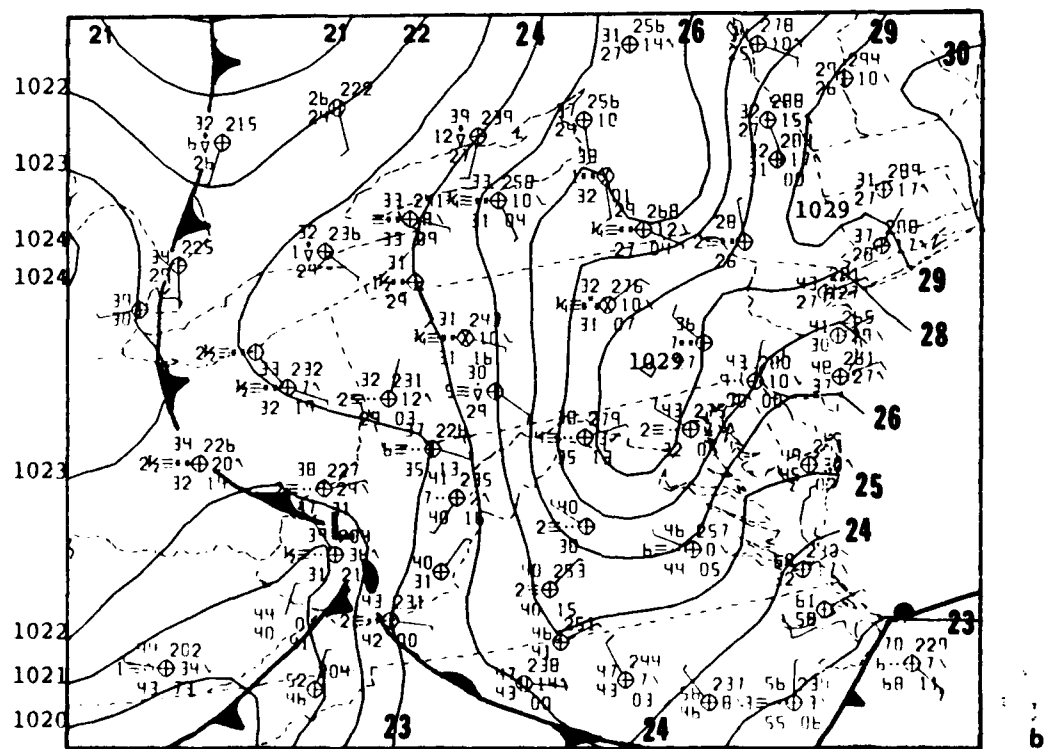
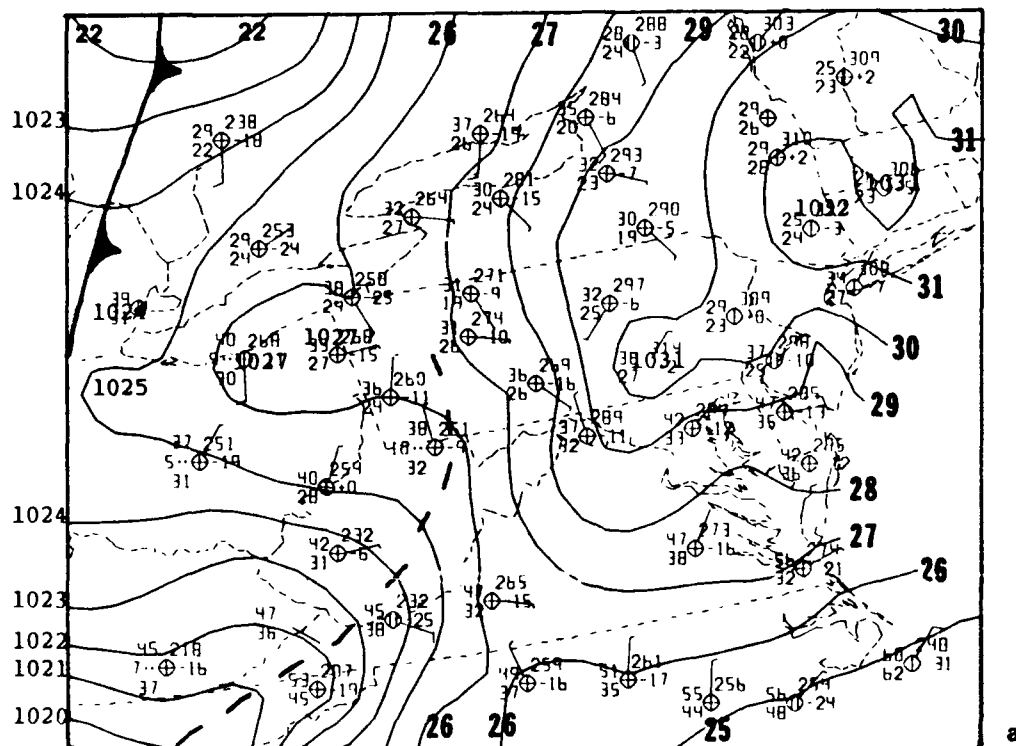


Figure 4.3. Surface observations and sea-level pressure isobars (solid, at 1 mb intervals) on 11 November 1986. (a) 0700 UTC; (b) 1200 UTC; (c) 1900 UTC.

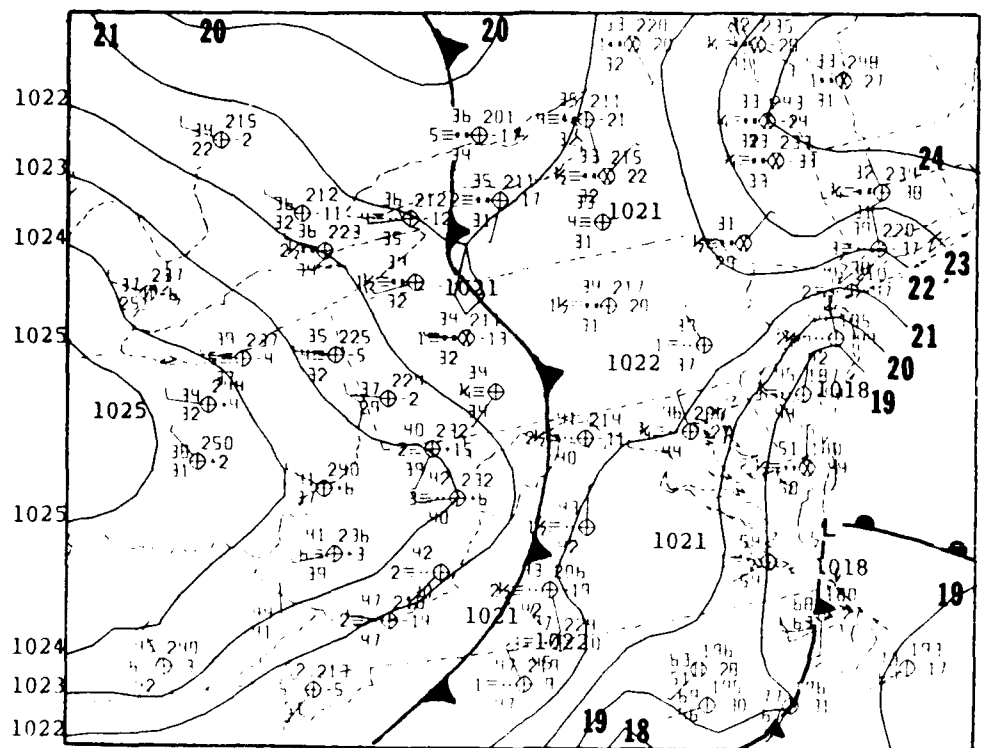


Figure 4.3. Surface observations and sea-level pressure isobars (solid, at 1 mb intervals) on 11 November 1986. (c) 1900 UTC.

that time, and entered the profiler baseline about 1800 UTC.

Figure 4.4 shows the time-height sections of the winds observed at the Crown and McAlevy's Fort, PA wind profiler sites. While a sloping zone of maximum winds can be seen at each site, no dramatic wind shifts are evident. At McAlevy's Fort, the sloping zone of maximum winds can be seen near 3 km at 1800 UTC and near 8 km at 2300 UTC. This wind maximum is likely to be found in association with, and just above, the mid- to upper-level front of Fig. 4.2, which is pushing eastward with time while sloping upward to the west.

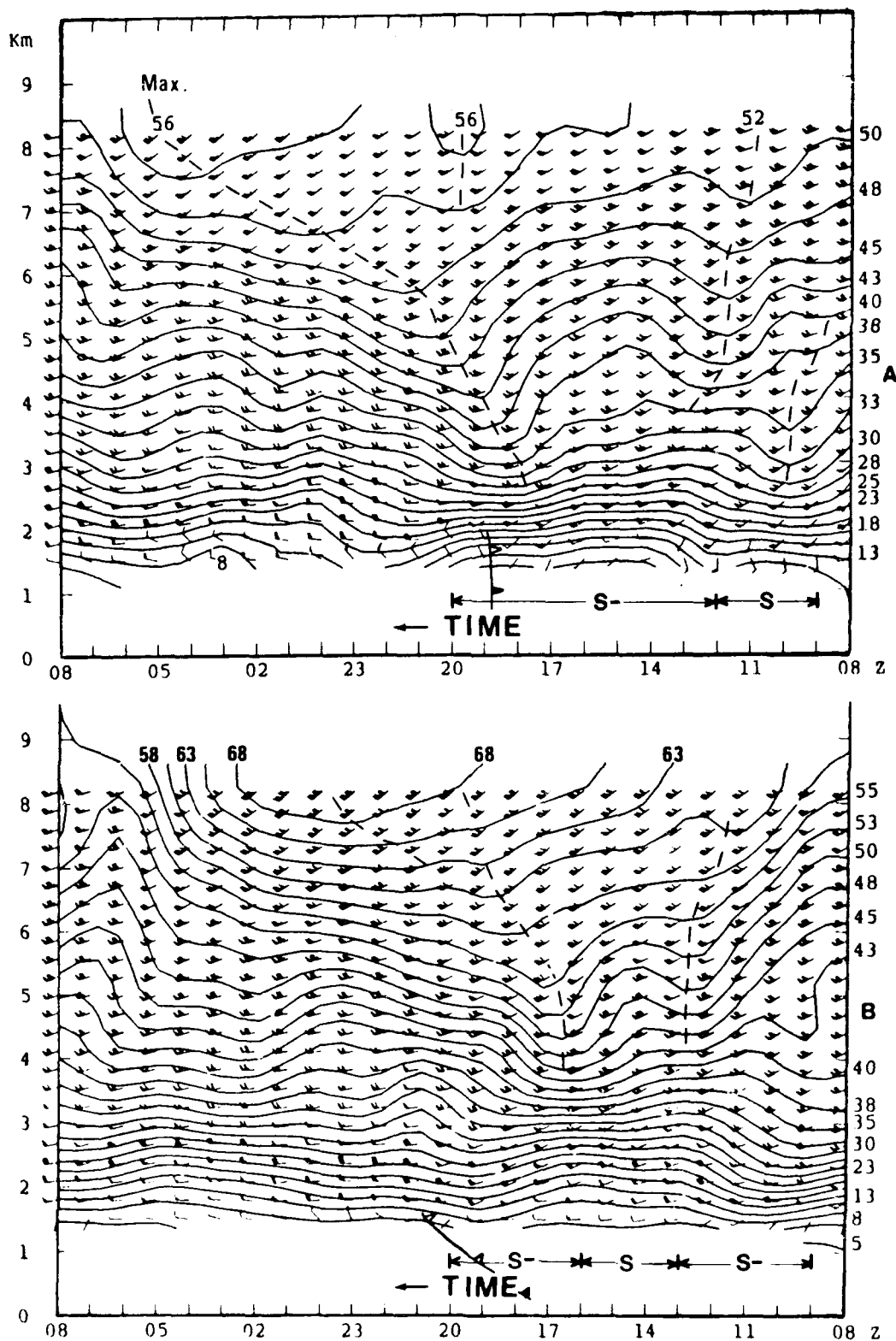


Figure 4.4. Time-height section of profiler winds for the 24 hours beginning 0800 UTC on 11 November 1986 (right). A full barb represents 5 m/s; isotachs are at 2.5 m/s intervals.

- a. McAlevy's Fort, PA
- b. Crown, PA

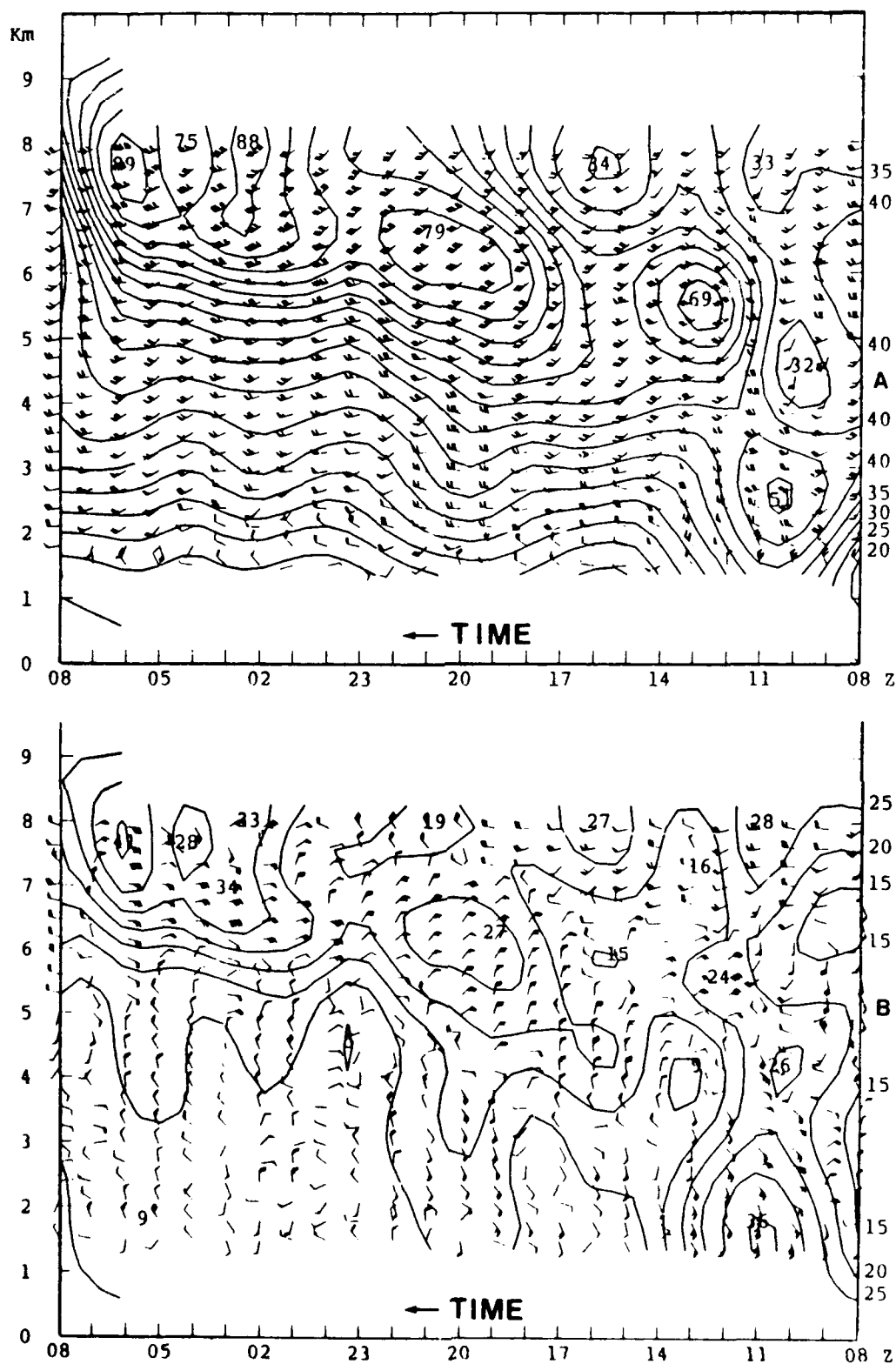


Figure 4.3. Time-height sections of two-profiler-derived geostrophic velocities (a) and ageostrophic velocities (b) beginning at 0800 UTC on 11 November 1986 (right). Isotachs are at 5 m/s intervals.

Figure 4.5 shows time-height sections of the geostrophic and ageostrophic wind velocities derived from the 2-profiler network. The geostrophic winds are not too dissimilar, qualitatively, from the observed winds (Fig. 4.4), especially after 1800 UTC. However, the geostrophic winds show a more dramatic pattern of maximum velocities in the zone of sloping maximum winds. The ageostrophic velocities appear to exhibit noise in a few places, but generally show a coherent pattern. Above the sloping zone of maximum geostrophic winds, the ageostrophic winds generally show an easterly component. At levels below 4 km, two periods of strong south-southeasterly ageostrophic flow can be seen at about 1100 UTC and 2000 UTC. As in other cases, as noted by Forbes et al. (1989), these wind maxima were affiliated with precipitation periods, especially the earlier one. The second maximum was affiliated with the arrival of the surface-based front of Fig. 4.2 into the profiler baseline.

Figure 4.6 shows a time-height section of the 2-profiler kinematic vertical velocities for this case. Ascending motion can be seen throughout the section aloft, corresponding well to the layers and periods having easterly or southerly ageostrophic winds in Fig. 4.5. Two periods of maximum ascent can be seen, centered at about 1100 UTC 11 November and 0300 UTC 12 November. The first period corresponds well to the time of the low-level south-southeasterly ageostrophic winds of Fig. 4.5, and to the period of heaviest precipitation. The weak secondary maximum of ascent (5 cm/s at 1900 UTC) appears to correspond to the second

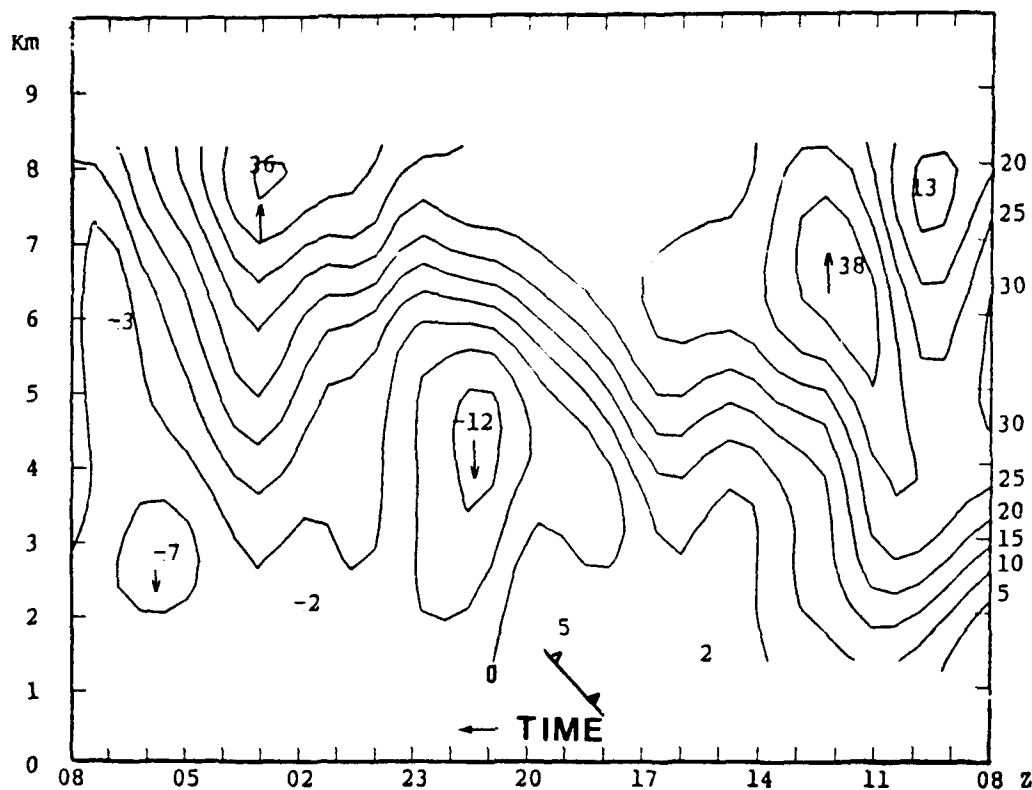


Figure 4.6. Time-height section of two-profiler-derived kinematic vertical velocities (cm/s), beginning at 0800 UTC 11 November 1986 (right). Positive values denote upward vertical velocity. Vertical velocity at the ground has been set to 0.

period of south-southeasterly ageostrophic winds and to the low-level front. However, the ascent appears to be too trivial in relation to the ageostrophic velocities, which seem to convey the more useful message for the forecaster in this case. The descent thereafter, peaking at about 2200 UTC, follows the front passage.

Figure 4.7 shows the time-height section of the Q-vector forcing of (4.4). Ageostrophic velocities are large where the gradients of  $Q$  are large, and are illustrated qualitatively by arrows. Two periods of lower-tropospheric ascent are diagnosed and correspond very well to the periods having south-southeasterly ageostrophic wind maxima.

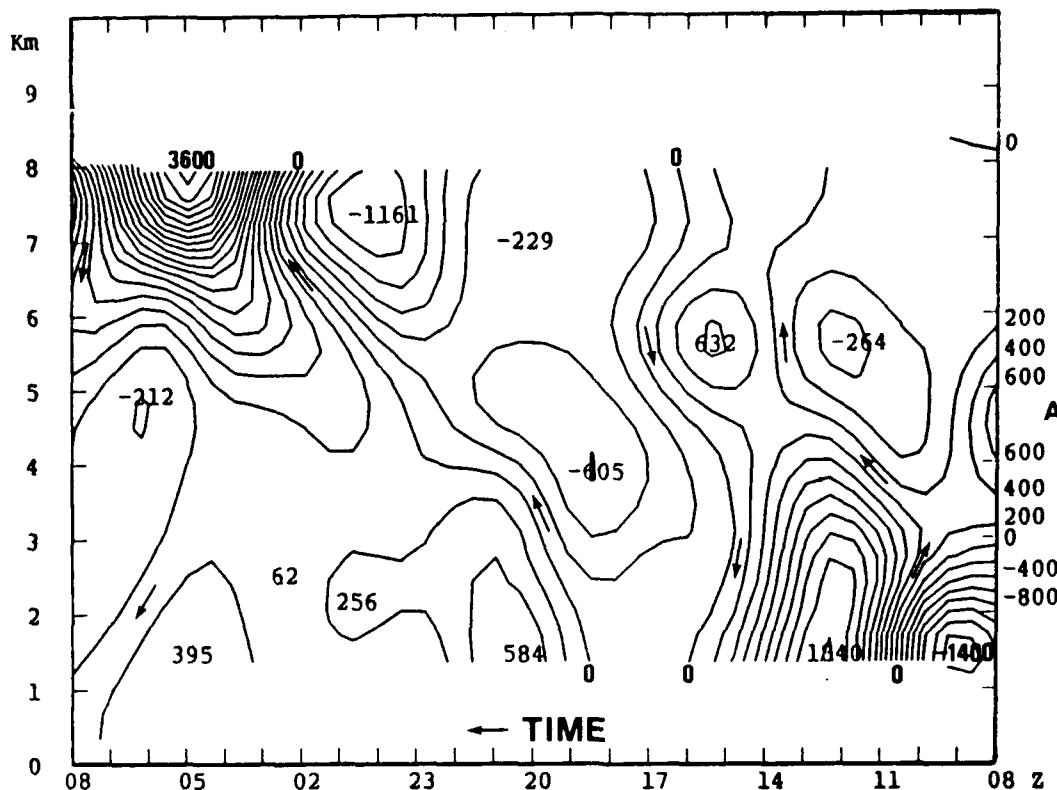


Figure 4.7. Time-height section of two-profiler-derived Q-vector forcing (solid; at intervals of  $200 \times 10^{-8} \text{ s}^{-2}$ ) and inferred ageostrophic circulations (vectors), beginning at 0800 UTC 11 November 1986 (right).

Thus, in this case of 2-profiler computations, the ageostrophic velocities and the Q-vector forcing fields seem to have given the best diagnoses regarding the most significant weather events: the 1100 UTC period of heaviest precipitation and the 1900 UTC low-level front passage. The kinematic vertical velocity gave a similar result overall, but did not highlight the low-level front passage.

There were small but non-trivial differences between the diagnosed circulations computed using 2-station versus 3-station VHF wind profiler networks in Colorado. That case featured a

highly curved jet stream and frontal system, in which appreciable along-front variations were present. It is suggested that for the PA case, in which the jet stream and front were less curved, the two-station-diagnosed circulations were more accurate.

Figure 4.8 shows cross-sections through the Colorado profiler triangle at 0000 and 1200 UTC on 29 September 1985. A front can be seen extending from the surface near Monett, MO (72349) to 400 mb near Denver (72469), and moving slowly eastward.

Figure 4.9 shows time-height sections of the 2-profiler and 3-profiler mean winds on 28-29 September. The isotach pattern is somewhat similar to that of Fig. 4.4, although the sloping wind maximum is not as pronounced.

Figure 4.10 shows time-height sections of the geostrophic wind velocities. As in the PA case, the 2-profiler geostrophic wind field shows the sloping wind maximum (affiliated with a frontal zone) more clearly than did the observed winds. The 3-profiler field is quite similar.

Figure 4.11 shows the ageostrophic winds for the 2-profiler and 3-profiler calculations. These are similar, although the 2-site values at about 0000-0400 UTC 29 September in the lower troposphere are stronger than those from the 3-profiler calculations. Moderate snow fell from about 2100 UTC 28 September to 0500 UTC 29 September, and heavy snow fell near 0000 UTC. Each section of Fig. 4.11 correctly diagnosed that the later period of strong ageostrophic southeasterlies (after 1000 UTC 29 September) would affect primarily the middle and upper-troposphere,



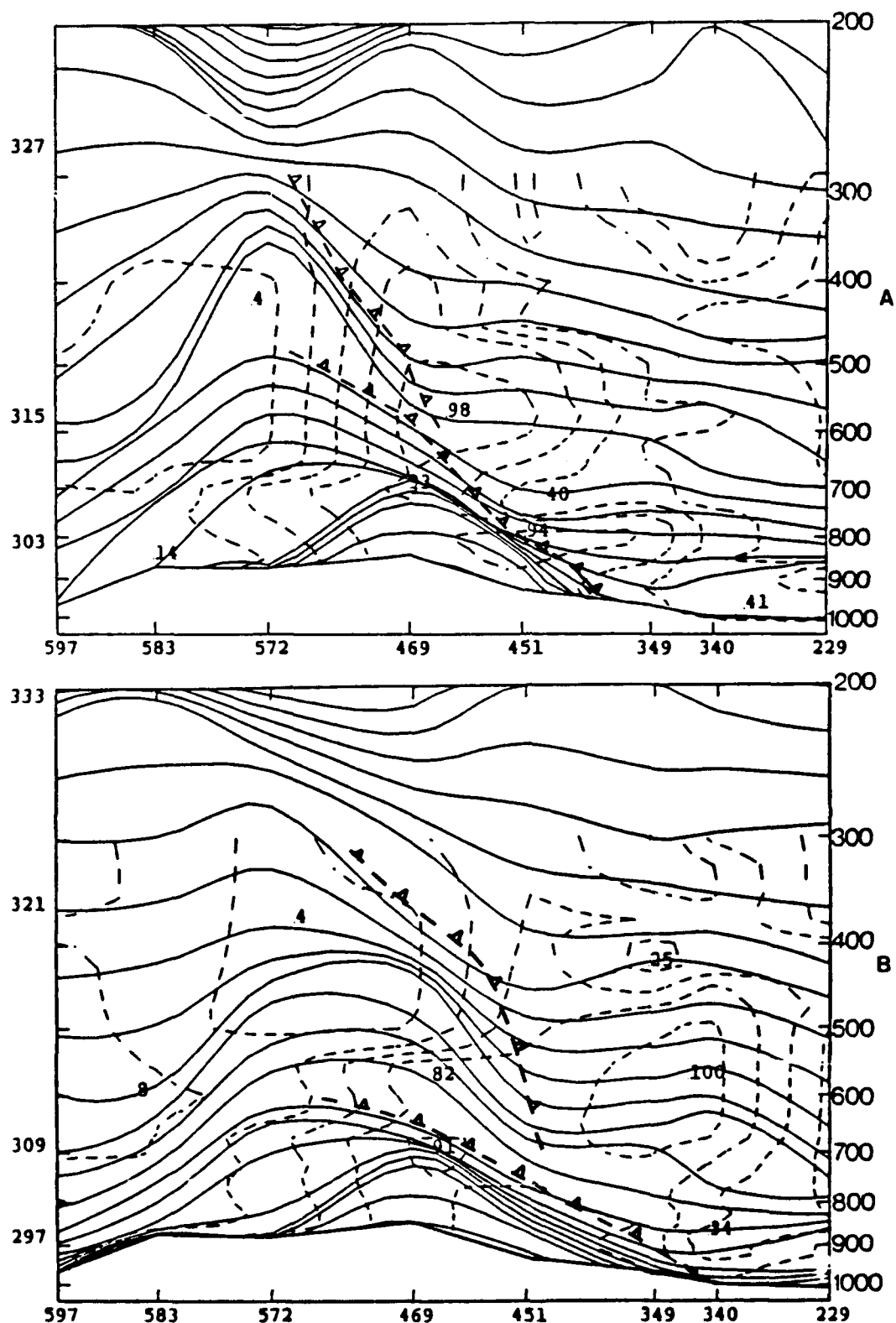


Figure 4.8. West-northwest-to-east-southeast cross-sections of potential temperature (solid) and relative humidity (dashed) for 0000 UTC 29 September 1985 (a) and 1200 UTC 29 September 1985 (b). Observing sites are shown by WMO number (with '72' missing): Medford, OR -- 72597; Winnemucca, NV -- 72583; Salt Lake City, UT -- 72572; Denver, CO -- 72469; Dodge City, KS -- 72451; Monett, MO -- 72349; Little Rock, AR -- 72340; Centreville, AL -- 72229.

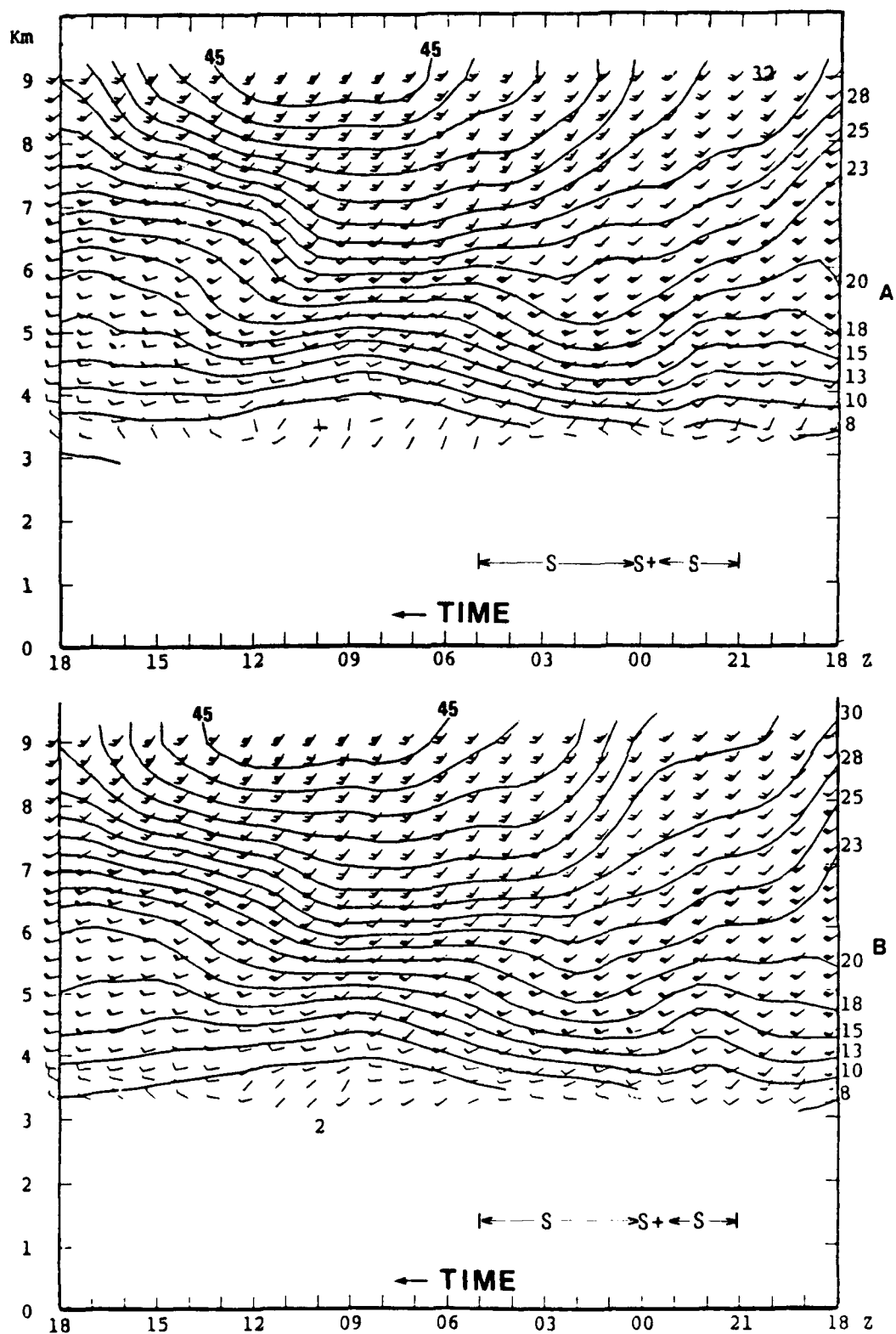


Figure 4.9. Time-height sections of mean profiler winds beginning at 1800 UTC 29 September 1985 (right). Isotachs are at 2.5 m/s intervals. (a) Two-profiler mean. (b) Three-profiler mean.

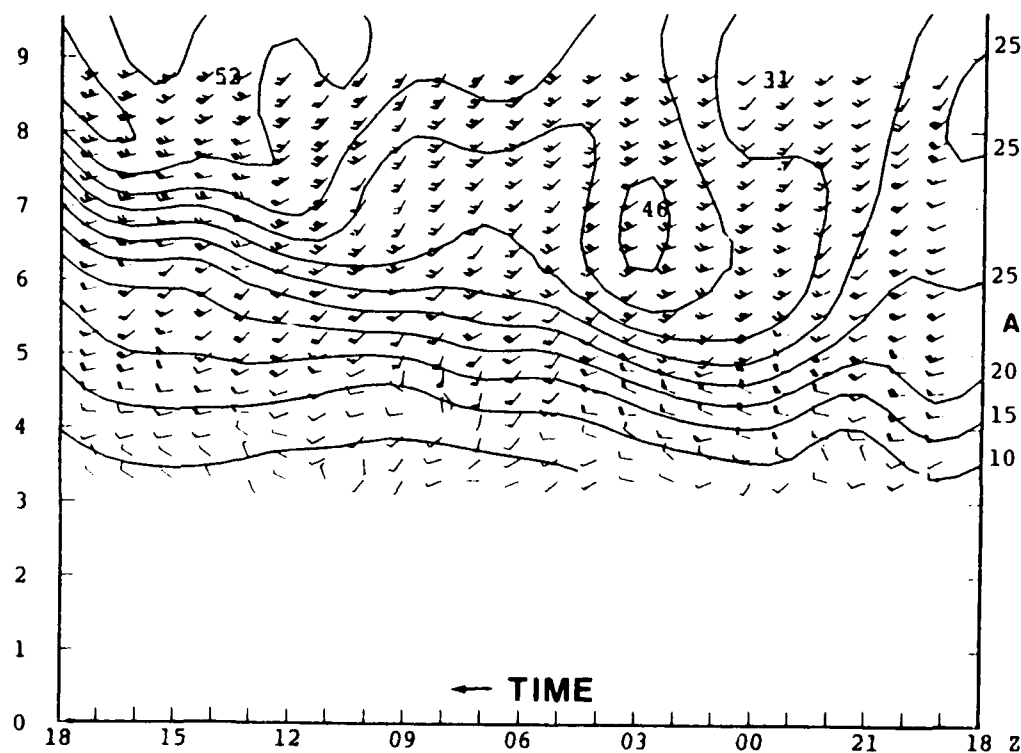
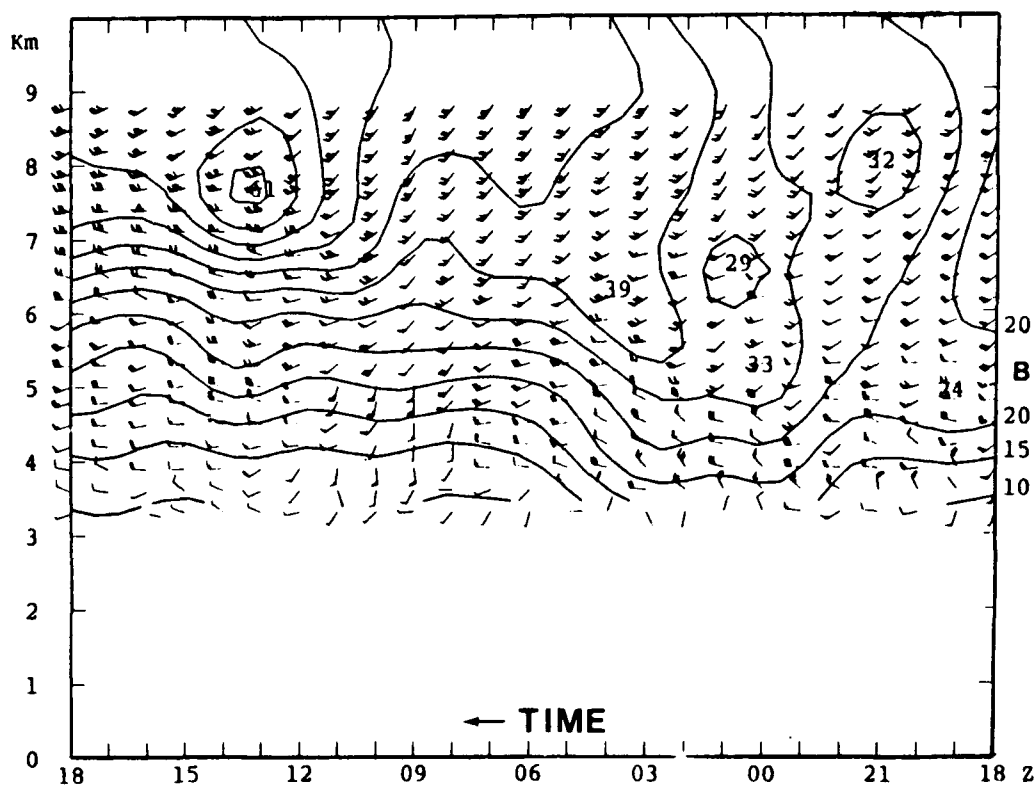


Figure 4.10. Time-height sections of profiler-derived geostrophic winds, beginning at 1800 UTC 29 September 1985 (right). Isotachs are at 5 m/s intervals. (a) Two-profiler calculations. (b) Three-profiler calculations.

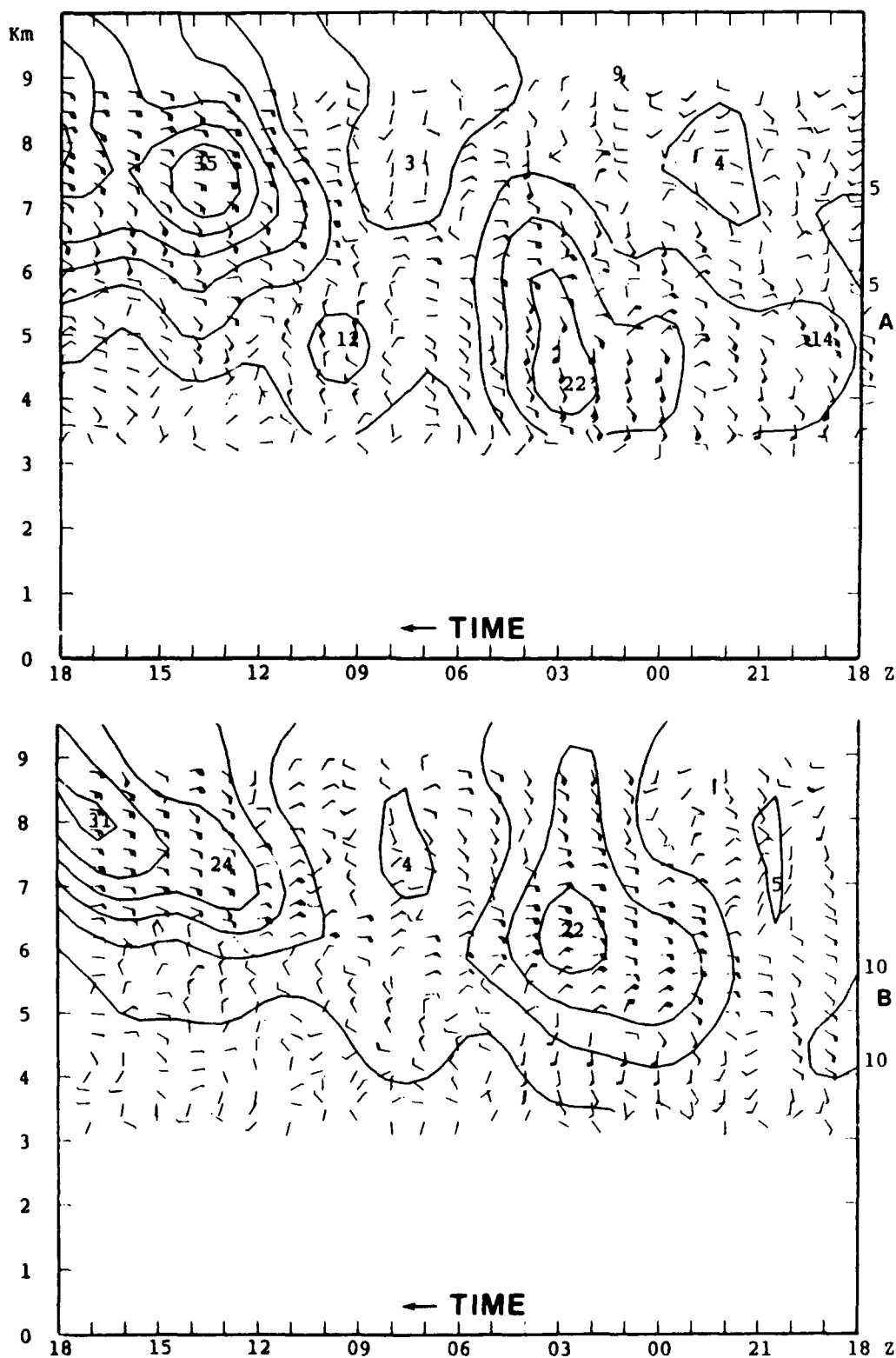


Figure 4.11. Time-height sections of profiler-derived ageostrophic velocities, beginning at 1800 UTC 29 September 1985 (right). Isotachs are at 5 m/s intervals. (a) Two-profiler calculations. (b) Three-profiler calculations.

thereby being drier and less likely to induce precipitation. The two-profiler diagnosis might have an edge in that the southerlies are stronger and occur lower than in the 3-profiler diagnosis. However, the 3-profiler technique shows stronger easterly ageostrophic components, which seem to correspond better to the timing of the moderate to heavy snow event in this case.

Figure 4.12 shows time-height sections of 2-profiler and 3-profiler kinematic vertical velocities. Both sections show two periods of ascent, with the 3-profiler diagnosis perhaps relating somewhat better to the precipitation observations.

Figure 4.13 shows time-height sections of the Q-vector forcing of ageostrophic circulations. Again, each section shows two periods of ascent. The 2-profiler diagnosis focuses better on the time of heaviest precipitation, but it must be concluded that the moderate precipitation was treated better by the 3-profiler diagnosis. In the latter, ascent would be present by 2100 UTC, since the circulation about the -200 isopleth would be clockwise.

The very preliminary conclusion that can be drawn from these two case studies is that 2-profiler calculations can give quite meaningful results when the front happens to be oriented almost normal to the baseline. Three-profiler calculations performed in such a situation are not too different from those using two profilers. In each case, ageostrophic velocities and Q-vector-derived circulations seemed to give a diagnostic signal that was better correlated to the significant weather than did the kinematic vertical velocity. Overall, a gratifying result is that hourly wind profiler velocities can be used to compute fields that have diagnostic value regarding mesoscale weather events.

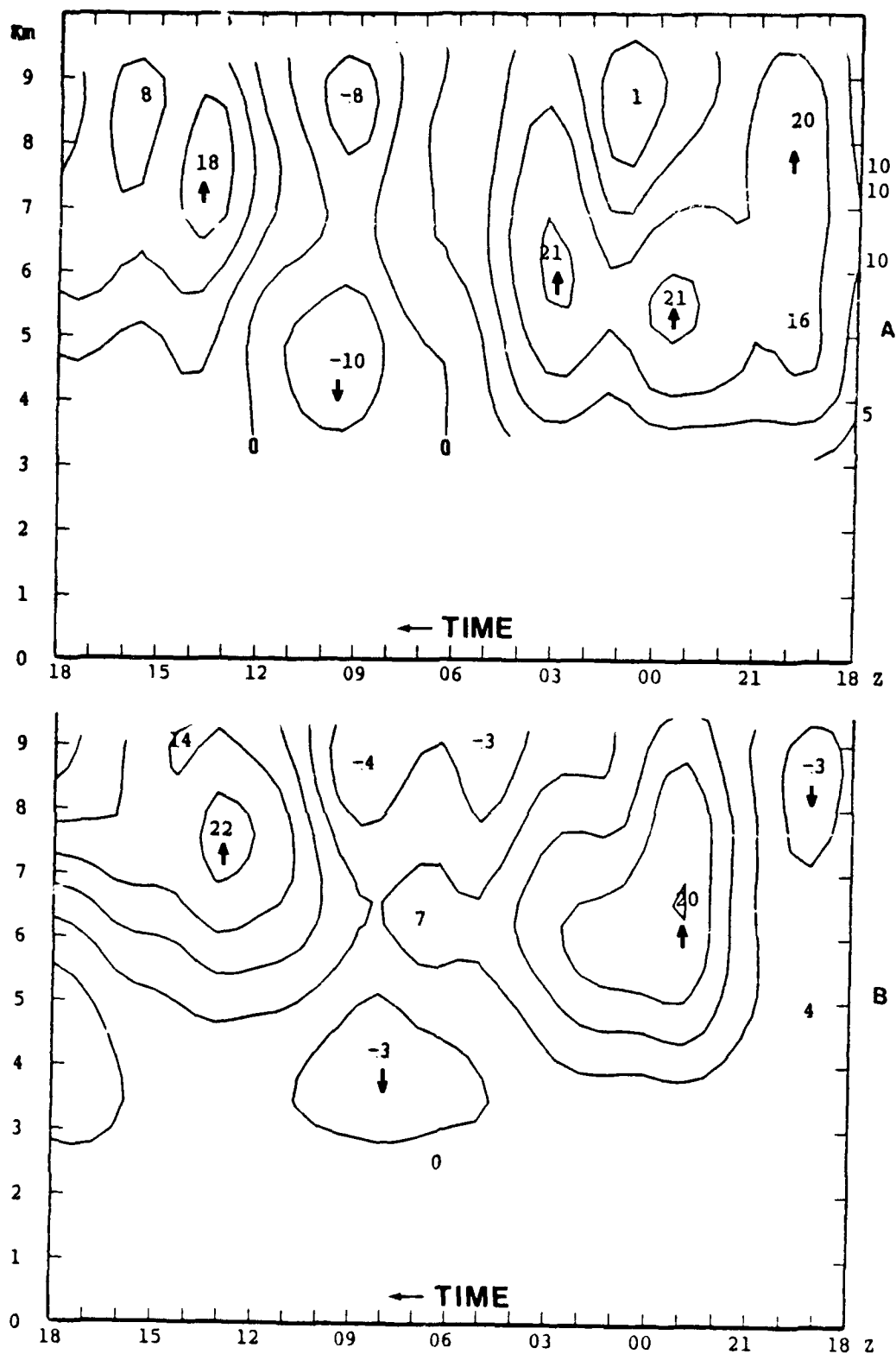


Figure 4.12. Time-height sections of profiler-derived kinematic vertical velocities, beginning at 1800 UTC 29 September 1985 (right). Isotachs are at 5 cm/s intervals. (a) Two-profiler calculations. (b) Three-profiler calculations.

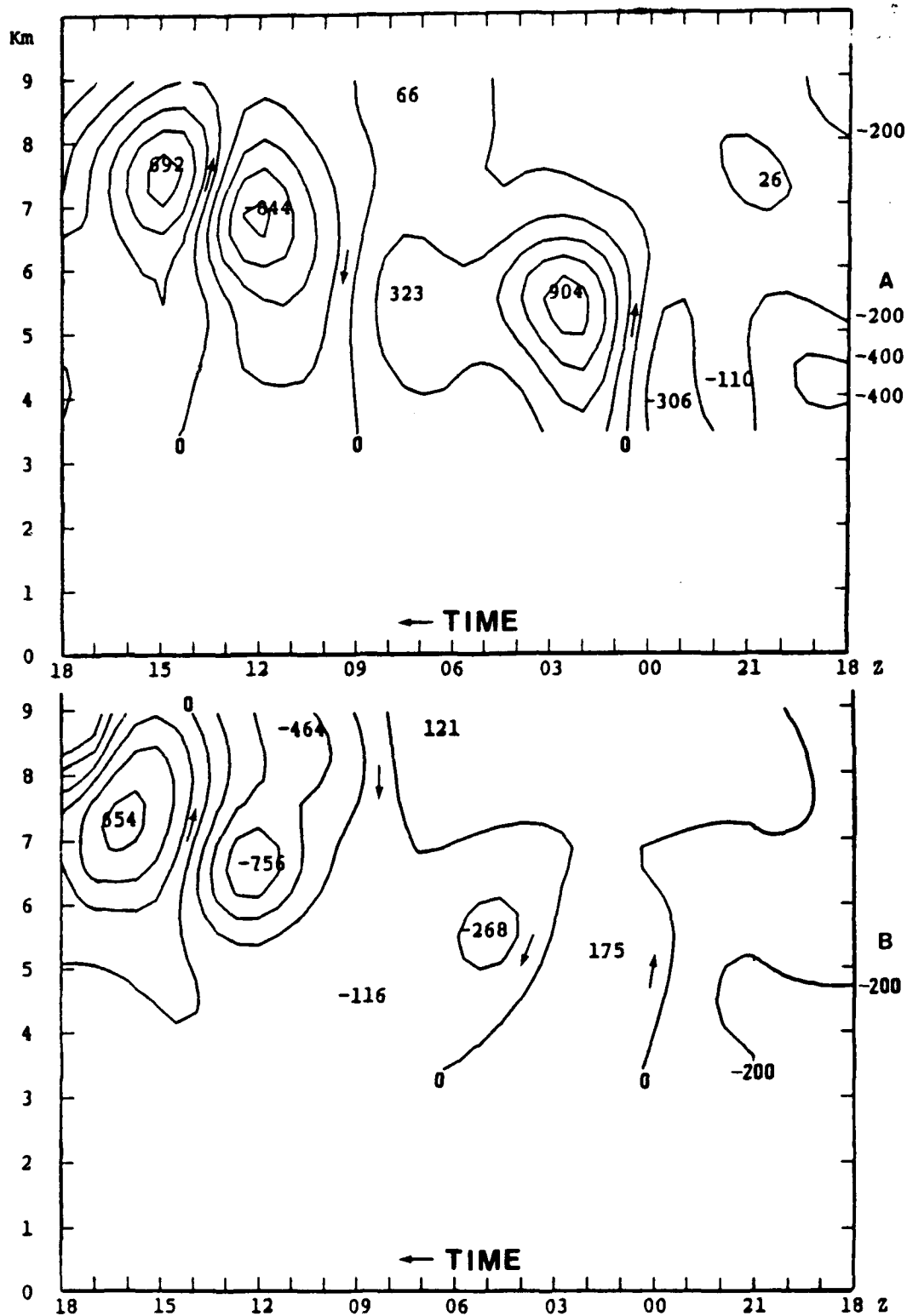


Figure 4.13. Time-height sections of Q-vector forcing (intervals of  $200 \times 10^{-8} \text{ s}^{-2}$ ), beginning at 1800 UTC 29 September 1985 (right). Arrows indicate direction of inferred ageostrophic circulations. (a) Two-profiler calculations. (b) Three-profiler calculations.

## 5. CONCLUDING REMARKS

A number of analysis techniques were examined during the course of the research funded by AFGL. Some of the key techniques are critiqued briefly here.

Time-Height Sections of Total Winds--These are most useful when the background flow is weak or moderate and the magnitude of the velocity variations associated with the travelling mesoscale disturbances is comparable to that of the background flow. In such situations, wind shifts, wind maxima and minima, and patterns of direction variations can be inspected visually and yield useful diagnostic information. By monitoring the trends of wind direction in conjunction with general estimates of cyclone or anticyclone movement, it is possible to infer where the centers of cyclones and anticyclones are passing relative to the profiler site (e.g., to its north or south).

Time-Height Sections of Perturbation Winds--When background flow is strong, or when mesoscale disturbances are weak, removal of the background velocity can reveal coherent patterns of wind variations that reveal mesoscale structure; whereas the variations may appear to have been noise on the total wind display. Mesoscale precipitation events or bands are often associated with modest strengthening of the southerly or easterly wind component, and can be highlighted using this technique.

Time-Height Sections of Relative Winds--In this technique a single velocity is subtracted from all levels; namely, the propagation velocity of the mesoscale weather feature of interest. Vertical wind shears are more evident in this technique than in



the perturbation velocity sections, in which the mean velocity was subtracted, level by level. Knowledge of the prevailing wind shear, together with the vertical velocity, can give insights into air and precipitation trajectories. Relative streamlines of the two-dimensional (x-z) flow are useful for depicting rainband circulations.

Horizontal charts--The addition of profiler-measured winds to synoptic upper-level charts often yields an improvement in the analysis of the location of fronts, trough lines, and ridge axes.

Horizontal Charts with Time-Space Conversion--The use of time-space conversion of hourly profiler winds for periods of up to +/- 6h appears to have value for mesoscale analysis of traveling meso-alpha-scale features. For meso-beta-scale features, shorter measurement intervals are needed, along with shorter windows of steady-state assumption.

Vertical Velocities--A number of studies have shown that profiler-measured vertical velocities, when processed carefully and appropriately, can yield useful information on the meteorological phenomenon of interest. Care must be taken to remove the effects of turbulence and gravity waves which often contaminate high-temporal-frequency measurements, and the effects of precipitation when using UHF-measured velocities.

Thermal Wind-Assumed Temperature Gradients--Vertical shears of the observed winds can generally be used to gain a qualitative sense of the temperature gradient at levels above the friction layer. However, ageostrophic effects (that are implicitly ignored) can greatly reduce the correlation between the observed shears and the geostrophic shears.

Q-Vector Forcing Streamfunctions--Preliminary studies by Knowlton (1987) showed these to be of value. Further evaluation is merited.

Kinematic Vertical Velocities; Other Kinematic Quantities--Carlson (1987) and Knowlton (1987) showed that kinematic quantities derived from multi-profiler networks could yield tremendous amounts of mesoscale information. However, when the mesoscale systems are smaller than the profiler triangle (for example) the kinematic quantities cannot fully resolve the magnitudes of the weather system's velocity perturbations, circulations, or divergences. Two-profiler kinematic vertical velocities appear to have some value when used in situations where the phenomenon of interest is largely two-dimensional, such as fronts and rainbands.

The full benefit of wind profilers is yet to be realized. The deployment of a network of wind profilers across the Midwest will allow for real-time analysis improvements using the techniques described above, and these improved diagnoses should lead to improvements in nowcasting and very-short-term forecasting. Further, the insertion of time-height series of data from the profiler network into mesoscale numerical weather prediction models, via four-dimensional data assimilation, will allow for impressive improvements in mesoscale short-term forecasting. If, in addition, efficient real-time and research use can be made of the wind measuring and profiling capabilities of the NEXRAD network of weather radars, the next decade promises to be one of the most exciting in the history of meteorology.

## ACKNOWLEDGEMENTS

Development of the Penn State VHF Doppler wind profilers has been in progress for more than 7 years, under the direction of Prof. Dennis W. Thomson. Funding for the instrumentation development and deployment program has been provided by Dept. of Defense University Instrumentation Research Grants AFOSR-83-0275 and AFOSR-85-0067, by the Office of Naval Research (N00014-86-K-0068) and by the Pennsylvania State University. Success of the instrumentation program would not have been possible without the outstanding technical assistance of the Profiler Development Group at NOAA-ERL-WPL: Richard Strauch, Ken Moran, and Dave Merritt. The control and signal processor and the data processor and executive controller of the radar were constructed by Bob Peters, Dick Thompson, and Jim Breon of Penn State, in consultation with WPL and using WPL concepts, designs, and software. Tycho Technology, Inc., manufactured the transmitters, receivers and antennae for these systems. Analyses of the VHF and UHF wind profiler data in this report has been supported by the Air Force Geophysics Laboratory under Contract F19628-86-C-0092.

## REFERENCES

- Carlson, C.A., 1987a: Kinematic quantities derived from a triangle of VHF Doppler wind profilers. M.S. Thesis, The Pennsylvania State University, University Park, PA, 136pp.
- Carlson, C.A., 1987b: Kinematic quantities derived from a triangle of VHF Doppler wind profilers. AFGL-TR-87-0265, Air Force Geophysics Lab, Hanscom AFB, MA, 136pp. ADA207542

- Carlson, C.A. and G.S. Forbes, 1989: A case study using kinematic quantities derived from a triangle of VHF Doppler wind profilers. J. Atmos. Oceanic Tech., 6, 769-778.
- Carlson, T.N., 1980: Airflow through midlatitude cyclones and the comma cloud pattern. Mon. Wea. Rev., 108, 1498-1509.
- Dye, T.S., 1990: Structure and circulation of mesoscale rainbands deduced from a VHF and UHF Doppler wind profiler. M.S. Thesis, The Pennsylvania State University, 187pp.
- Forbes, G.S., R.A. Anthes, D.W. Thomson, 1987: Synoptic and mesoscale aspects of an Appalachian ice storm associated with cold-air damming. Mon. Wea. Rev., 115, 564-591.
- Forbes, G.S. and R. Bankert, 1987: Satellite imagery and conceptual models in mesoscale forecasting. Proc., Symposium on Mesoscale Analysis and Forecasting, Vancouver, Canada, ESA SP-282, 251-261.
- Forbes, G.S., R.L. Scheinhart, E. Araujo, W.D. Lottes, and J.J. Cahir, 1984: Short-term forecasting using a REMOS approach. Proc., Nowcasting-II Symposium, European Space Agency Special Publication 208, 379-384.
- Forbes, G.S. et. al, 1989: Analysis of significant weather on meso-alpha scales using conventional and remotely-sensed data -- exploratory studies. Final Report on Contract F19628-85-K-0011, The Pennsylvania State University,
- Fujita, T.T., 1955: Results of detailed studies of squall lines. Tellus, 7, 405-436.
- Fujita, T.T., 1963: Analytical mesometeorology: A review. Meteor. Monogr., 5(27), 77-125.
- Keyser, D. and T.N. Carlson, 1984: Transverse ageostrophic circulations associated with elevated mixed layers. Mon. Wea. Rev., 112, 2465-2478.
- Knowlton, L.W., 1987: Kinematic diagnoses of frontal structure and circulations derived from two and three-station VHF Doppler wind profiler networks. M.S. Thesis, The Pennsylvania State Univ., 84pp.
- Lee, M.-T., 1990: Analysis of mesoscale substructure of cyclones and jet streams, using time-space conversion of VHF Doppler wind profiler and rawinsonde data. M.S. Thesis, The Pennsylvania State University, 189pp.
- Miller, J.E., 1948: On the concept of frontogenesis. J. Meteor., 5, 169-171.

- Neiman, P., 1987: Wind profiler-derived temperature gradients and advections. M.S. Thesis, The Pennsylvania State University, University Park, PA, 214 pp.
- Thomson, D.W. and S.R. Williams, 1990: Analysis of comparative wind profiler and radiosonde measurements. Preprints, 10th Int'l. Geosc. Rem. Sensing Symp., College Park, MD, pp. 537-540.
- Weldon, R.B., 1979: Cloud patterns and the upper air wind field. AWS/TR 79/003, Air Weather Service, United States Air Force, 80pp.

## APPENDIX 1

## PROJECT PERSONNEL

The following personnel were supported, in part, by AFGL Contract  
F19628-86-C-0092:

John J. Cahir  
Catherine A. Carlson  
Timotjy Dye  
Gregory S. Forbes  
Larry Knowlton  
Ming-Tzer Lee  
Paul Neiman  
Arthur A. Person  
Dennis W. Thomson  
Scott Williams

## APPENDIX 2

## REPORTS AND PUBLICATIONS PREPARED

- arlson, C.A., 1987a: Kinematic quantities derived from a triangle of VHF Doppler wind profilers. M.S. Thesis, The Pennsylvania State University, University Park, PA, 136pp.
- arlson, C.A., 1987b: Kinematic quantities derived from a triangle of VHF Doppler wind profilers. AFGL-TR-87-0265, Air Force Geophysics Lab, Hanscom AFB, MA, 136pp. ADA207542
- arlson, C.A. and G.S. Forbes, 1989: A case study using kinematic quantities derived from a triangle of VHF Doppler wind profilers. J. Atmos. Oceanic Tech., 6, 769-778.
- ye, T.S., 1990: Structure and circulation of mesoscale rainbands deduced from a VHF and UHF Doppler wind profiler. M.S. Thesis, The Pennsylvania State University, 187pp.
- orbes, G.S., 1986: Examples of mesoscale structures and short-term wind variations detected by VHF Doppler radar. Workshop on Technical Aspects of MST Radar, Aguadilla, Puerto Rico, 1985. Middle Atmosphere Handbook, 20, 17-29. [SCOSTEP Secretariat, Univ. of Illinois, 1406 Green St., Urbana, IL 61801]
- orbes, G.S. and R. Bankert, 1987: Satellite imagery and conceptual models in mesoscale forecasting. Proc., Symposium on Mesoscale Analysis and Forecasting, Vancouver, Canada, ESA SP-282, 251-261.
- owilton, L.W., 1987: Kinematic diagnoses of frontal structure and circulations derived from two and three-station VHF Doppler wind profiler networks. M.S. Thesis, The Pennsylvania State Univ., 84pp.
- Lee, M.-T., 1990: Analysis of mesoscale substructure of cyclones and jet streams, using time-space conversion of VHF Doppler wind profiler and rawinsonde data. M.S. Thesis, The Pennsylvania State University, 189pp.
- veiman, P., 1987: Wind profiler-derived temperature gradients and advections. M.S. Thesis, The Pennsylvania State University, University Park, PA, 214 pp.
- Thomson, D.W., 1988: New perspectives on atmospheric structure and dynamics. Earth and Mineral Sciences, 57(1), 1-6.

Williams, S.R. and R.M. Peters, 1986: The Penn State Doppler network progress report. Workshop on Technical Aspects of MST Radar, Aguadilla, Puerto Rico, 1985. Middle Atmosphere Handbook, 20, 339-341. [SCOSTEP Secretariat, Univ. of Illinois, 1406 Green St., Urbana, IL 61801]

Williams, S.R. and D.W. Thomson, 1984: An evaluation of errors observed in the measurement of low wind velocities.



## APPENDIX 3

## ACCURACY OF PROFILER MEASUREMENTS

## REPRINT OF

Thomson, D.W. and S.R. Williams, 1990: Analysis of comparative wind profiler and radiosonde measurements. Preprints, 10th Int'l. Geosc. Rem. Sensing Symp., College Park, MD, pp. 537-540.

## Analysis of Comparative Wind Profiler and Radiosonde Measurements

Dennis W. Thomson  
Scott R. Williams

Department of Meteorology  
Penn State University  
University Park, PA 16802

### ABSTRACT

During the last three years a variety of wind profiler "calibration" experiments were performed at Penn State University. These included a variety of profiler-radiosonde intercomparison measurements, multiple tracking and analysis of the same sondes, profiler measurements with parallel antenna beams and, finally, comparisons with a conventional 10 cm Doppler radar. The results demonstrate that the primary source of uncertainty in earlier published comparative studies was the result of the time dependent physical separation between the profilers being evaluated and the reference radiosonde balloons. We estimate the accuracy of profiler-derived velocities to be better than  $\pm 1 \text{ m sec}^{-1}$  and recommend that consideration be given to using Doppler radar, optical or acoustic systems rather than radiosondes as standards for atmospheric wind measurements.

### INTRODUCTION

Questions regarding the precision, accuracy and representativeness of wind profiler measurements have been sporadically researched for more than a decade. However, although a number of "calibration" experiments comparing profiler with raob-derived winds have been performed [5, 2, 9, 12, 1, 3, 7, 6, 8] no single one of these experiments has been able to resolve all of the outstanding questions.

It is precisely because measurements made with remote sensing Doppler radars are so different from those obtained with balloon-borne radiosondes that calibration by comparison is problematical. Profiler-measured winds are derived by spectrally processing thousands (typically  $> 75,000$ ) of independent samples of a relatively noisy signal from a stationary volume ( $\sim 10^6$  to  $10^8 \text{ m}^3/\text{range gate}$ ) through which the radar signal scattering refractive inhomogeneities are translated at a wind speed dependent rate. In contrast radiosondes provide only a series of "snapshots" of the winds along the particular trajectory taken by the balloon. There is no guarantee that an individual radiosonde datum will be a representative sample.

The spectral estimates from which individual profiler velocity values are extracted are typically 30 to 90 sec averages. Typical sampling intervals for digital radiosondes range from 5 to 30 sec. However, due to the methods used to analyze the balloon's changing position winds are rarely reported more frequently than once or twice per minute. Thus, the change in altitude

between such samples from a radiosonde ascending at 3 to  $5 \text{ m sec}^{-1}$  corresponds roughly to the maximum vertical resolution of a profiler;  $\sim 100$  and  $300 \text{ m}$  for UHF and VHF systems, respectively.

Profiler measurements of the radial velocities are derived from beams which are typically separated by about  $15^\circ$ . Beam separation is, thus, a function of altitude but the effective horizontal spatial resolution also depends upon the average wind speed at the altitude of interest. Recent articles discussing multibeam profiler measurements include references [10] and [14]. The uncertainties resulting from the separated beams are not usually considered to be a problem.

However, atmospheric motions such as those associated with convective or wave motions can also be quite variable on much larger spatial scales than those corresponding to the separated beams. The effective spatial scales over which profiler signals are averaged due to continuous renewal by the wind of the volume being sampled also correspond to the range of distances, 10 to  $100 \text{ km}$ , typically traversed by an ascending radiosonde.

In this paper we will show that the variability of the atmosphere is such that if one is interested in comparing profiler-raob winds, or in constructing a database with combined (integrated) profiler and raob data, it is necessary to consider the separation between the sample locations. First, we present a series of measurements which help to define the operational precision of radiosonde-measured winds. A variety of raob-based and profiler-derived winds are then compared. Finally we show measurements obtained using two colocated, parallel, like pointed antennas. The results of all these comparisons clearly show that calibration experiments can be seriously compromised not only as a consequence of undersampling by raobs but also by uncertainties which result from the varying separations in the spatially inhomogeneous atmosphere.

### DESCRIPTION OF THE PENN STATE EXPERIMENTS

During a series of optical and radar propagation-related experiments conducted principally in April and May, 1986 near State College, PA winds were measured with both Penn State's "Shantytown" VHF (50 MHz) wind profiler and two LORAN-based raob wind profiling systems; one belonging to Air Force Geophysical Laboratory (AFGL) and the second to the Naval Postgraduate School (NPS). During these experiments a total of 35 radiosondes were launched. During 16 soundings profiler winds were recorded at 5 min or

shorter intervals. During 14 of the soundings the same balloon was simultaneously and independently tracked using both the AFGL and NPS analysis and recording systems.

All of the above radiosondes were launched from the lab on the roof of the Walker Building on campus. Penn State's Shantytown profiler is located about 16.4 km south of the Walker Building. Using the high resolution mode ( $Z = 290$  m) individual wind profiles were usually logged with the profiler for 90 sec at 5 min intervals. The average ascent rate of the radiosonde balloons was about  $5 \text{ m sec}^{-1}$ . Thus, in the time required for the balloon to reach 8 km (max. range in the profiler's high resolution mode), about 5 separate wind profiles were logged with the radar. Since clear skies were a necessary condition for the optical measurements, wind directions during the individual experimental runs were generally northwesterly. Fig. 1 shows the radar and balloon launch sites and a composite map of these raob trajectories.

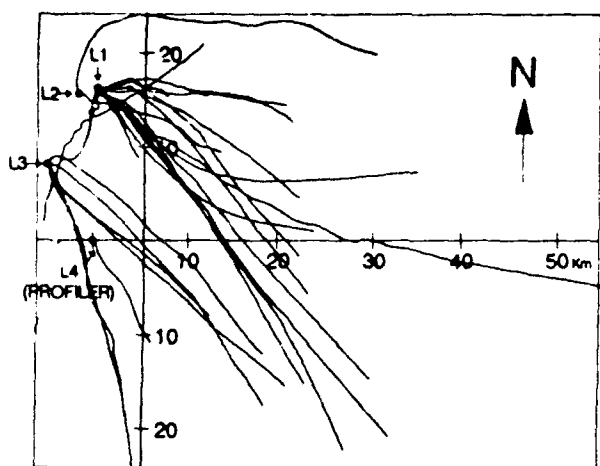


Figure 1. Trajectories for all balloons launched in 1986 and 1988. All 1986 launches were from L1, Walker Bldg. on campus. Three additional launch sites were used in 1988 so that the balloons would approach L4, the Shantytown profiler site.

The next set of profiler-raob comparison measurements was completed on selected days between 2 August and 14 October 1988. During this period a total of 16 raobs were launched. The purpose of these soundings was to gather additional comparative values for minimal separations between the profiler volume and the balloon's changing location. In order to do this the raobs were launched on selected days at four different sites which were nominally upwind of the profiler. The trajectories for these balloons are also shown on Fig. 1.

During the 1988 experiments our UHF profiler was set up at its Circleville Farm location which is approximately 15 km N of the VHF Shantytown site. The next section of this paper also includes the results of 744 hours ( $\sim 1$  month) of winds at one altitude ( $\sim 1.8$  km agl) measured concurrently with the UHF and VHF profilers.

Yet another additional set of comparative values consisted of winds measured independently with the UHF profiler and NCAR's CP-2 10 cm Doppler radar during the 1986 MIST project [11].

Finally in an attempt to absolutely minimize the possibility of variability associated with separated

measurement volumes, during July 1989 we set up the two Co-Co antennas for the UHF profiler side by side with the same polarization and pointing angle. With the antennas in this configuration measurements of the wind velocity along the antenna azimuthal pointing direction were made from 21Z on 14 July to 5Z on 16 July 1989.

## RESULTS

Table I includes not only the results of our measurements but also values reported in references [6], [5], and [11]. Insofar as possible Table I includes values of the relevant standard deviations, bias's and correlation coefficients.

Table I. Direction and speed statistics from assorted published experiments and the Penn State measurements.

Type (Ref)	Stand. Dev.	Bias	Corr. Corr.
GMD vs. GMD (6)	6-7.7 dg. 1.4-3.1 m/s		
AFGL LORAN vs. NPS LORAN	1.90 dg. 1.20 m/s	-0.31 dg. 0.15 m/s	0.99 0.94
SUNSET PROF. vs. GMD (5)	5.0 m/s		0.84
NSSL PROF. vs. GMD (6)	3.6 m/s		
PSU PROF. vs. Raobs at PSU	4.61 dg. <sup>1</sup> 3.31 m/s	1.45 dg. <sup>1</sup> -0.00 m/s	0.98 <sup>1</sup> 0.95
PSU 50 MHz vs. PSU 400 MHz	22.63 dg. 2.88 m/s	-1.23 dg. 1.26 m/s	0.88 0.79
PSU 400 MHz vs. NCAR CP-2 (11)	0.94 m/s	-0.29 m/s	0.90
UHF ANT1 vs. UHF ANT2	0.91 m/s	0.04 m/s	0.95

<sup>1</sup> LORAN sondes only

**Raob-Raob Comparisons**—In order to evaluate the relative precision of the radiosonde-measured winds we first constructed a scatter diagram (Fig. 2) of the wind values which were derived from seven profiles which included simultaneous tracking of a single sonde with the AFGL and NPS systems. Measured speeds ranged from 3.5 to  $48.5 \text{ m sec}^{-1}$ . Values which departed by more than  $\pm 2 \sigma$  from the first regression fit were rejected. With few exceptions these data,  $\sim 12\%$  of the total, could be clearly identified to be the consequence of substandard LORAN signals. The correlation coefficient for linear regression was  $r = 0.994$ . We were unable to determine the source of a  $0.42 \text{ m sec}^{-1}$  bias. Only 144 points are shown on Fig. 2 because it illustrates only the values at about 500 m height intervals.

**Profiler-Raob Comparisons**—Fig. 3 shows the scatter diagram for our profiler versus raob-measured speeds. Speed values for this comparison were chosen by first applying a 7-point triangular filter to the time series of raob wind values. This was done in order to produce vertical smoothing which might be comparable to the

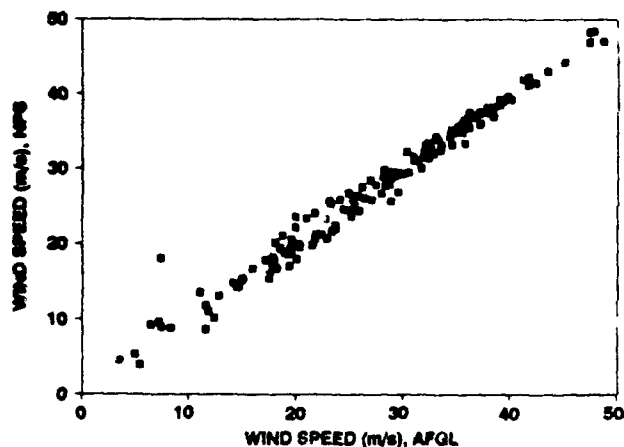


Figure 2. Scatter plot of 144 wind speeds recorded during seven launches. Each balloon was concurrently tracked using separate LORAN signal receivers and processors.

"averaging" associated with the 290 m vertical resolution of the profiler. Individual wind values were then extracted at the heights corresponding most closely ( $\pm 20$  m) to the midpoint of each profiler range gate. Again values departing by more than  $\pm 2\sigma$  were rejected ( $\sim 13\%$ ). The rejected data points in this case were such that if they had been subjected to consensus checks, they would not have been used in calculating, for example, an hourly wind profile. Although the correlation coefficient, 0.93, might appear to be satisfactory, we questioned the source of the evident scatter.

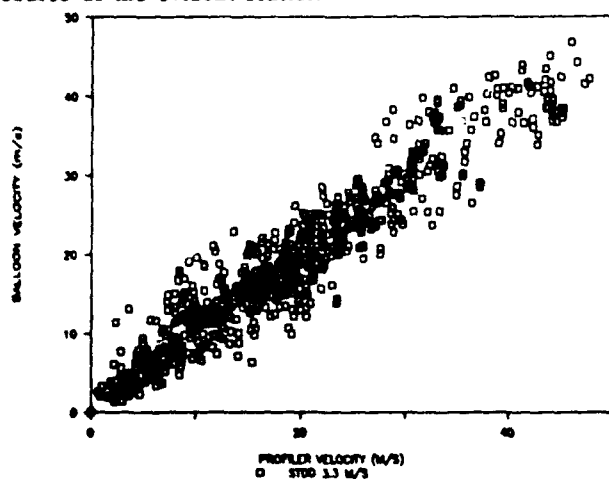


Figure 3. Scatter plot comparing profiler and raob-measured wind speeds. Database compiled from all 1986 and 1988 launches included 817 values.

**Percentile Absolute Speed Differences**--Previous comparative studies had reported only rms or standard deviations of raob-raob or raob-profiler differences. Furthermore, most of the reported measurements were made for relatively light wind speeds. In order to provide a measure of performance which would not be dependent upon relative numbers of high and low wind speed values we chose, in addition, to calculate the percentile of the absolute speed difference.

$$\text{PASD} = \frac{U_2 - U_1}{U_1} \times 100 \quad (1)$$

The mean PASD for all the wind speed values derived from the seven simultaneously tracked balloons was 4.1%. This is representative, we believe, of the precision which can be expected of the LORAN-based radiosondes which are commonly in use today. Using the Doppler frequency-measuring profiler with its stationary beam as a reference, the mean PASD for all the wind speed values shown in Fig. 3 was calculated to be 15.8%. Was this large PASD primarily the consequence of temporal fluctuations combined with undersampling by the raobs or a result of spatial or temporal variability in the winds?

**Dependence Upon Separation**--To examine the dependence of the PASD on profiler-raob separation ( $s$ ) raob trajectories were calculated to establish the position of each balloon with respect to the profiler for each wind speed datum. Fig. 4 was constructed by stratifying the PASD values into various separation classes (1 km bins to 23 km, 4 km bins to 38 km, and a final bin for values  $>38$  km). In order to establish whether or not the PASD's would change at even larger separations we added the following additional data to Fig. 4. For  $s = 145$  km the mean PASD was calculated for differences between hourly winds measured with our Shantytown and Crown PA profilers during Jan, 1987. For  $s = 228$  and 257 km, respectively, the winds at 12 hr intervals during Jan 1987 from the Shantytown profiler and the National Weather Service (NWS) upper air soundings from Pittsburgh, PA and Buffalo, NY, were used. Finally, for the largest nearly synoptic-scale separation,  $s = 297$  km, the PASD values were calculated using the January 1987 NWS upper air data from Pittsburgh and Buffalo.

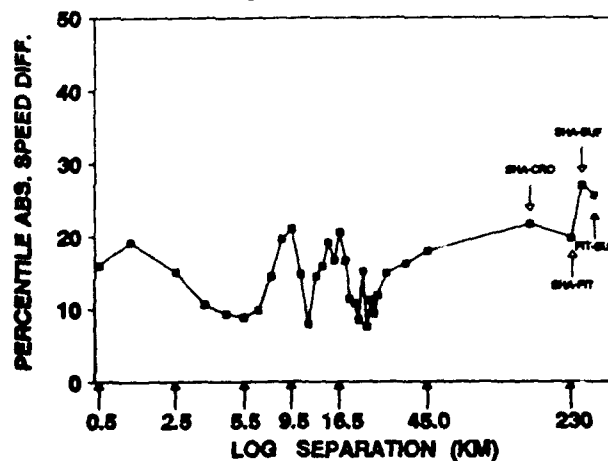


Figure 4. Percentile absolute speed difference, PASD, as a function of the log of the separation between locations of measurement. Unlabeled points are grouped means from the 1986 and 88 launches near Penn State. Labeled points include one month of hourly values from the Shantytown and Crown VHF profilers, one month of 12 hourly Shantytown profiler winds compared with NWS operational Pittsburgh and Buffalo soundings, and one month of 12 hourly operational soundings from Pittsburgh and Buffalo.

**Temporal Variability**--Ideally one would like to be able to discriminate between those contributions to the variance resulting from spatial gradients and those associated with temporal changes. We performed the parallel beam experiment to evaluate how well the velocities measured

in one beam would correspond to those in a second. Fig. 5 shows a 3 hour time series of winds at 1.5 km agl recorded with antennas 1 and 2. The velocities derived from the separate beams track one another closely but also clearly show the natural variability of the winds. The time labeled "onset of convection" (10:12 LT) we believe corresponded to the onset of cumulus convection at the measurement altitude. Such changes in velocity variability are also characteristic of boundary layer winds and the development of thermal "plume" convection. Fig. 6 shows the scatter diagram for the two antennas for the entire 33 hour measurement period. The standard deviation was  $0.91 \text{ m sec}^{-1}$ . This result is comparable to that obtained by Walikis & Forbes [11] who compared velocities measured with our UHF profiler with those obtained with NCAR's CP-2 Doppler radar.

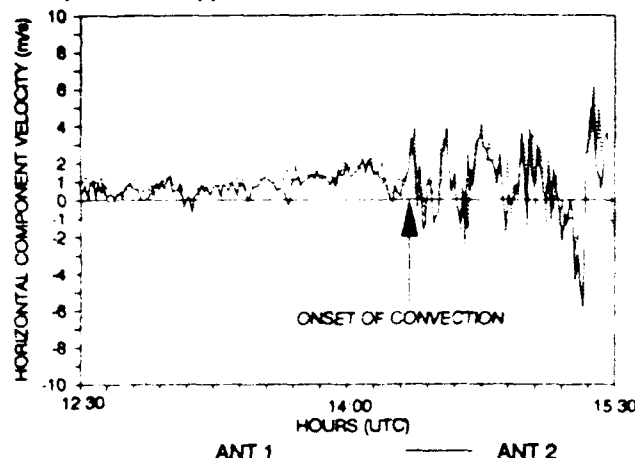


Figure 5. Example of time series (3 hours at 1 min resol.) velocities recorded on 14 July 1987 using the two co-located, like-oriented UHF antennas.

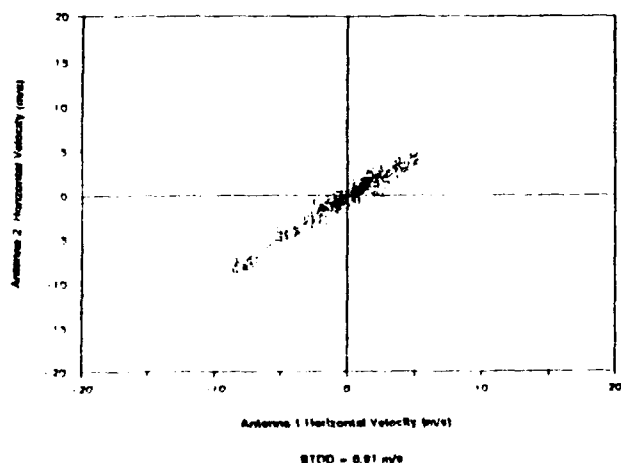


Figure 6. Scatter plot of horizontal velocities recorded with the 400 MHz UHF profiler in Gate 8 (1.5 km agl) using two co-located, like-oriented antennas. More than 2000 comparative values were recorded between 21Z July 14 and 5Z 16 July 1989.

## CONCLUSIONS

Our results indicate that the accuracy of profiler measured winds is substantially better than has been previously reported, less than  $\pm 1 \text{ m sec}^{-1}$ . The uncertainty in profiler-derived wind speeds and direction is clearly significantly less than the natural variability of the wind. Rather than using radiosondes which are highly prone to undersampling errors as a measurement "standard", we recommend that serious consideration should now be given to developing a standard for atmospheric velocity measurements which is based on analysis of signal Doppler frequency shifts. For that purpose profiling radar, lidar or sodar (or some combination thereof) systems could be used.

## ACKNOWLEDGEMENTS

This research was supported by ONR Contract No. N00014-86-5-0688. We gratefully acknowledge the assistance of AFGL and NPS for assistance with the 1986 raob measurements and Vaisala, Inc. (the Tycho Tech. Div. at Boulder, CO and K. Goss at Woburn, MA) for providing the system and sondes for the 1988 measurement program.

## REFERENCES

- [1] R.K. Crane, "Radar measurements of wind at Kwajalein", *Radio Sci.*, vol. 15, pp. 383-394, 1980.
- [2] W.L. Ecklund, et al., "Continuous measurements of upper atmospheric winds and turbulence using a VHF Doppler radar: preliminary results", *J. Atmos. Terr. Phys.*, vol. 41, pp. 983-944, 1978.
- [3] S.T. Fukao, et al., "Winds measured by a UHF Doppler radar and rawinsondes: comparisons made on twenty-six days (August - September 1977) at Arecibo, Puerto Rico", *J. Appl. Meteor.*, vol. 21, pp. 1357-1363, August 1982.
- [4] S.T. Fukao, et al., "VHF Doppler radar determination of the momentum flux in the upper troposphere and lower stratosphere: comparison between the three- and four-beam methods", *J. Atmos. Ocean. Tech.*, vol. 5, pp. 57-69, Feb. 1988.
- [5] J.L. Green, et al., "Studies of winds in the upper troposphere with a sensitive VHF radar", *Geophys. Res. Lett.*, vol. 2, pp. 19-21, 1975.
- [6] E.M. Kessler, "A look at profiler performance", in *Handbook of MAP, URSI/SCOSTEP Workshop on Technical and Scientific Aspects of MST Radar*, 1985, pp. 72-84.
- [7] M.F. Larsen, "Can a VHF Doppler radar provide synoptic wind data? A comparison of 30 days of radar and radiosonde data", *Mon. Wea. Rev.*, vol. 111, pp. 2047-2057, 1983.
- [8] T.R. Lawrence, et al., "A comparison of Doppler lidar, rawinsonde, and 915 MHz VHF wind profiler measurements of tropospheric winds", *NOAA Tech. Memo., ERL/WPL-130*, 1986.
- [9] J. Röttger, et al., "Remote sensing of the atmosphere by VHF radar experiments", *Naturwissenschaften*, vol. 65, pp. 285-296, 1978.
- [10] R.G. Strauch, et al., "The precision and relative accuracy of profiler wind measurements", *J. Atmos. Ocean. Tech.*, vol. 4, pp. 563-571, December 1987.
- [11] R.J. Walikis, and G. Forbes, "Retrieval of summertime raindrop size-concentration data using the Penn State VHF wind profiler", To be presented at IEEE International Geoscience and Remote Sensing Symposium, College Park, MD, May 20-24 1990.
- [12] J.M. Warnock, et al., "Comparison between wind profiles measured by Doppler radar and by rawinsonde balloons", *Geophys. Res. Lett.*, vol. 5, pp. 109-112, 1978.

## APPENDIX 4

## NOTES ON THE QUALITY CONTROL OF WIND PROFILER DATA

adapted from an unpublished manuscript

by Tim Dye

The Pennsylvania State University

May, 1990

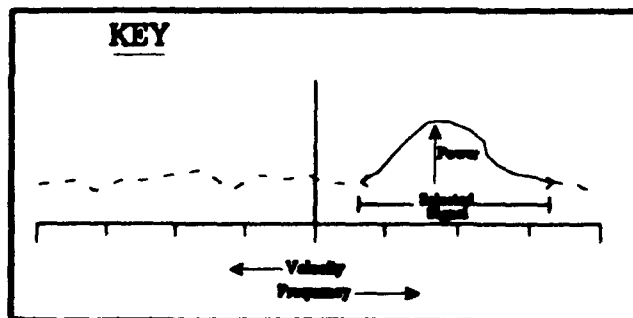
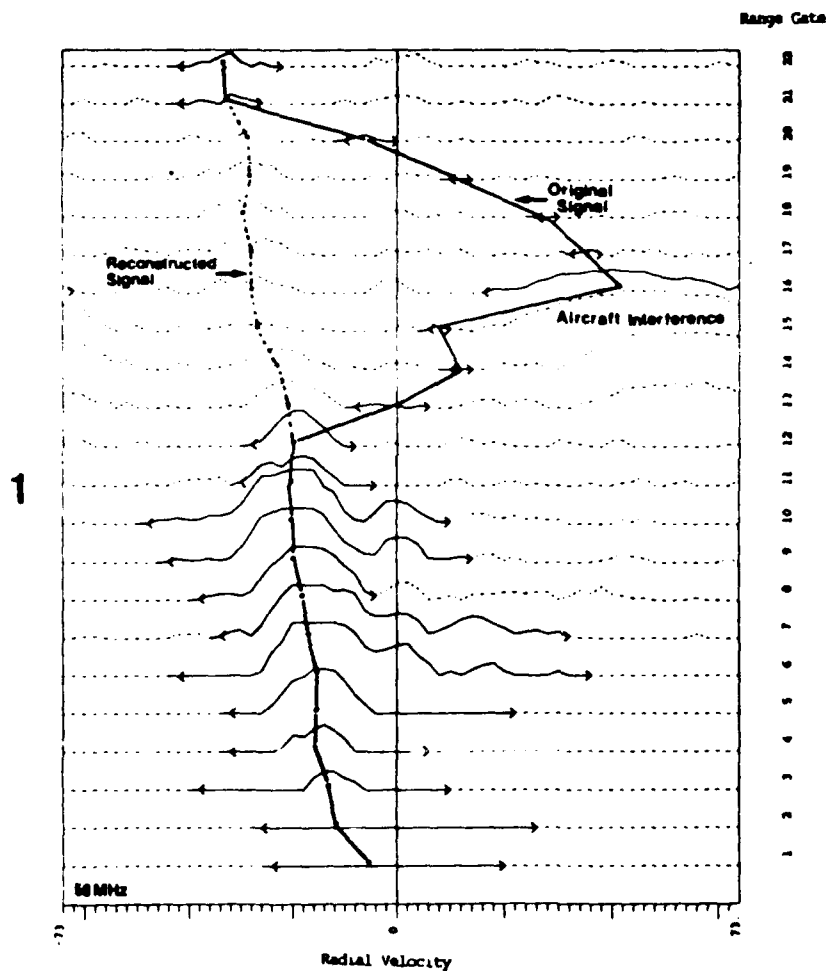
# A. Quality control of wind profiler measurements -- Overview

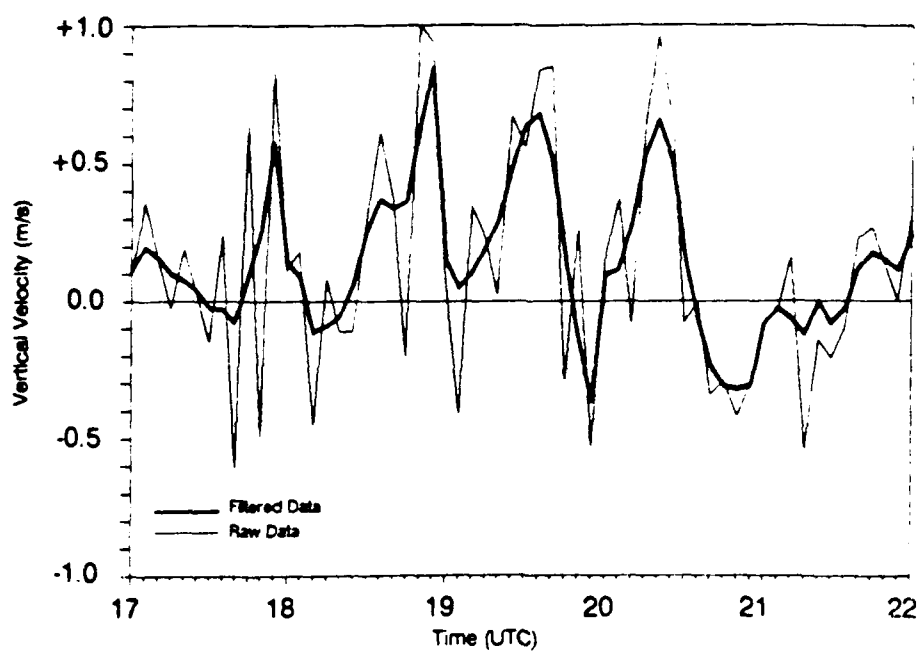
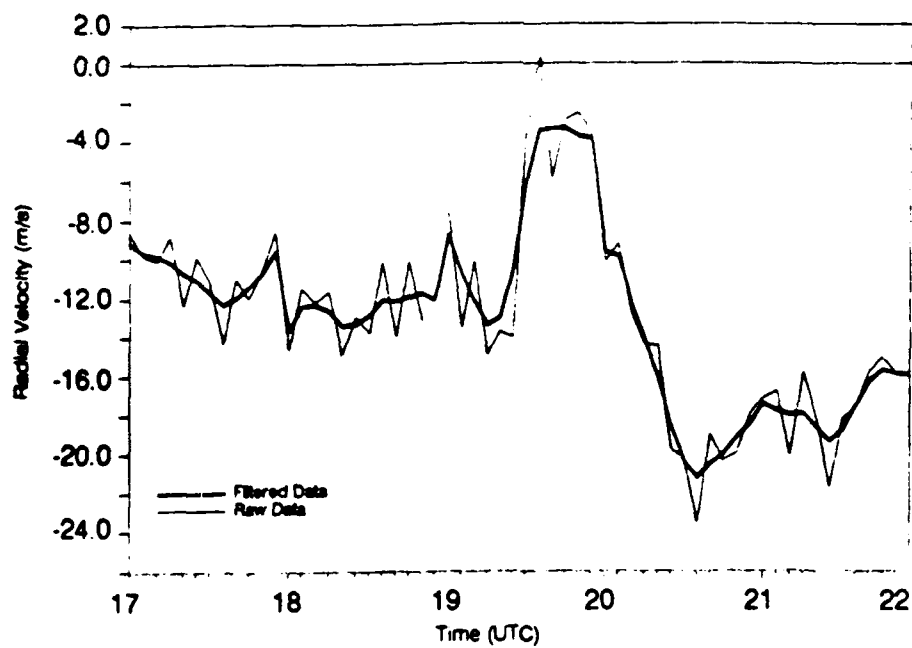
**Goal:** Remove spurious data from high-temporal (5-minute) 404 MHz and 50 MHz wind profiler data sets

**Method:** Sequentially applied a 3-step process:

1. interactive spectral reconstruction of the Doppler signal (1)
2. deletion of vertically and temporally inconsistent observations
3. use of a 1-3-5-3-1 moving filter to reduce small-scale fluctuations (2)

**Results:** Produced dynamically, vertically, and temporally consistent wind profiler data which enabled diagnoses of the phenomena being studied (eg. mesoscale rainbands)



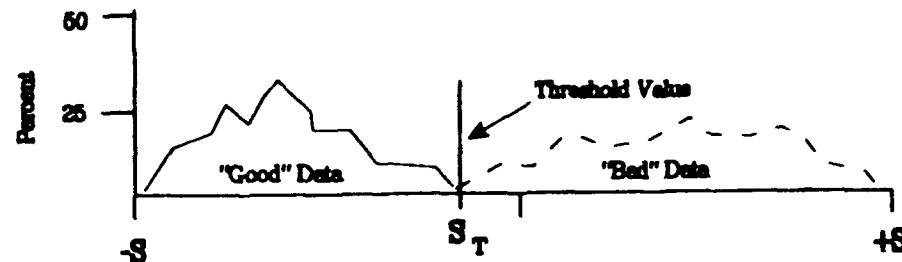
**Raw and Filtered Vertical Velocity****2****Raw and Filtered East Beam Velocity**



## B. Quality Control of Profiler Data -- Additional Details

### 1. Search for a threshold which selectively filters "good" and "bad" profiler data

**Goal:** Process known "good" and "bad" profiler data to determine if a threshold can be chosen to filter the "bad" data. Ideally (schematically shown below), the "good" and "bad" data should significantly differ.

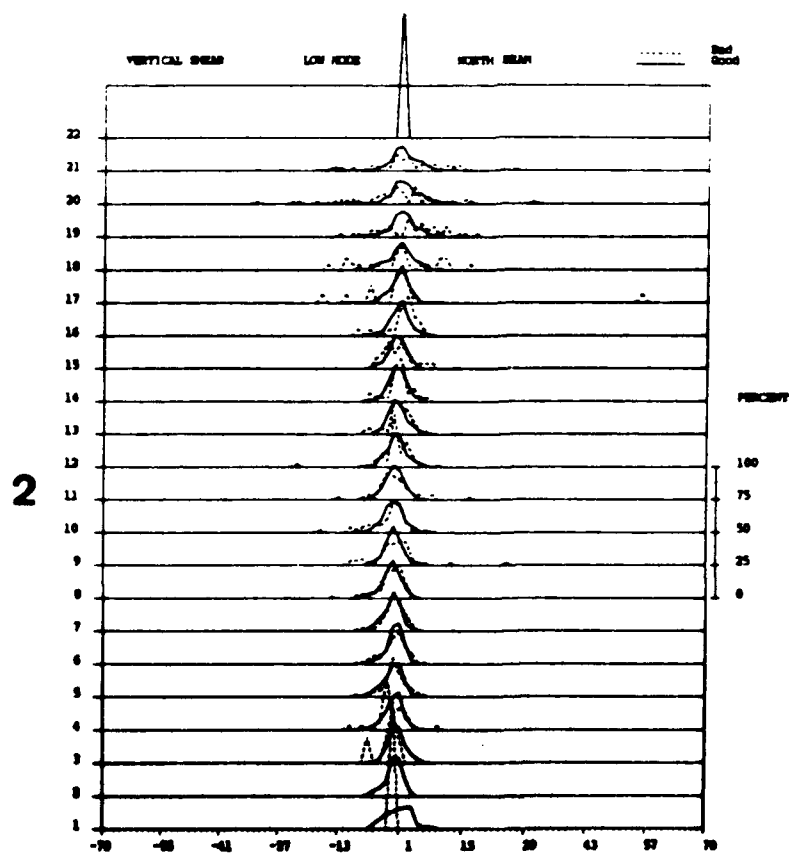
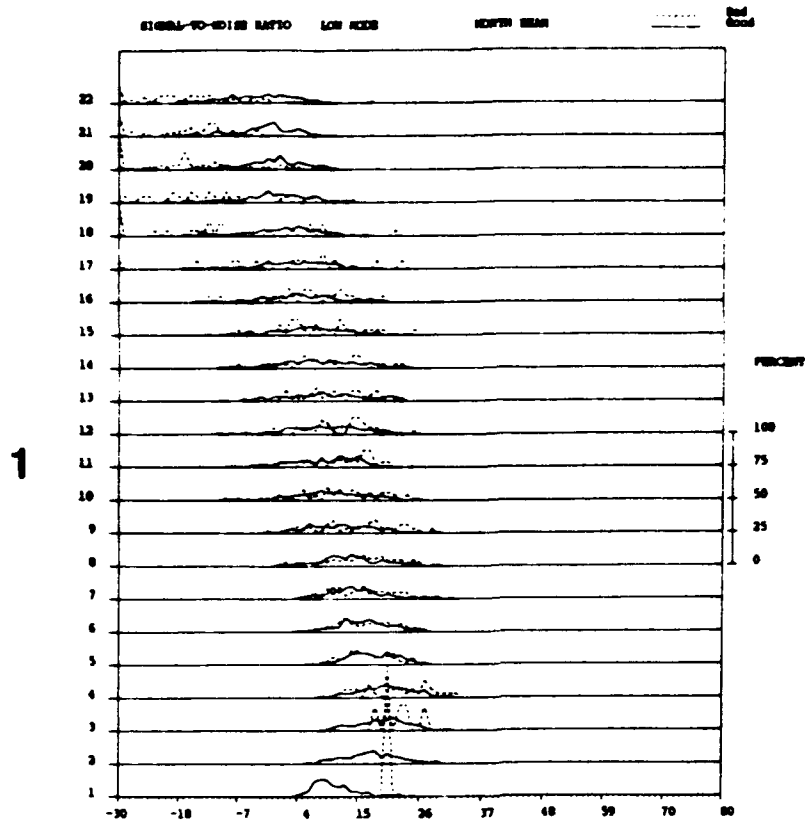


**Method:**

- used the 0, 1<sup>st</sup>, and 2<sup>nd</sup> moments (return power, radial velocity, and spectrum width), signal-to-noise ratio, noise, divergence, and vertical shear as criteria to test for a threshold
- applied to 5-minute data ( $\approx 10,000$  observations), which were subjectively stratified into "good" and "bad" observations using the technique described in I.A.
- created histograms of "good" and "bad" data

**Results:**

- histograms, shown below for signal-to-noise ratio (1) and vertical wind shear (2), indicate that "good" and "bad" histograms coincide; thus, a threshold method of quality control will not selectively filter "good" and "bad" data
- these results suggest that quality control must be performed with the Doppler spectra



## 2. Identification of errors in spectra

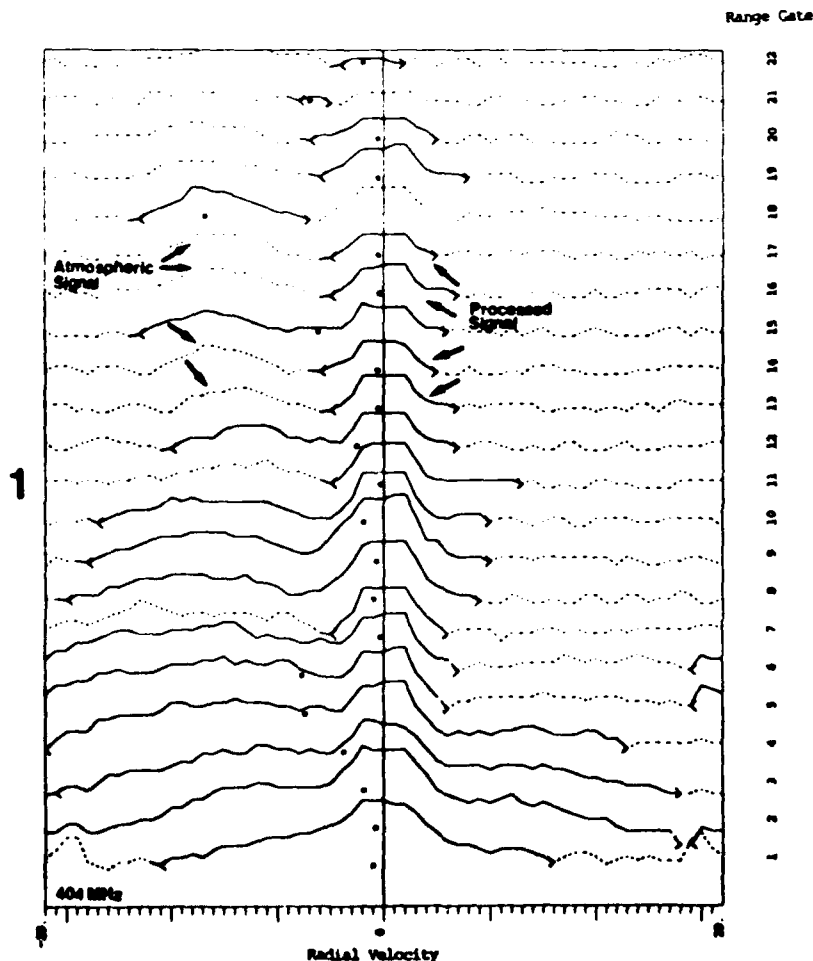
**Goal:** Understand the shortcomings of Doppler signal processing and identify any consistent error patterns

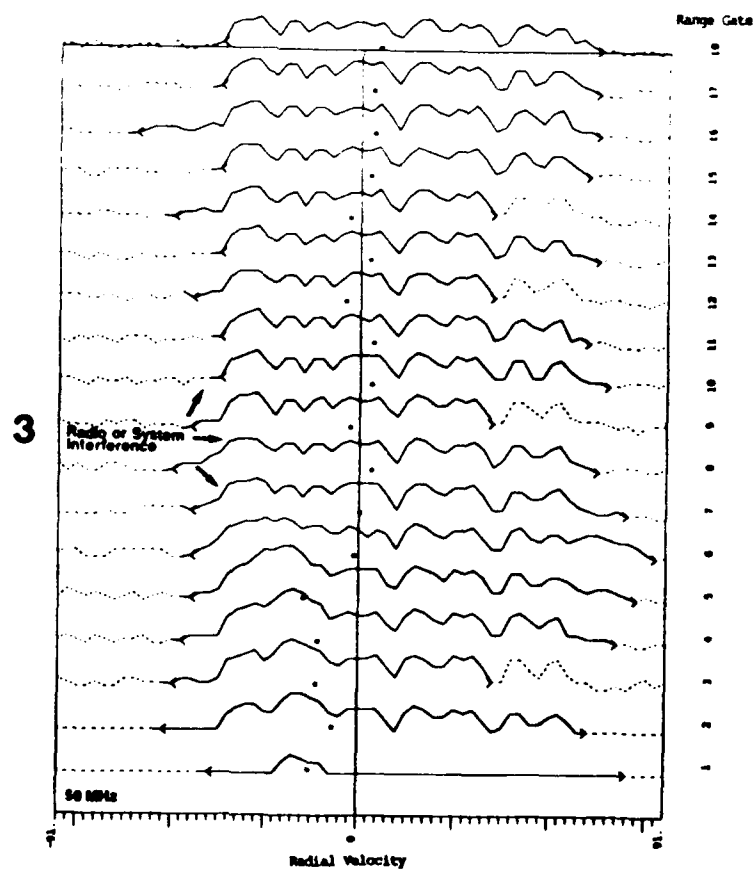
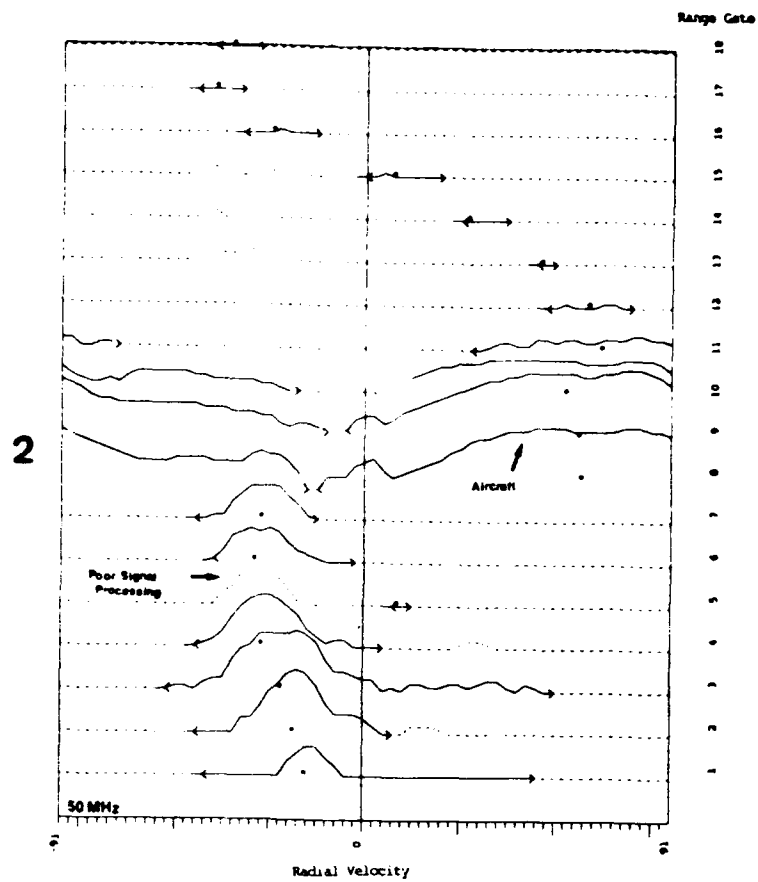
**Method:**

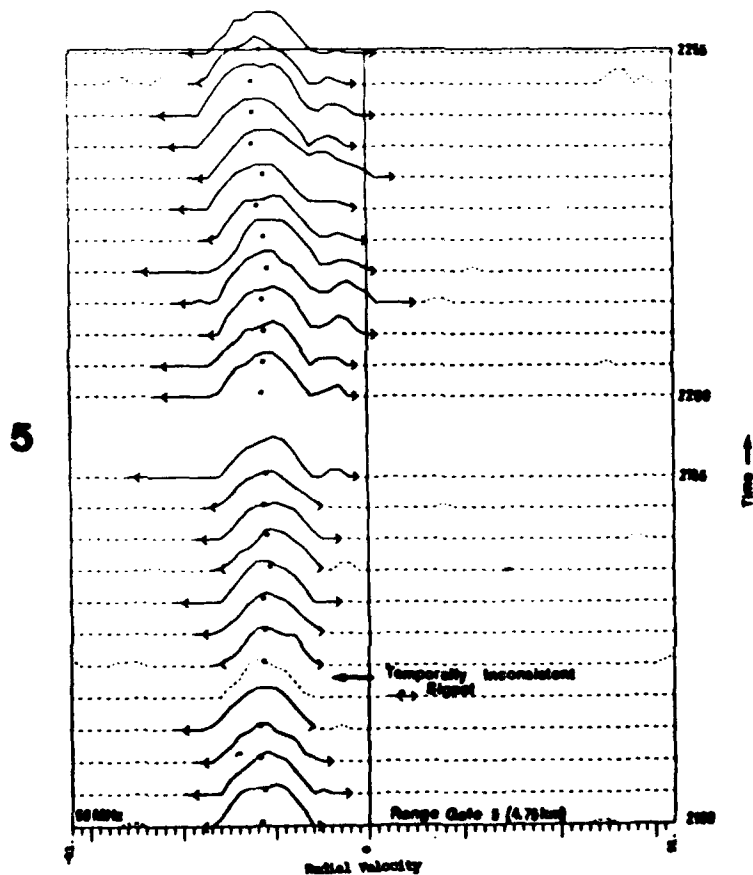
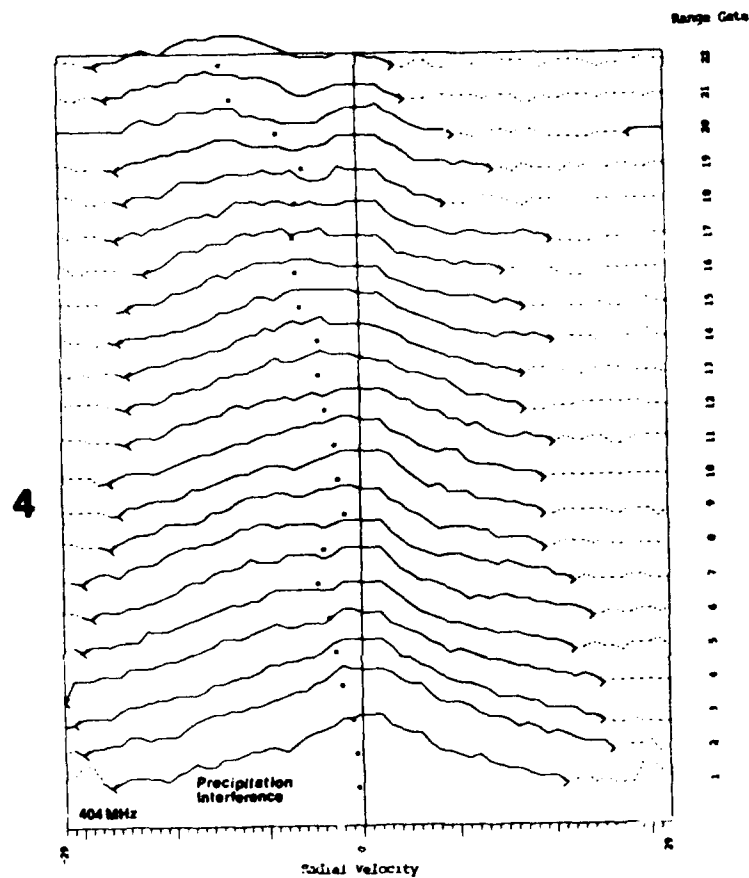
- used both 404 MHz and 50 MHz Doppler spectra
- displayed Doppler spectra as a time series at a particular height and, as previously shown, as a function of height

**Results:** Numerous errors in 404 MHz and 50 MHz wind profiler Doppler spectra were identified:

- Spectra (height section)
  - non-atmospheric signals were processed (1)
  - aircraft interference (2)
  - radio or system interference (3)
  - precipitation being sensed (can be corrected using the vertical velocity) (4)
- Spectra (time section)
  - non-atmospheric signal was processed (5)





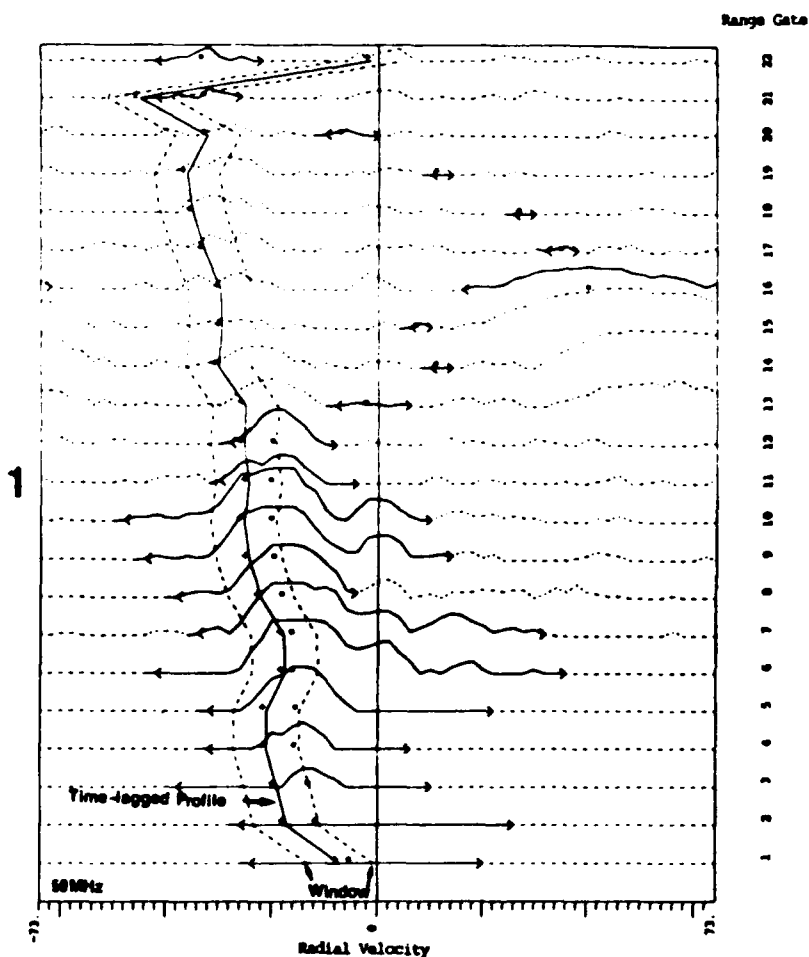


### 3) Methods of quality control utilizing Doppler spectra (research in progress)

**Goal:** Develop quality control with Doppler spectra that utilize the quasi-persistent nature of the atmosphere

**Method:** Utilized a 30-minute, consensus-averaged, time-lagged profile with a  $\pm 7\text{ms}^{-1}$  window to identify poor signal processing; if the chosen Doppler signal occurs outside the window, a new signal should be analyzed within the window

**Results:** As a first guess, a time-lagged profile is useful to identify poor signal processing (1)



### C. Studies of wind profiler-measured vertical velocity

**Goal:** Determine the representativeness of wind profiler-measured vertical velocity

1. **Experiment I** Research conducted for a paper written for Indirect Atmospheric Probing (graduate course in remote sensing)

**Tests**

**Performed:**

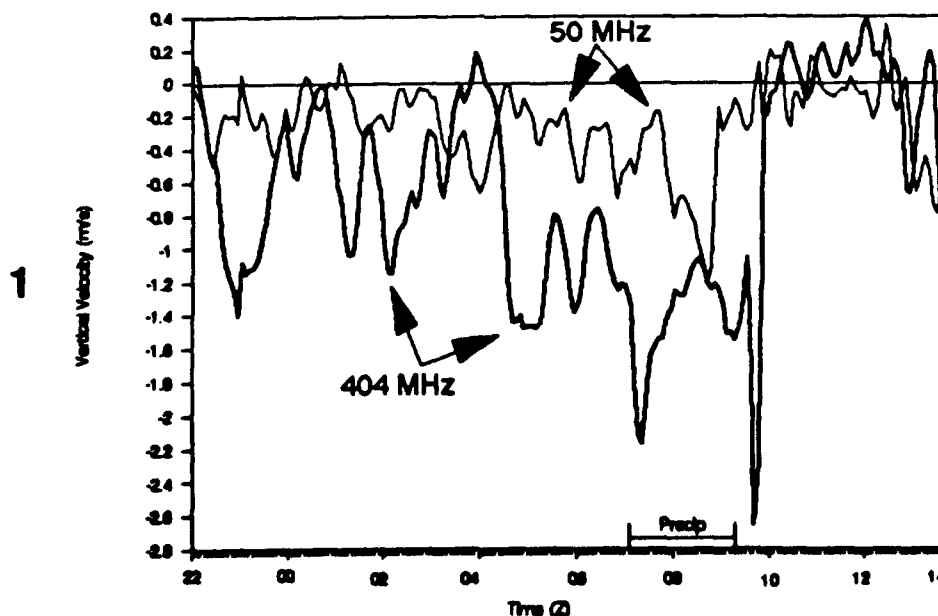
- Analyzed zenith beam Doppler spectra to determine the nature of the signal
- Tested weighted, moving filters on vertical velocity data
- Attempted to produce well-defined Doppler spectra by altering wind profiler sampling rates
- Compared 404 MHz and 50 MHz wind profiler-measured vertical velocities, these sites were separated by 15 km

**Test**

**Results:**

- Doppler spectra were broad, typical of multiple velocities being sensed
- Weighted filters reduced the noise and the variability (associated with turbulent and cumulus scale motions) while preserving the mean signal
- Altering wind profiler sampling rates produced mixed and inconclusive results
- Comparison of 404 MHz and 50 MHz vertical velocity (displayed below) showed agreement in direction, but differed in magnitude (the 404 MHz wind profiler measured stronger velocities) (1)

**50 MHz and 404 MHz Vertical Velocities**



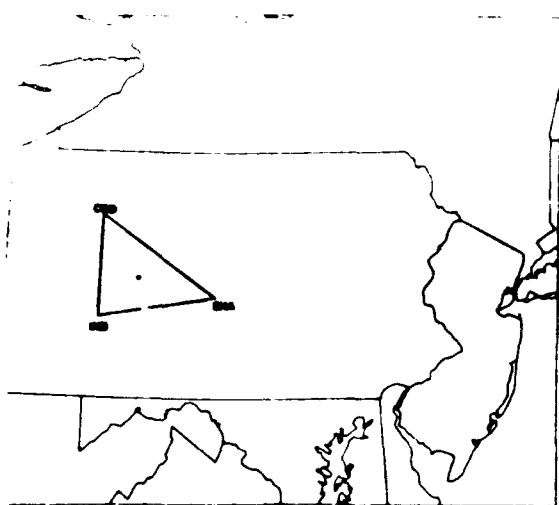
2. Experiment II Comparison of hourly averaged 50 MHz wind profiler-measured vertical velocity and kinematically derived vertical velocity from a triangle of 50 MHz wind profilers

Method:

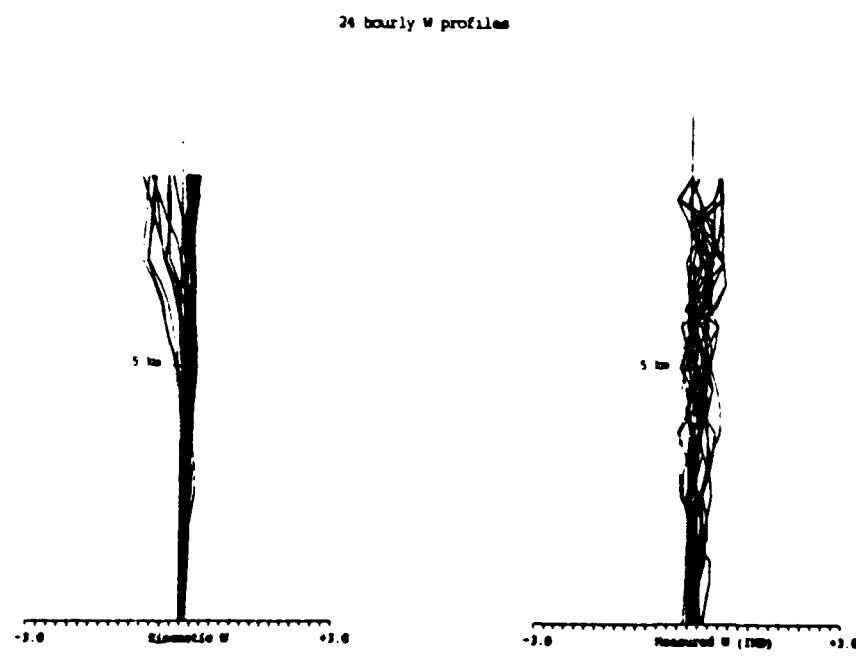
- Used profiler-measured horizontal winds from a triangle of three 50 MHz wind profilers to kinematically derive vertical velocity for the centroid of the triangle (1), shown below) and compare to hourly averaged profiler-measured vertical velocities at Indiana, PA (IND), 50 MHz wind profiler
- Applied to March 7, 1990, data

Results:

- Individual vertical velocity profiles had a large degree of variability, as indicated by the 24 hourly vertical velocity profiles (2) and the scatter plot (4)
- The 24-hour mean profiles (3) were similar below 5 km.
- Other days studied varied, with some days showing strong agreement while others had less agreement

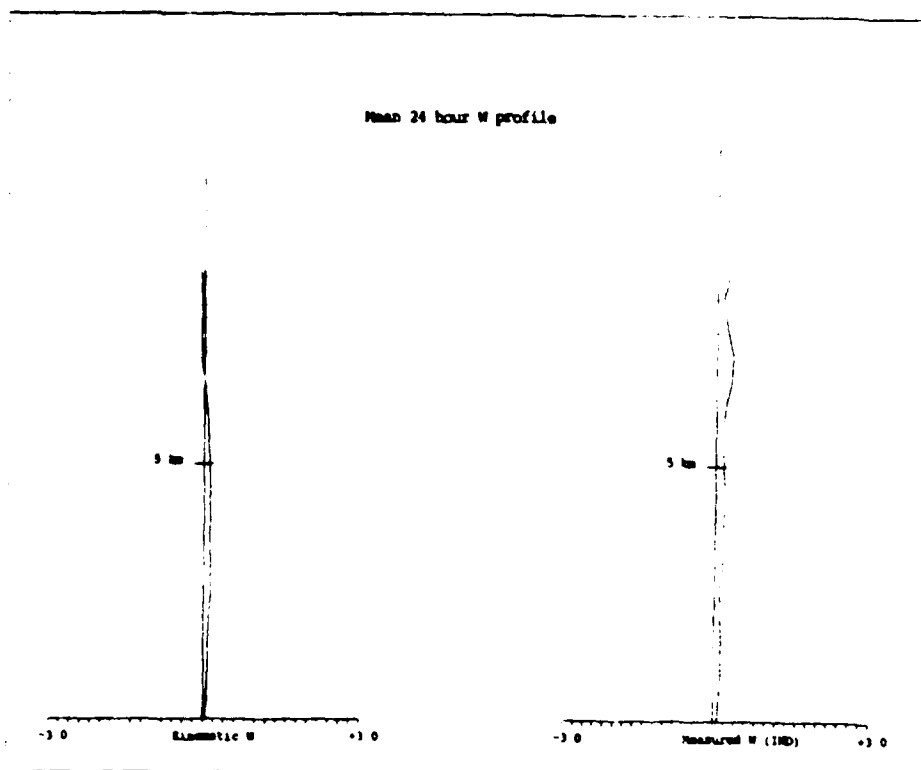


2





3



4

